AN ANALYSIS OF A DUOPLASMATRON ION SOURCE FOR ION BEAM DEPOSITION

by

Chin-Chi Tsai

Submitted in partial fulfillment of
the requirements for the degree
of Master of Science

DEPARTMENT OF ELECTRICAL ENGINEERING
FACULTY OF PURE AND APPLIED SCIENCE
UNIVERSITY OF OTTAWA
OTTAWA, CANADA

1968

SUMMARY

This thesis describes a continuation of work of another author, on a source of a controllable beam of ions of solid elements. The source is of the Duoplasmatron type, and was originally intended for use in the fabrication of microcircuits.

A review of the principles of operation of ion-sources is included to provide a theoretical background for the description of the investigations of the existing ion source. The purpose of these investigations was to find the ways of increasing the current of silver ions from a fraction of a microampere to one of at least a few milliamperes. Basic measurements had to be made to determine the detailed characteristics of the magnetic field system, the heating, and the cooling systems. These measurements provided the basis for an analysis of the source, and for recommending modifications to bring it to the expected performance. Among others, a definite proposal of the pole shape modification has been made.

Since the temperature of the oven used for evaporating silver could not be controlled in the existing source, a simple control system had been designed and incorporated in the apparatus.

ACKNOWLEDGEMENTS

I wish to express my sincere gratitude to Prof. O. Celinski for his efforts to introduce me to scientific work, and for many stimulating discussions which we had in the course of this research.

I would also like to express my thanks to Mr. René LeHenaff from the Electrical Engineering Department, to Mr. Nelson Goodchild from the Physics Department, to Mr. C. B. Jeffery of Geospace Engineering Company, Ottawa, and to others who helped me in the experimental work.

Financial assistance was received from the National Research Council through grant number A-871, and this is gratefully acknowledged.

AN ANALYSIS OF A DUOPLASMATRON ION SOURCE FOR ION BEAM DEPOSITION

Tables of Contents

Tables of Figures*

*See also Tables of Figures in "Principles of Operation of Ion Sources"

INTRODUCTION

Following World War II, the development of electronics expanded greatly. Electronic circuits found ever increasing applications in defence, industry, scientific research, medicine, business, and entertainment fields; e. g. in automatic weapon systems, airbone equipment, missiles, satellites, industrial automation, television, etc (Stern, 1964).

Man, as the controlling agent, is being eliminated by its electronic counterpart whenever possible. The increasing quantity of electronic equipment (e. g. in aircraft) produced a necessity of not only increasing its reliability but also reducing its size, weight, cost, and power consumption (Carroll, 1965).

The introduction of miniature and subminiature vacuum tubes seemed to have been the first step towards the miniaturization at the end of the World War II. Transistors, introduced commercially in the early fifties, whose process of adoption by the industry took some ten years, made possible the size reduction of equipment by a whole order of magnitude (Danko, 1961). Integrated circuits, introduced in the early sixties, added, perhaps, as much as two more orders of magnitude to the size reduction of the equipment (Alberts, 1961).

The integrated circuits are manufactured by photo-etching process which puts a lower limit (about 10 μ) to the minimum size of the components. The dimensions of the

components have to be much greater than the wave length of the light used in the process (about 0.3 μ for the ultra violet light). To further reduce the size of the electronic circuits, different manufacturing techniques with better resolution than that of a light beam would have to be used. Since the wave length of electrons and ions within the commonly used range of energies is below one Angstrom, therefore, the use of electron and ion beams to construct and investigate the micron-size devices became the next step in the development of the microcircuits (Shoulders, 1961).

Early in 1962, following the general trend towards miniaturization, G. S. Glinski proposed to build an experimental tool (Glinski et al., 1962), using scanning electron-, and ion-beam techniques, for construction, observation, and measurement of micron-size electronic circuits. This resulted in the Multipurpose Microelectronic Processor (MMP) the construction of which was started in 1962 by Samaroo and Mousseau in this department (Glinski et al., 1964). The MMP, when completed, will perform controlled ion-beam deposition, electron beam micromachining, and topological and chemical inspection using a scanning electron microscope (Samaroo, 1965). In this process, the photo-etching technique of making circuits will be replaced by deposition of ions of suitable elements on a passive substrate (glasses, ceramics, etc.) to produce circuit elements and their interconnections. A wide variety of ions of different elements are required for making semiconductors (Si, Ge, B, P, etc.), resistors (SiO_2, Sb_2O_5, TiO_2, Al_2O_3, etc.), conductors (Au, Al, etc.), capacitors (Al, SiO_2, etc.), and insulators (SiO_2, TiO_2, etc.). To produce beams of ions of all these elements a versatile ion source had to be

designed and constructed. At the end of 1965, W. J. Jirafe started the design and development of an ion source of the Duoplasmatron type (Jirafe, 1966). This ion source was first tested in Dec. 1966 and produced an ion current of less than one microampere. After the departure of W. J. Jirafe the ion-source project was continued by O. Celinski with the assistance of the writer.

The object of the work was to find the ways of increasing the ion current from less than a microampere, to at least a few milliamperes. The following program was suggested at the outset of the work:

A study of the principles of operation of ion sources.

Measurement and analysis of the performance of the existing equipment.

Deciding about the modifications which would improve the performance of the existing ion-source.

Incorporation and testing of the modifications.

The first three stages of the execution of this program are described in this thesis. The last one could not be done because of the equipment breakdowns and consequent delays, which were beyond the author's control.

References:

1. Alberts, Richard D.
'Microminiaturization and Molecular Electronics',
Miniaturization, P. 32, 1961

2. Carroll, John M.,
'Microelectronic Circuits and Applications',
N. Y. McGraw-Hill, P. 2, 1965

3. Danko, S.F.,
'The Micromodule Approach to Microminiaturization',
Microminiaturization, P. 101, 1961.

4. Glinski, G.S., Mousseau, T., Samaroo, W.R.,
'Microelectronix Research Laboratory Equipment',
University of Ottawa, Oct., 1962

5. Glinski, G.S., Mousseau, T., and Samaroo, W.R.,
'The Multipurpose Integrated Electronic Processor',
Proc. of IEEE, P. 1475-78, Vol. 52, 1964

6. Jirafe, W.J.,
'A Duoplasmatron Ion Source for Ion Beam Deposition',
University of Ottawa, TR NO 66-15, 1966

7. Samaroo, W.R.
'The Multipurpose Microelectronic Processor',
Ph. D. Thesis, University of Ottawa, 1965

8. Shoulders, K.R.
'Advanced in Computers',
Academic Press, P. 137-289, Vol. 2, 1961

9. Stern, Arthur P.
'Preface to the Integrated Electronics Issue',
Proc. of IEEE, P. 1395-99, Vol. 52, 1964

THE UNIVERSITY OF OTTAWA
Department of Electrical Engineering
OTTAWA, CANADA

Technical Report No. 68 - 1
January, 1968

PRINCIPLES OF OPERATION OF ION SOURCES

by
Chin-Chi Tsai

All the work reported here was supported by the National Research Council of Canada, under Grant No. A-871

An ion beam source, of the von Ardenne type has been designed and built in 1966, for use in the Multipurpose Microelectronics Processor. The ultimate purpose of the processor was the fabrication of microelectronic circuits by means of ion and electron beams to produce patterns of interconnected circuit components.

This report deals with principles of operation of ion sources and is preliminary to further work on the existing apparatus towards its intended purpose.

TABLE OF CONTENTS

TABLE OF FIGURES

TABLE OF FIGURES (cont'd)

PRINCIPLES OF OPERATION OF ION SOURCES

Chin-Chi Tsai

Introduction:

An ion is an atom, or a molecularly-bound group of atoms, which has gained or lost one or more electrons, and which thus has a negative or positive electric charge.

An ion source is an apparatus used to produce ions in the form of a beam, usually consisting of one variety of ions.

Ion sources are used in a number of scientific and industrial applications, such as the studies of the channeling and blocking effects in crystals(Nelson, 1967), the manufacture of semiconductor devices by ion implantation(Chopra et al., 1967), or the studies of the impurities in solids(McCaldin, 1965). An interesting application of ion sources is in their intended use for propulsion in space travel(Brewer et al., 1961).

Ion formation:

Ions can be formed in a solid, liquid, or gas state. In general, to form an ion, one or more electrons have to be detached from, or attached to an atom or a molecular group of atoms. To detach an electron from an atom to form a positive ion, a certain amount of energy has to be imparted to the atom. In attaching an electron to an atom to form a negative ion, an energetic free-electron has to be collided and captured by the atom. These processes are called ionization processes.

Negative ions can be formed(Field, 1957) either by an electron capture process or by a pair-production process. The process of the capture of an electron 'e' by an atom 'A' to form a negative ion A^- can be represented by the following physicochemical reaction:

$$A + e + KE_1 = A^- + KE_2 + U_a$$

where KE_1 and KE_2 are the total kinetic energies before and after the ionization, respectively, and U_a is electron affinity, which is the energy required to form a positive ion and/or a negative ion from a neutral molecule, it also represents the binding energy of an attached electron(Cambel, 1963). If the sum of the kinetic energy and the electron affinity in the right-hand side of the last equation is liberated(primarily by radiation) then A^- becomes stable, otherwise the reverse process of loosing an electron is likely to happen. Because of this reversibility,the electron capture process is called a resonance process. In contrast, the pair-production process, i.e. the process in which the molecule AB is split into two ions A^+ and B^- as follows,

$$AB + e + KE_1 = A^+ + B^- + e + KE_2 + U_a$$

in which an emitted electron carries away the excess energy,is a stable,non-resonance process.

The formation of a positive ion may occur in different ways by means of a variety of mechanisms which are basically collision processes. These processes may be categorized under three broad classifications as follows:

a) Thermal ionization phenomena:

These are due to the collisions by the agitated particles constituting the gas. The collision agents may be energetic electrons, positive ions, or neutral atoms. If a rest atom is ionized in a single collision, the increase of potential energy of this atom due to this collision must be at least equal to the ionization energy U_i of the atom. The maximum energy U_{max} that may be absorbed by a particle m_2 at rest,involved in an inelastic collision with an impinging particle m_1 with a velocity v_1 is

$$U_{max} = \frac{m_2}{m_1 + m_2} \frac{m_1 v_1^2}{2} = \frac{m_2}{m_1 + m_2} KE_1$$

If $m_1 \ll m_2$ then $U_{max} \simeq KE_1$

$m_1 = m_2$ $U_{max} = \frac{1}{2} KE_1$

$m_1 \gg m_2$ $U_{max} \simeq 0$

Hence, if the impinging particle is an electron, its kinetic energy must be at least equal to U_i of the atom to be able to ionize the atom, while if the particle is one of positive ions or neutral atoms then its KE must be not less than twice U_i. Actually, an ion becomes an effective ionizer when its velocity is as great as that of an electron whose KE is equal to the ionization energy of the atom. Since, to excite positive ions and neutral atoms to high velocities is more difficult than to excite electrons, therefore, the ionization by the positive ion collisions, and by the neutral atom collisions, are improbable(Cobine, 1958).

b) Ionization by radiation:

When an atom absorbs radiation energy such as photon, it becomes excited, or ionized, if the absorbed energy is not less than the ionization energy of the atom. The radiation energy is given by Planck's formula, $U = h\nu$, where 'h' is Planck's constant and 'ν' is the frequency of radiation. From this formula, the lowest-frequency of a photon that will ionize an atom can be calculated. Frequencies higher than this lowest-frequency tend to release an electron from an inner shell of the atom. The ionization by radiation is generally less important than the ionization by electron collisions(Cambel, 1963).

c) Cumulative ionization:

In this process, an atom is ionized in two or more stages. An atom excited by one of the processes may have its ionization completed by a repetition of the same process or by one or more other processes, e. g. an atom may become excited by a collision and then ionized by radiation. Such an ionization combines a variety of ionization processes and is probably the most common manner in which atoms become ionized in a plasma state.

From the above three ionization processes, the thermal ionization process is the only one of practical importance in ion

sources. Since electrons are easy to produce, control, and accelerate in the form of a beam of an arbitrary energy, therefore, the electron collision ionization process is the most common way of artificial ion production.

Ion sources:

As ions are formed, they are extracted from the ionization chamber by an electrostatic field and acclerated and collimated by an electromagnetic field to form an ion beam. An apparatus which produces an ion beam is called an ion source.

A wide variety of ion sources has been developed for uses in electromagnetic isotope separators, in the high current or the high voltage accelerators used in thermonuclear research, etc. These ion sources have been developed for variety of purposes and for the use of various charge materials.

As mentioned before, the ionization by electron collision process is the most common way of ion formation. With the exception of the contact ion source virtually all other ion sources, such as RF ion source, magnetic ion source, duoplasmatron ion source, sputtering ion source, and electron gun ion source etc., use this process.

The starting charge material used in an ion source may be a solid, liquid, or gas. For gas charge material, all we have to do is to feed the gas into the ionization chamber of the ion source, such as RF ion source, magnetic ion source, and duoplasmatron ion source. However, the charge material in solid or liquid state, has to be evaporated prior to its ionization. Such ion sources are oven-ionizer ion source, sputtering ion source, contact ion source, and electron gun ion source. In order to extend the use of the duoplasmatron ion source, this principle has been adopted in the duoplasmatron designed by W.J. Jirafe (1966).

The source designed and built by the above author was expected to have an efficiency of better than 90 % and the ion current of at least on the order of milliamperes. When tested, however, the performance fell short of the expectations. The ion current was less than one microampere and the efficiency, because of the smallness of the beam current, could not be measured. It was, therefore, necessary to find why the current was

so small, and propose ways of overcoming this defect. For this purpose the ionization mechanisms of different ion sources were considered in some detail as follows:

A. Radio-frequency ion source:

The charge material, in the form of gas, is invariably at such pressure ($p < 10\mu$) that the gas breakdown does not occur under the working conditions, because of the low probability of collision (long mean free path of electron, $\lambda_e \gtrsim 30$ cm). To ensure a continuous ionization of charge material, radio-frequency power may be used to excite and maintain the discharge in a highly rarefied gas ($p \leq 50\mu$) by lengthening the effective path of electrons, i.e. increasing the probability of the collisions with other atoms and thus ionization. There are two methods of transferring this RF power from the oscillator to the ionization chamber: one is by inductive coupling to the chamber by several turns of wire (Eubank et al., 1954; Narinsek et al., 1963); the other is by direct connection to two internal or external electrodes of the chamber (Moak et al., 1951; Hall, 1948). An axial magnetic field is often used (Hall, 1948) which makes the electrons move in a spiral path, thus greatly increasing the probability of collision, and considerably enhancing the ion yield. Because of the use of the RF power this ion source is called a radio-frequency ion source (Fig. 1).

To investigate the behavior of electrons in this source, we shall consider an electron moving in a vacuum with both, the electric and the magnetic, fields applied in the 'z' direction, i.e. $B = B_z$ and $E = E_z$ as shown in Fig. 2. From Lorentz's relation, a charged particle moving in superimposed E and B fields is subject to a force,

$$F = qE + q(v \times B) \qquad (1)$$

where 'q' is the charge of the particle and 'v' is its velocity, and the equation of its motion is

$$M \frac{dv}{dt} = F = qE + q(v \times B) \qquad (2)$$

where M is the mass of the charged particle. Similarly, if the charged particle is an electron, then Eqs. (1) & (2) can be rewritten as

$$F = - eE - e(v \times B) \qquad (3)$$

and

$$m\frac{dv}{dt} = F = - eE - e(v \times B) \qquad (4)$$

where 'e' is the electron charge; m, the electron mass; and v, the electron velocity. If $E = E_z$ and $B = B_z$ then

$$F = - eE_z - e(v \times B_z) \qquad (5)$$

and

$$m\frac{dv}{dt} = - eE_z - e(v \times B_z) \qquad (6)$$

Equations (5) and (6) indicate that the electron motion is a function of the parameters E_z, B_z, and v. Since the distributions of the electric and the magnetic fields are complex and non-uniform, the behavior of electrons in the ion source is difficult to evaluate. Nevertheless, by making certain assumptions, one may evaluate it in simple cases.

a) Consider an electron at rest(initial velocity zero) at the origin of the coordinates in Fig. 2 in the presence of the E_z and B_z fields. Since E_z will accelerate the electron along the 'z' direction only, i.e. $v = v_z$, and $v_z \times B_z = 0$, therefore, Eq. (6) becomes

$$m\frac{dv_z}{dt} = - eE_z$$

If 'e' and 'm' are constant, then the electron motion depends on E_z only. The electric field E_z can be any

function of time or space. For simplicity, we consider the electron motion in a static electric field and a sinusoidal electric field respectively.

ai) Substituting the static electric field, $E_z = - E_o$ = constant, into Eq. (6) and integrating twice, we get

$$v_z = \frac{eE_o}{m} t + C_1$$

and

$$S_z = \frac{eE_o}{2m} t^2 + C_1 t + C_2$$

where S_z is the displacement of the electron in the 'z' direction. From the initial conditions at $t = 0$, $v_z = 0$ and $S_z = 0$, we get $C_1 = C_2 = 0$, thus

$$v = v_z = \frac{eE_o}{m} t$$

$$S = S_z = \frac{eE_o}{2m} t^2$$

The curves of E_z, v_z, and S_z are shown in Fig. 3.

aii) In the case of purely sinusoidal electric field, i.e. $E_z = - E_1 \sin(\omega t + \phi)$, where '$\phi$' is the phase angle of the field at $t = 0$ and 'ω' is its angular frequency. Substituting this relation into Eq. (6), we have

$$m \frac{dv_z}{dt} = eE_1 \sin(\omega t + \phi)$$

and the corresponding velocity and displacement of an electron are

$$v_z = -\frac{eE_1}{m\omega}\cos(\omega t + \phi) + C_3$$

$$S_z = -\frac{eE_1}{m\omega^2}\sin(\omega t + \phi) + C_3 t + C_4$$

Taking $v_z = 0$ and $S_z = 0$ at $t = 0$, we get $C_3 = \frac{eE_1}{m\omega}\cos\phi$ and $C_4 = \frac{eE_1}{m\omega^2}\sin\phi$. Thus,

$$v_z = \frac{eE_1}{m\omega}(\cos\phi - \cos(\omega t + \phi)) \qquad (7)$$

$$S_z = (\frac{eE_1}{m\omega}\cos\phi)t + \frac{eE_1}{m\omega^2}(\sin\phi - \sin(\omega t + \phi)) \qquad (8)$$

The curves of the electron motion in Fig. 4 show that the electron will move forward along the 'z' direction and oscillate at the same time.

b) Assume now that an electron is moving in the xy plane in a uniform and constant field B_z, with $E = 0$, and with an initial position and velocity S_{xo}, and v_{yo}, respectively. In this case, Eq. (6) becomes

$$m\frac{dv}{dt} = -e(v_{yo} \times B_z)$$

Since the vector $v_{yo} \times B_z$ is perpendicular to both v_{yo} and B_z, the force $m\frac{dv}{dt}$ will be at right angles to both v_{yo} and B_z. Due to the uniform B_z, the magnitude of v will not change but its direction will, and the electron will follow a circular path in the xy plane (Fig. 5). We now set the force on the electron due to B_z numerically equal to the centrifugal force, $\frac{mv_{yo}^2}{r_c}$, where r_c is the cyclotron radius. Thus

$$ev_{yo}B_z = \frac{m(v_{yo})^2}{r_c}$$

or $$r_c = \frac{mv_{yo}}{eB_z} \qquad (9)$$

The cyclotron frequency associated with the electron gyration is

$$\omega_c = \frac{v_{yo}}{r_c} = \frac{eB_z}{m} \qquad (10)$$

Since the electron moves in a circular path(Fig. 5) with the initial conditions, $v = v_{yo}$ and $S = S_{xo}$ at $t = 0$,

then the velocity and displacement of the electron at time t are

$$v = v_x\, i + v_y\, j + v_z\, k = v_x\, i + v_y\, j + 0\, k$$

$$= -(v_{yo} \sin\omega_c t)\, i + (v_{yo} \cos\omega_c t)\, j \qquad (11)$$

$$S = S_x\, i + S_y\, j + S_z\, k = S_x\, i + S_y\, j + 0\, k$$

$$= (S_{xo} - r_c + r_c \cos\omega_c t)\, i + (r_c \sin\omega_c t)\, j \qquad (12)$$

c) In the presence of a sinusoidal electric field, $E_z = -E_1 \sin(\omega t + \Phi)$, and a constant and uniform magnetic field B_z, and with initial conditions, $v = v_{yo}$ and $S = S_{xo} = r_c$, at $t = 0$, we can rewrite Eq. (6) as

$$m\frac{dv_z}{dt} = eE_1 \sin(\omega t + \phi)$$

$$m\frac{dv_{xy}}{dt} = e(v_{yo} \times B_z)$$

where $v_{xy} = v_x\, i + v_y\, j$, and from Eqs. (7), (8), (11), and(12), we have

$$v = v_x\, i + v_y\, j + v_z\, k$$

$$= -(v_{yo} \sin\omega_c t)\, i + (v_{yo} \cos\omega_c t)\, j + \frac{eE_1}{m\omega}(\cos\phi - \cos(\omega t + \phi))\, k \qquad (13)$$

$$S = S_x\, i + S_y\, j + S_z\, k$$

$$= (r_c \cos\omega_c t)\, i + (r_c \sin\omega_c t)\, j + ((\frac{eE_1}{m\omega}\cos\phi)t + \frac{eE_1}{m\omega^2}(\sin\phi - \sin(\omega t + \phi)))\, k \qquad (14)$$

where r_c and ω_c are the same as in Eqs. (9) & (10). The electron will move in a helix around the cylindrical surface, oscillating along the 'z' axis at the same time (Fig. 6).

Up to now we have been considering electron motion in a perfect vacuum. In fact, the gas pressure in an ion source is not zero, but usually above 10μ. Thus, an accelerated electron does not move unimpeded as in a vacuum, but it will collide with some atoms and, in general, be reflected. If its energy is high enough(i.e. during the accelerating half cycle of the RF field), it will ionize the collided atom and produce an ion-electron pair. The reflected primary and the secondary electrons produced in the collision will be accelerated again in the next half cycle in the opposite directions. Under favourable conditions electrons will follow the RF field, oscillating back and forth, getting their energy from the field. Thus, the streams of electrons go from end to end of the ionization chamber continually ionizing the charge material.

To find the order of magnitudes of the quantities encountered in the operation of an ion source we can use the published data. We can approximately calculate the maximum velocity of the electron in the 'z' direction v_{zmax} and its corresponding displacement S_{zmax} from the data given in the paper of Moak et al.(1951) and Eqs. (13) & (14).

Given: L = the length of the ionization chamber; 8.75"(or 22.2 cm).

p = the pressure in the ionization chamber is less than 50μ.

ω = the angular frequency of the RF field is from 20 to 450 MHZ.

On these bases let us assume the values of the parameters as follows,

$p = 40\mu = 0.04$ mmHg

$\omega = 8\pi \times 10^7$ rad/sec

ϕ = the initial phase angle of the RF electric field = 0

E_1 = the peak value of the RF electric field = $5 \times 10^3 \frac{V}{m}$

The velocity v_z will be maximum at the end of the accelerating half cycle, $t = \pi/\omega = 1.25 \times 10^{-8}$ sec, thus

$$v_{zmax} = 2\frac{eE_1}{m\omega} = 7 \times 10^6 \quad m/sec$$

and

$$S_{zmax} = \frac{eE_1}{m\omega} \times \frac{\pi}{\omega} = 0.04375 \text{ m} = 4.375 \text{ cm}$$

where $\frac{e}{m} = \frac{\text{electron charge}}{\text{electron mass}} = 1.76 \times 10^{11} \frac{\text{coul.}}{\text{Kg.}}$.

The mean free path of the electron (Loeb. 1961) is

$$\lambda_e = \left(\pi \left(\frac{\sigma}{2}\right)^2 N \right)^{-1} = 0.08 \text{ m} = 8 \text{ cm}$$

where N is the concentration of atoms($N = 3 \times 10^{25} \frac{\text{atoms}}{m^3} \times$

$\frac{0.04\ \text{mmHg}}{760\ \text{mmHg}}$) and σ is the diameter of the gas atom(e.g. for hydrogen $\sigma = 10^{-10}$ m). Since the mean free path of the electron is greater than its maximum displacement at $t = 1.25 \times 10^{-8}$ sec, therefore the probability of collision is less than unity and, in this case, about $S_{zmax}/\lambda_e = 54.7\%$. The maximum kinetic energy corresponding to v_{zmax} of the electron is

$$KE_{max} = \frac{m(v_{zmax})^2}{2} = 139 \text{ eV}$$

If the electron-atom collision is an elastic one the electron can transfer $\frac{2m}{M}$ of its kinetic energy($2 \times \frac{9.1 \times 10^{-31}}{1.673 \times 10^{-27}} \times 139$ = 0.15 eV) to the hydrogen atom. The electron will be reflected and change its phase angle but its velocity will remain in the same order. On the other hand the hydrogen atom will only become excited but not ionized. If the collision is inelastic, the atom can obtain almost the whole kinetic energy of the electron and become ionized. The electron will be scattered from the original beam and become a, so called, ultimate electron, whose kinetic energy is less than the ionization energy of the atom, which moves through the gas in a random fashion (Cobine, 1958).

Since the maximum KE of the impinging electron is higher than the ionization energy of gas atom, and the probability of collision during the accelerating half cycle is only 54.7%, therefore, if we wish to sustain the ionization process and to speed-up the gas breakdown under a fixed set of parameters as that in the above case, we have to increase the electron path and its lifetime. A convienent method to serve this purpose is to superimpose an axial magnetic field B_z. If a primary electron scatters from the original beam, due to a collision, it will gyrate in the axial magnetic flux. If the initial velocity of the scattered electron in the transverse directrion is 10^6 m/sec(i.e. one seventh of its maximum velocity in the 'z' direction before a collision), then the electron will travel through a distance of about 1.25 cm in a circular path in the time from t=0 to $t = 1.25 \times 10^{-8}$ sec. Thus the effective path of the electron increases from 4.37 cm(in the above case S_{zmax} = 4.37 cm) to 4.65 cm, and the probability of collision increases from 54.7% to 58.1% during this interval. From

this example, the presence of the axial magnetic field in the system seems insignificant. But, when we consider the lifetime of an electron, the axial magnetic field is really very important. The scattered electron in the absence of this field, would be absorbed by the walls of the ionization chamber. The presence of it, makes the scattered electrons gyrate and, under suitable conditions, oscillate between both ends of the ionization chamber several times before reaching the wall, thus prolonging the scattered electron's lifetime. Therefore, the presence of an axial magnetic field not only can sustain the ionization process but, under favourable working conditions, can also speed-up the process of gas breakdown.

So far, we have only considered the RF power which was transfered to the chamber by a capacitive method. In the case of an inductive coupling, a rapidly alternating current flows in the solenoid which surrounds the chamber. This current produces a high frequency magnetic flux along the axis of the solenoid. An induced electric field appears in the transverse plane of the solenoid. The electrons in the gas will be acclerated by the EM field, and move in a spiral path in the transverse plane. When the working conditions are favourable, the discharge will occur in the form of a bright ring. It is called a 'ring discharge' (Thomson, 1933)

B. Magnetic ion source:

The construction of this source is shown in Fig. 7. The ionization chamber consists of two planar cathodes (top and bottom plates) separated by a cylindrical anode, and of an emission filament at the cathode potential (ground). The primary electrons emitted from the filament oscillate between two cathodes (as described below) and are accelerated to the positive anode. The presence of an axial magnetic field lengthens the path of the electrons by twisting their paths into spirals. Hence the increase of the lifetime of the electrons, and of the probability of ionization. Because of this, this source has been called 'magnetic ion source' (Kistemaker et al., 1950; Nielsen, 1957; Almen et al., 1957). This kind of ionization in which the oscillating electrons follow spiral paths along the axis and ionize the gas molecules by collisions in crossed EM fields

is called 'Penning ionization'. The discharge in this source is of this type and called 'Penning discharge'. The source is thus also known as P. I. G. (Penning ionization gauge, or Philips ionization gauge) ion source (Mohamed, 1967; Bennett, 1967).

The charge material of the source can be either solid, liquid, or gas. If it is used as a metal-ion source, the metal has to be evaporated in an oven, and the vapor introduced into the ionization chamber. This source is thus also called an 'oven-ionizer' ion source (Nielsen, 1957). If the charge material is a gas, a special gasinlet is used to introduce the gas into the ionization chamber.

To investigate the behavior of the electrons in the source, let us consider an electron moving in a vacuum with a uniform axial magnetic field B_z and an electric field whose potential distribution is shown as in Fig. 8 (Kistemaker, 1950). Using Lorentz's relation, the electron motion in the fields can be represented as follows,

$$m \frac{dv}{dt} = - eE - e(v \times B_z) \qquad (15)$$

where $E = - \nabla V$, and $E = E_r a_r + E_\theta a_\theta + E_z a_z$,

$$\nabla V = \frac{\partial V}{\partial r} a_r + \frac{1}{r} \frac{\partial V}{\partial \theta} a_\theta + \frac{\partial V}{\partial z} a_z$$

Since the potential distribution in the ionization chamber is very complex, the behavior of the electrons in the source is difficult to calculate. However, we can do this in simplified cases.

a) Assume $B_z = 0$ and $E = - \nabla V$, the potential distribution is shown in Fig. 9a. The electric field components (Fig. 9b) are $E_r = E_\theta = 0$ and

$$E_z = \begin{cases} \dfrac{V_A}{S_c - S_b} & S_b < S_z < S_c \\ 0 & S_c < S_z < S_e \\ \dfrac{V_A}{S_f - S_e} & S_e < S_z < S_e \end{cases}$$

If the distances are $S_b - S_a = S_c - S_b = S_e - S_d = S_f - S_e = D$ then

$$E_z = \begin{cases} -E_1 & S_b < S_z < S_c \\ 0 & S_c < S_z < S_e \\ E_1 & S_e < S_z < S_f \end{cases}$$

where $E_1 = V_A / D$ and V_A is the potential of the anode. Rewriting Eq. (15) as

$$m \frac{dv_z}{dt} = -eE_z = \begin{cases} eE_1 & S_b < S_z < S_c \\ 0 & S_c < S_z < S_e \\ -eE_1 & S_e < S_z < S_f \end{cases}$$

From the last differential equation, we can find its general solution v_z, the velocity of an electron in the 'z' direction. If the initial velocity of the electron at point 'b' is only in 'z' direction, then the electron will move in that direction only, i.e. $v=v_z$ and $S = S_z$. The general equations are given below, separated into three groups corresponding to the three sections of its path.

1) $S_b < S_z < S_c$

$$v_z = v_{bo} + \frac{eE_1}{m}(t - t_b)$$

$$S_z = S_b + v_{bo}(t - t_b) + \frac{eE_1}{2m}(t - t_b)^2$$

or $$v_z = \left(v_{bo}^2 + 2\frac{eE_1}{m}(S_z - S_b)\right)^{1/2}$$

at point 'c' $$v_{zc} = (v_{bo}^2 + 2eV_A/m)$$

2) $S_c < S_z < S_e$

$$v_z = v_{zc}$$

$$S_z = S_c + v_{zc}(t - t_c)$$

3) $S_e < S_z < S_f$

$$v_z = v_{zc} - \frac{eE_1}{m}(t - t_e)$$

$$S_z = S_e + v_{zc}(t - t_e) + \frac{eE_1}{2m}(t - t_e)^2$$

$$\text{or} \quad v_z = \left(v_{bo}^2 + 2\,\frac{eV_A(S_f - S_z)}{m(S_f - S_e)}\right)^{1/2}$$

at point 'f' the velocity of the electron is $v_f = v_{bo}$.

If an electron leaves the filament with zero initial velocity, it will be accelerated between points 'b' and 'c', then it will travel over the path cde with constant velocity, then it will decelerate between points 'e' and 'f', and at last stop at 'f'. A similar motion will be repeated now in the reverse direction. This oscillating motion of the electron between the top cathode and the filament is shown in Fig. 9c. If the initial velocities of the emitted electrons are not zero, the electrons will strike the top plate with their initial kinetic energy and become absorbed by it. Obviously, these electrons cannot oscillate. Since the probability of collision in a single passage between the cathodes is small the contribution of these electrons to the ionization process is insignificant.

b) The potential distribution of the system as shown in Fig. 9a is idealized and simplified. To simulate the real case of the potential distribution,as shown in Fig. 8, let us assume the potential distribution to be that in Fig. 10a. In this case, due to the symmetry of the field, the electrons on the axis of the anode cylinder will oscillate as described in a). But the electrons at other points, will receive a small accelerating force in the radial direction due to the radial electric field E_r. Now let us investigate the electron motion under this condition with absence of B_z and zero initial velocity at point 'b', and the distances $S_b - S_a = S_c - S_b = S_d - S_c = S_e - S_d = S_f - S_e = D$, where D is the radius of the anode cylinder. From Eq. (15), we get

$$m\frac{dv_z}{dt} = -eE_z \quad \text{and} \quad m\frac{dv_r}{dt} = -eE_r \qquad (16)$$

where the E_z and E_r components of the electric field vary in the 'z' direction as shown in Fig. 10b. Their distribution functions are

$$E_z = \begin{cases} -E_1 & S_b < S_z < S_c \\ -E_2 & S_c < S_z < S_d \\ E_2 & S_d < S_z < S_e \\ E_1 & S_e < S_z < S_f \end{cases}$$

$$-E_r = \begin{cases} p(S_z - S_b) & S_b < S_z < S_c \\ E_{r3} - q(S_z - S_c) & S_c < S_z < S_d \\ E_{r4} + q(S_z - S_d) & S_d < S_z < S_e \\ E_{r3} - p(S_z - S_e) & S_e < S_z < S_f \end{cases}$$

in which $E_1 = V_c/D$, $E_2 = (V_d - V_c)/D$, $E_{r3} = (V_A - V_c)/D$ $= pD$, $E_{r4} = (V_A - V_d)/D = (p - q)D$, and p & q are slopes of E_r distribution in the 'z' direction. Substituting the distribution functions to Eq. (16) and solving it, we find the velocity and the displacement of an electron at any point of the ionization chamber. We separate the resulting equations into four groups, describing an electron starting from plane 'b', and corresponding to the four sections of its path.

1) $S_b < S_z < S_c$

In this region $m\frac{dv_z}{dt} = eE_1$ and $m\frac{dv_r}{dt} = ep(S_z - S_b)$,

we can get the velocity and the displacement both in 'z' and in 'r' directions of an electron with an initial condition, i.e. at $t=0=t_b$, $S_z = S_b$, $v_{zb} = 0$, $S_r = S_{rb}$, and $v_{rb} = 0$, as follows,

$$v_z = \frac{eE_1}{m}(t - t_b)$$

$$S_z = S_b + \frac{eE_1}{2m}(t - t_b)^2$$

$$t - t_b = \left(\frac{2m}{eE_1}(S_z - S_b)\right)^{1/2}$$

or $$v_z = \left(2\frac{eE_1}{m}(S_z - S_b)\right)^{1/2}$$

$$v_r = \frac{e^2pE_1}{6m^2}(t - t_b)^3$$

$$S_r = S_{rb} + \frac{e^2pE_1}{24m^2}(t - t_b)^4$$

2) $S_c < S_z < S_d$

Since $m\frac{dv_z}{dt} = eE_2$ and $m\frac{dv_r}{dt} = e(E_{r3} - q(S_z - S_c))$

then, $$v_z = v_{zc} + \frac{eE_2}{m}(t - t_c)$$

$$S_z = S_c + v_{zc}(t - t_c) + \frac{eE_2}{2m}(t - t_c)^2$$

$$t - t_c = \frac{m}{eE_2}\left(-v_{zc} + \left(v_{zc}^2 + 2\frac{eE_2}{m}(S_z - S_c)\right)^{1/2}\right)$$

or $$v_z = \left(v_{zc}^2 + 2\frac{eE_2}{m}(S_z - S_c)\right)^{1/2}$$

$$v_r = v_{rc} + \frac{eE_{r3}}{m}(t - t_c) - \frac{eqv_{zc}}{2m}(t - t_c)^2 - \frac{e^2qE_2}{6m^2}(t - t_c)^3$$

$$S_r = S_{rc} + v_{rc}(t - t_c) + \frac{eE_{r3}}{2m}(t - t_c)^2 - \frac{eqv_{zc}}{6m}(t - t_c)^3 - \frac{e^2qE_2}{24m^2}(t - t_c)^4$$

3) $S_d < S_z < S_e$

Since $m\frac{dv_z}{dt} = -eE_2$ and $m\frac{dv_r}{dt} = e(E_4 + q(S_z - S_d))$

then $$v_z = v_{zd} - \frac{eE_2}{m}(t - t_d)$$

$$S_z = S_d + v_{zd}(t - t_d) - \frac{eE_2}{2m}(t - t_d)^2$$

$$t - t_d = \frac{m}{eE_2}(v_{zd} - (v_{zd}^2 - 2(\frac{eE_2}{m})(S_z - S_d))^{\frac{1}{2}})$$

or $$v_z = (v_{zd}^2 - 2\frac{eE_2}{m}(S_z - S_d))^{1/2}$$

$$v_r = v_{rd} + \frac{eE_{r4}}{m}(t - t_d) + \frac{eqv_{zd}}{2m}(t - t_d)^2 - \frac{e^2qE_2}{6m^2}(t - t_d)^3$$

$$S_r = S_{rd} + v_{rd}(t - t_d) + \frac{eE_{r4}}{2m}(t - t_d)^2 + \frac{eqv_{zd}}{6m}(t - t_d)^3 - \frac{e^2qE_2}{24m^2}(t - t_d)^4$$

4) $S_e < S_z < S_f$

Since $m\frac{dv_z}{dt} = -eE_1$ and $m\frac{dv_r}{dt} = e(E_{r3} - p(S_z - S_e))$

$$v_z = v_{ze} - \frac{eE_1}{m}(t - t_e)$$

$$S_z = S_e + v_{ze}(t - t_e) - \frac{eE_1}{2m}(t - t_e)^2$$

$$t - t_e = \frac{m}{eE_1}\left(v_{ze} - \left(v_{ze}^2 - 2\frac{eE_1}{m}(S_z - S_e)\right)^{1/2}\right)$$

or $$v_z = \left(v_{ze}^2 - 2\frac{eE_1}{m}(S_z - S_e)\right)^{1/2}$$

$$v_r = v_{re} + \frac{eE_{r3}}{m}(t - t_e) - \frac{epv_{ze}}{2m}(t - t_e)^2 + \frac{e^2pE_1}{6m^2}(t - t_e)^3$$

$$S_r = S_{re} + v_{re}(t - t_e) + \frac{eE_{r3}}{2m}(t - t_e)^2 - \frac{epv_{ze}}{6m}(t - t_e)^3 + \frac{e^2pE_1}{24m^2}(t - t_e)^4$$

From these equations, we canfind the motion of an electron in the system. Let us assume

$E_2 = \frac{1}{2}E_1$, $q = \frac{1}{2}p$, $E_1 = pD = E_{r3}$, $E_2 = E_{r4}$,

$S_c - S_b = S_d - S_c = S_e - S_d = S_f - S_e = D$, and the

electron starting in the plane 'b' at $t = t_b = 0$ in which its position and velocity are

$S_b = 0$, $S_r = S_{rb}$, $v_{zb} = 0$, and $v_{rb} = 0$.

then, in the plane 'c', $v_{zc} = \left(2\frac{eE_1}{m}D\right)^{1/2}$

$$T = t_c - t_b = \left(\frac{2mD}{eE_1}\right)^{1/2}$$

$$v_{rc} = \frac{1}{3}v_{zc}, \qquad S_{rc} - S_{rb} = \frac{1}{6}D.$$

in the plane 'd', $v_{zd} = 1.225\, v_{zc}$, $t_d - t_c = 0.45\, T$

$v_{rd} = 0.676\, v_{zc}$, $S_{rd} - S_{rb} = 0.636\, D$.

in the plane 'e', $v_{ze} = v_{zc}$, $t_e - t_d = 0.45\, T$,

$v_{re} = 1.01 v_{zc}$, $S_{re} - S_{rd} = 1.37\ D$,

in the plane 'f', $v_{zf} = 0$, $t_f - t_e = T$,

$v_{rf} = 1.35\ v_{zc}$, $S_{rf} - S_{rb} = 3.91\ D$

Since the displacement of an electron in the radial direction when travelling from plane 'b' to plane 'f', $S_{rf} - S_{rb}$, is greater than the radius of the anode cylinder 'D', therefore, the electron can not return to the inside of the anode region after it recoils from the top plate. But if we increase the relative value of the axial field E_z with respect to the radial field E_r by a factor of 10, i.e. $E_1 = 10\ E_{r3}$ and $E_2 = 10\ E_{r4}$, then $v_{rf} = 0.135\ v_{zc}$, and

$S_{rf} - S_{rb} = 0.391\ D$. Since $(S_{rf} - S_{rb})$ is less than D,

the electron will oscillate several times between the top plate and the filament before it collides with the anode surface.

Therefore, if $E_1 \gg E_{r3}$, then the drift of the electrons in the radial direction is very small. This ensures that an electron will oscillate between the plates before it strikes the anode surface and becomes removed from the oscillation process(Fig. 11a). In contrast, if $E_1 \leq E_{r3}$, then the electrons not only cannot turn back to the inside of the anode cylinder(Fig. 11b), but also may be captured by the anode even before reaching the top plate(Fig. 11c).

c) An electron which moves in a uniform magnetic field will, in the absence of an electric field, follow a circular path in a plane perpendicular to the lines of the magnetic flux (Fig. 12a). If we apply an electric field E_y in the direction normal to that of the magnetic field, the electron will follow a cycloidal path with a drift velocity $v_D = kE_y/B_z$ perpendicular to both B_z and E_y, as shown in Fig. 12b (see e.g. Alfven, 1963). If the electric field E is in the radial direction of the cylinder, the electron path will be like that in a magnetron(Fig. 12c). Now if we also apply a uniform electric field along the 'z' axis, the electron will drift from the bottom to the top of the ionization chamber (Fig. 12d). It follows from the above description, that the electric field distribution as described in b), with an accompanying axial magnetic field, will result in the

oscillations of electrons between the bottom and the top plates, the individial electron path being similar to that of Fig. 12e. The presence of the magnetic field is therefore not only decreasing the probability of the electron's capture by the anode, but also increasing the length of the path of the electron motion.

As an example of the orders of magnitudes involved in such a motion we may use the data from the description of the ion source of Kistemaker et al. (1950). In this source

$S_b - S_a = 0.3$ cm, $S_c - S_b = 1.1$ cm, $S_d - S_c = 4$ cm,

$S_f - S_e = 3.9$ cm, $D = 1.85$ cm, $V_A = 50$ to 250 volts,

and $p = 10^{-4}$ to 5×10^{-4} mmHg.

To make a detailed calculation let us assume specific values:

$$V_A = 120 \text{ V}, \quad V_c = 110 \text{ V}, \quad V_d = 115 \text{ V}, \quad p = 10^{-4} \text{ mmHg}.$$

then $E_1 = 100$ V/cm, $E_2 = 1.25$ V/cm $= \frac{1}{80} E_1$, $E_{ef} = \frac{11}{39} E_1$,

$E_{r3} = \frac{1}{20} E_1$, and $E_{r4} = \frac{1}{40} E_1$.

If the initial conditions of an electron in the plane normal to the axis at point 'b' are $v_z = 0$, $v_r = 0$, $S_z = S_b$, and $S_r = S_{rb}$ then we can find these constants at any transverse plane along the axis by applying the equations derived in b). The values of the velocities and displacements at planes c, d, e, and f are given as follows,

the plane 'c', $v_{zc} = \left(\frac{2eV_c}{m}\right)^{1/2} = 6.2 \times 10^6$ m/sec.

$$T = t_c - t_b = 3.54 \times 10^{-8} \text{ sec}.$$

$$v_{rc} = \frac{1}{60} v_{zc}, \quad S_{rc} - S_{rb} = \frac{1.1}{120} \text{ cm}.$$

the plane 'd', $v_{zd} = 1.025\, v_{zc}$, $t_d - t_c = 2T$,

$v_{rd} = 0.1\, v_{zc}$, $S_{rd} - S_{rb} = 0.143$ cm.

the plane 'e', $v_{ze} = v_{zc}$, $t_e - t_d = 2T$,

$v_{re} = 0.167\, v_{zc}$, $S_{re} - S_{rb} = 0.44$ cm.

the plane 'f', $v_{zf} = 0$, $t_f - t_e = 3.7\ T$

$v_{rf} = 0.177\, v_{zc}$, $S_{rf} - S_{rb} = 1.331$ cm. $= 0.72\ D$

In this source, the pressure p is assumed as 10^{-4} mmHg which indicates the concentration of gas atoms

$$N = 3 \times 10^{25} \frac{\text{atoms}}{m^3} \times \frac{10^{-4}\ \text{mmHg}}{760\ \text{mmHg}} \simeq 4 \times 10^{18} \frac{\text{atoms}}{m^3}$$

and the electron mean free path, under these conditions, is

about 32 m($\lambda_e = \frac{1}{\pi (\sigma/2)^2 N}$), i.e. about 250 times of the length

of the ionization chamber. Since $S_{rf} - S_{rb} = 0.72\ D$, an electron will reach the anode surface in about one oscillation, and obviously, has no chance to collide with gas atoms. However, as soon as the axial magnetic field appears in the system, the motion of primary electrons becomes different. Assume

$B_z = 1000$ gauses $= 0.01$ weber/m^2, and

$v_{rmax} = 10^7$ m/sec, Here v_{rmax} is always less than v_{zmax}

then the cyclotron radius can be estimated from Eq. (9)

$$r_{cmax} = \frac{m v_{rmax}}{e B_z} = 0.58 \text{ cm}$$

Since the maximum cyclotron radius is smaller than the radius of the anode cylinder, the primary electrons will, therefore, oscillate between both plates until they collide with the gas atoms and diffuse to the anode.

The electron with the zero initial energy will acquire a kinetic energy from the E_z field, equal to the potential at its position in the system. The magnitude of the field is adjusted so that this energy is high enough to produce ionization. Secondary electrons, produced in the process of ionization, are liberated with appreciable energies, ions with practically none(Bohm, 1949). Because of their small mass and high energy, electrons rapidly leave the region in which they are liberated and approach the top and the bottom plates. If they stop before reaching both plates they will oscillate like primary electrons. Otherwise, they are captured by the plates. The heavy ions, first, diffuse to both plates due to the concentration gradient, then they are accelerated to both plates by the potential across the plasma sheath near the plates. Their impact on the plates produces a large number of the secondary electrons, which contribute greatly to the ionization process. Now both plates are charged negatively with respect to the plasma due to the accumulation of the negative electrons near them. Thus those plasma electrons which do not have enough energy to reach either of the plates are repelled, and subsequently oscillate between the top and the bottom plates until collected by the anode, or until they get enough energy to reach one of the plates(ground). The collisions of these plasma electrons result in a shuffling of their energies which will ultimately dissipate in the process of excitation and ionization. Thus an appreciable fraction of all ionization is caused by plasma electrons, which obtain their energy from the secondaries.

During the operation of the ion source, the product ions are continuously extracted from the discharge chamber, this process results in a pressure gradient having its minimum at the extraction hole. The charge material in the form of gas or vapour is introduced into the ionization chamber at the same time. Since the neutral gas molecules always diffuse down the pressure gradient, therefore the gas diffuses towards the ionization column from the gas inlet. If electron current density in the ionization column is high (e.g. 1 Amp. /cm^2) the neutral molecules will be converted into ions once they

enter the ionization column. This kind of ionization is called neutral ionization (Bohm, 1949). And it contributes a large fraction of all ionizations in this ion source.

C. Duoplasmatron Ion Source:

Duoplasmatron ion source, with its characteristics high ionization efficiency and high current density, was developed in 1956 by M. von Ardenne. As in the magnetic ion source, ionization is achieved by electron bombardment and the ion beam is extracted from the plasma. This ion source can produce ion current densities of more than 100 a/cm^2 as compared to about 1 a/cm^2 for the magnetic ion source. Figure 13 illustrates the basic configuration of this source. A low pressure arc is produced between cathode 'K' and anode 'A'. An intermediate electrode 'I', conical in shape, serves to constrict the discharge and increase the plasma density, it is also used as a magnetic core. The addition of a high intensity magnetic field between the intermediate electrode and the anode, acts as a further constraint of the discharge. These mechanical and magnetic constraints produce a very dense plasma in the vicinity of the extraction aperture. Plasma penetration through the anode button permits a large area of plasma boundary to emit a high current density ion beam on the application of a suitable negative potential to the extractor (cf. Fig. 14).

The complicated geometry of the duoplasmatron makes exact analysis of its operation virtually impossible. However, the basic mechanisms which determine its characteristics can be discussed qualitatively.

The arc inside the source has the characteristic of a low pressure discharge where the electron mean free path is of the same order as that of the discharge length. The free low pressure discharge, i.e. a discharge without physical or magnetic constraints, consists of three regions as shown in Fig. 15 (Cobine, 1958). A strong positive space charge region near the cathode supports a considerable voltage drop, called the 'cathode drop' region, approximately equal to the first ionization potential of the gas. Following this there is a 'positive column' extending to for a short distance from the anode. It is characterized by a small potential

gradient and a neutral plasma. At the other end of the discharge, near the anode, there is a domain of strong negative charge, called the 'anode drop' region. An electron emitted from the cathode acquires enough energy in the cathode drop region to ionize the neutral atoms in the positive column.

The electron-ion pairs produced by the electron-atom collisions are separated by the electric field in the positive column. The ions drift to the cathode and the corresponding electrons to the anode. The highly mobile electrons are able to to draw more energy from the field than the heavy ions, and thus reach higher temperatures. Since momentum exchange between electrons and ions is small, the two groups of particles do not reach thermal equilibrium (Burton, , 1961). Owing to the high mobility of electrons compared with that of the positive ions the arc current is due almost entirely to electrons.

In the actual operation the low pressure discharge in this source is not free. The mechanical and magnetic constraints due to the intermediate electrode force the electrons to the central part of the discharge. This causes electron-ion collisions that tend to rise the ion temperature closer to that of the electrons.

Because of the high temperature difference between plasma and the wall of the intermediate electrode, it is easy to attract positive ions from the plasma to the build-up of negative electrons near the wall. It was found that a stable ion sheath can be formed only when the positive ions reach the edge of the sheath with kinetic energy, KE_1, equal to at least one-half of the thermal energy of electrons (Bohm, 1949)

$$KE_1 = \frac{1}{2} m_i v_i^2 \geq \frac{kT_e}{2}$$

where m_i and v_i are the mass and the velocity of the positive ion, k is Boltzman's constant, and T_e is the electron temperature. The ion current density J_i at the sheath is

$$J_i = n_i q_i v_i \geq n_i q_i \left(\frac{kT_e}{m_i}\right)^{1/2}$$

where n_i and q_i are the density (No. of ions per cubic meter) and the charge of the positive ions respectively. The thickness of the sheath is approximately equal to the Debye length, L_D, given by

$$L_D = 6.9 \left(\frac{T_e}{n_e}\right)^{1/2}$$

where n_e is the electron density. The Debye length indicates the scale of the system, i.e. the order of the magnitude of the distance over which one may expect microscopic variation in plasma properties. The 'graininess' can be disregarded, and the plasma assumed to be homogeneous when observing regions large compared with L_D.

An important function of the sheath is that it protects the plasma from the wall, or the electrodes. This is due to the fact that the sheath sustains the potential difference between the plasma and the physical surface. Thus, the presence of the physical surface may shift the plasma boundary but cannot affect the plasma beyond the sheath.

With the presence of a constant and uniform strong magnetic field B, i.e. $\omega_c \tau > 1$ (Burton, 1961), the plasma will be confined by a magnetic pressure (Spitzer, 1951)

$$p = -\frac{1}{8\pi} B^2$$

This magnetic confinement will greatly reduce the diffusion losses of ions and electrons from the plasma to the physical surface. In spite of this reduction, there are still losses of plasma which diffuses across the magnetic field. These losses can be characterized by a diffusion coefficient

$$D \simeq \frac{D_o}{1 + (\omega_c \tau)^2}$$

where D_o is the ordinary diffusion coefficient without B field, ω_c is the cyclotron frequency, and τ is the mean free time of particles in the plasma.

The intermediate electrode 'I' in the ion source makes the discharge a subject to a mechanical constraint. For a given current, the narrow channel at the outlet of the 'I' electrode constricts the plasma, thus producing a greater current density inside the channel than either at its entrance, or its outlet. This increased current density can be supported either by an increase in charge density or an increase in their velocity. In either case there must be certain potential and pressure gradients existing across the 'I' electrode to accelerate particles through its channel, and to give electrons enough energy to produce new ions on the anode side. In addition to the mechanical constraint the transverse magnetic field between anode and intermediate electrode (Fig. 16), forces the charged particles to the central part of the plasma. These two factors greatly increase the plasma density.

The differences in the plasma density caused by the magnetic and the mechanical constraints can trap and reflect electrons on the anode side (Fig. 17). this can greatly increase the electron density, and increase the frequency of electron-ion collisions. This tends to make the ion temperature approach the electron temperature. A hot dense plasma cloud thus can be formed on the anode side. This cloud prevents any neutral particles from escaping from the source before they become ionized. These further increase the ionization efficiency to the extent that the plasma appears as a 'fire ball'.

If the intermediate electrode channel is not too short, a true (neutral) plasma may exist within it. The tendency of recombination in the channel is greater the greater is the channel length in relation to the mean free path of electrons. This should be taken into account in choosing the channel length to secure a high current density.

To be able to use the ions in the plasma, they have to be 'extracted' from it, and arranged in the form of a beam. The problems of 'extraction' and of focussing will be considered in future reports.

References:

1. Alfen, H.; and Falthamar, C. G.
'Cosmical Electrodynamics, Fundamental Principles',
London, Oxford University Press, 1963.

2. Almen, O.; and Nielsen, K. O.
'Systematic Investigation of Magnetic Ion Source for
an Electromagnetic Isotope Separator',
Nuclear Instruments, Vol. 1, pp. 302-322, Dec., 1957.

3. Ardenne, M. von
'Tabellen der Elektronen-physik, Ionenphysik and Ubermikrosk',
VER Deutscher Verlag der Wissenschaften, Berlin, 1956.

4. Bennett, G. W.; and Turner, C. M.
'A Penning Discharge Ion Source for High Brightness',
IEEE Transactions on Nuclear Science, Vol. NS. 14,
No. 3, June, 1967.

5. Bohm, D.
'The Characteristics of Electric Discharges in Magnetic Fields',
McGraw-Hill Book Company, INC., 1949.

6. Brewer, G. R.; Currie, M. R.; and Knechtli, R. C.
'Ionic and Plasma Propulsion for Space Vehicles',
Proc. I. R. E., Vol. 49, pp. 1789-1821, Dec., 1961.

7. Burton, B. S.
'Electrostic Propulsion', Edited by D. B. Langmuir, E. Stuhlinger,
and J. M. Sellen., Academic Press INC., New York, 1961.

8. Cambel
'Plasmaphysics and Magnetofluidmechanics',
McGraw-Hill Book Company, INC., 1963.

9. Chopra, K. L.; and Randlet, M. R.
'Duoplasmatron Ion Beam Source for Vacuum Sputtering of
Thin Films',
The Rev. of Sci. Ins., Vol. 38, No. 8, Aug. 1967.

10. Cobine, J. D.
'Gaseous Conductors',
McGraw-Hill Book Company, INC., 1958.

11. Eubank, H. P.; Peck, R. P.; and Truell, R.
'Operating Characteristics of a High Yield R. F. Ion Source',
Rev. of Sci. Ins., Vol. 25, pp. 989-995, Oct., 1954.

12. Field, F. H.; Franklin, J. L.
'Electron Impact Phenomena and the Properties of Gaseous Ions',
Academic Press INC., New York, 1957.

13. Hall, R. N.
'High Frequency Proton Source',
Rev. of Sci. Ins., Vol. 19, No. 12, pp. 905-910, Dec. 1948.

14. Jirafe, W. J.
'A Duoplasmatron Ion Source for Ion Beam Deposition',
Technical Report No. 66-15, Elec. Eng. Dept.,
Univ. of Ottawa, Dec., 1966.

15. Kistemaker, J.; and Dekker, H. L. D.
'Investigation of a Magnetic Ion Source I',
Physica, Vol. 16, pp. 196-208, Mar., 1950.

16. Loeb, L. B.
'The Kinetic Theory of Gasses',
Dover Publications, INC., New York, 1961.

17. McCaldin, J. O.
'Ion Beams and Solid State Physics',
Nuclear Instruments and Methods, Vol. 38, pp. 153-164, 1965.

18. Moak, C. D.; Reese, H.; and Good, W. M.
'Design and Operation of a Radio-Frequency Ion Source for Particle Accelerators',
Nucleonics, Vol. 9, pp. 18-23, Sept., 1951.

19. Mohamed, E. A.; and Ahmed, M. G.
'Characteristics of a High Current P. I. G. Ion Source',
IEEE Transactions on Nuclear Science, Vol. NS. 14, No. 3,
June, 1967.

20. Narinsek, B.; Pozar, F.; and Marinkoric, V.
'An Ion Bombardment Apparatus with a High-Frequency Ion Source',
Journal of Scientific Instrument, Vol. 40, pp. 201-202, 1963

21. Nelson, R. S.
'Ion Implantation',
Science Journal, Vol. 3, No. 2, Feb. 1967.

22. Nielsen, K. O.
'The Development of Magnetic Ion Source for an Electromagnetic I Isotope Separator',
Nuclear Instruments, Vol. 1, pp. 289-301, Dec., 1957.

23. Spitzer, L. Jr.
'Physics of Fully Ionized Gases',
Interscience Publishers, INC., New York, 1956.

24. Thomson, J. J.; and Thomson, G. P.
'Conduction of Electricity Through Gases',
London, Cambridge University Press, 1933.

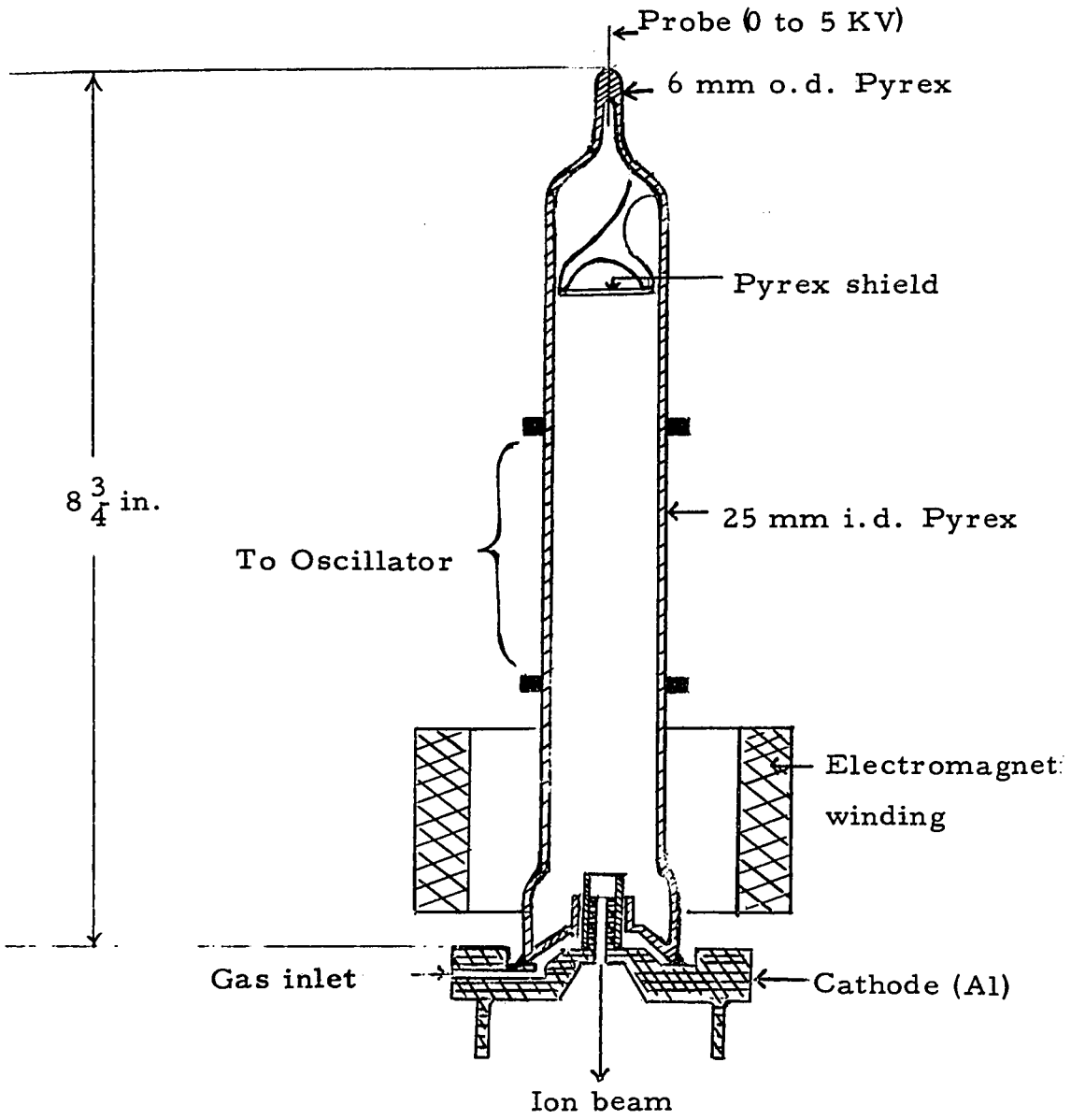

FIG. 1. Cross section of RF ion source (Moak et al., 1951).

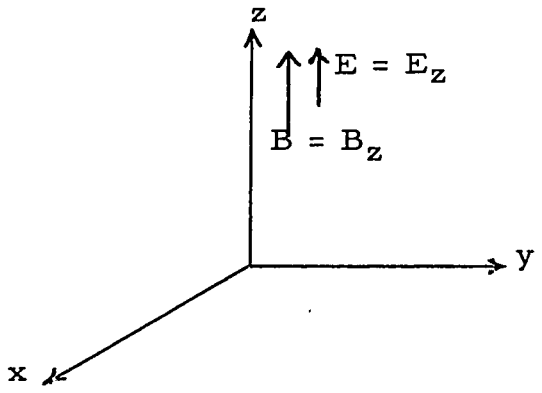

FIG. 2. The electric and the magnetic fields present in the 'z' direction.

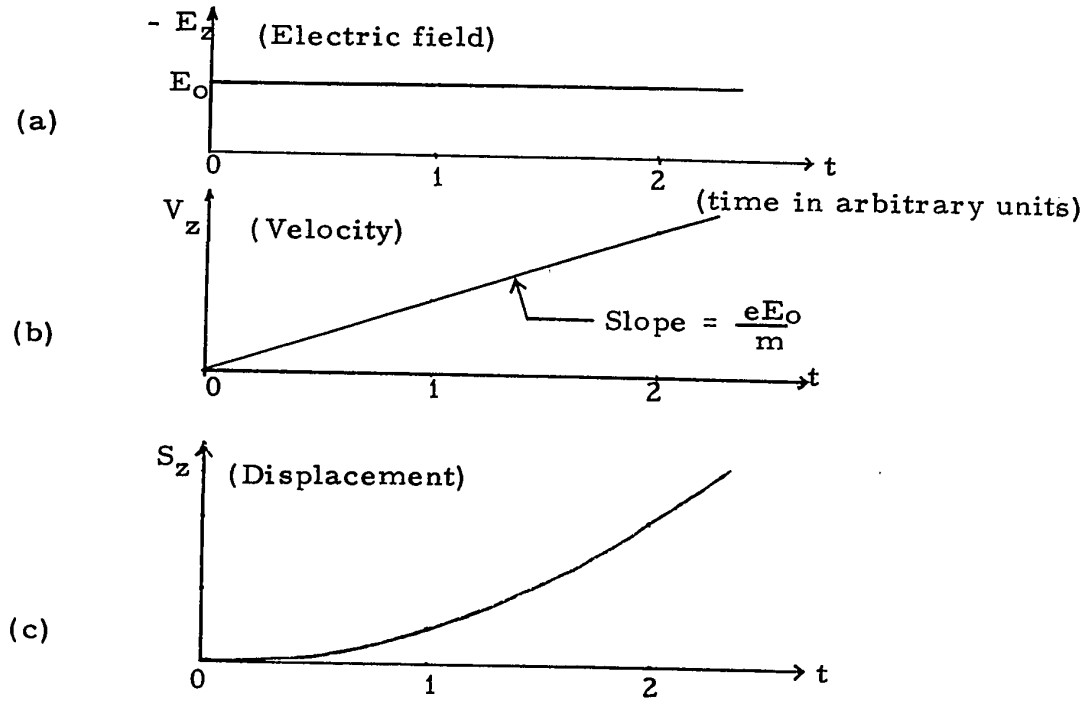

FIG. 3. The motion of an electron in a constant electric field, $E_z = - E_o$. The initial velocity and displacement are zero.

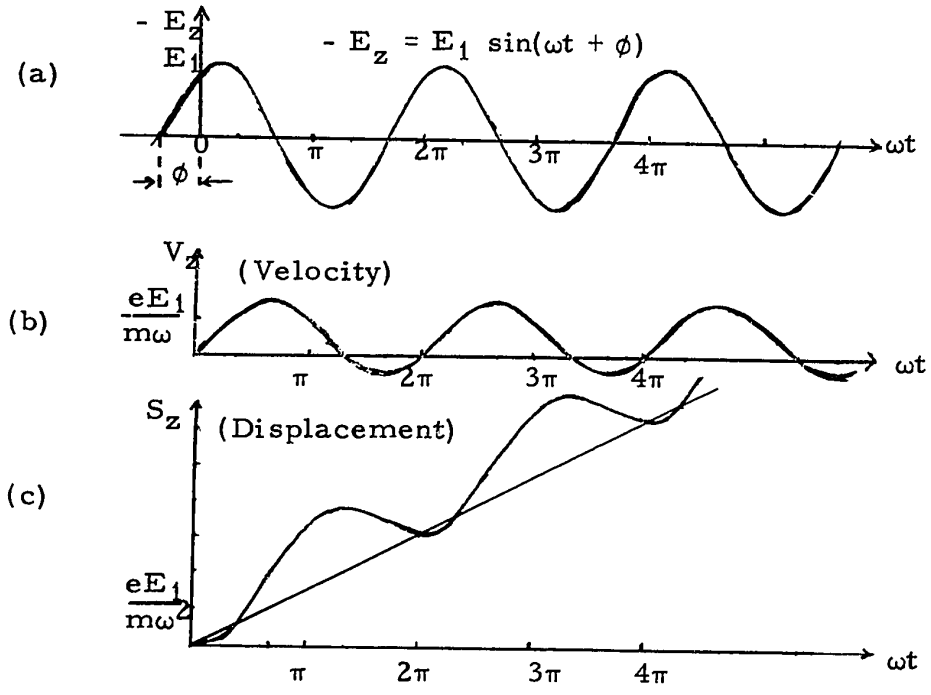

FIG. 4. The motion of an electron starting in a sinusoidal electric field. The initial velocity and displacement are zero and $\phi = 60°$.

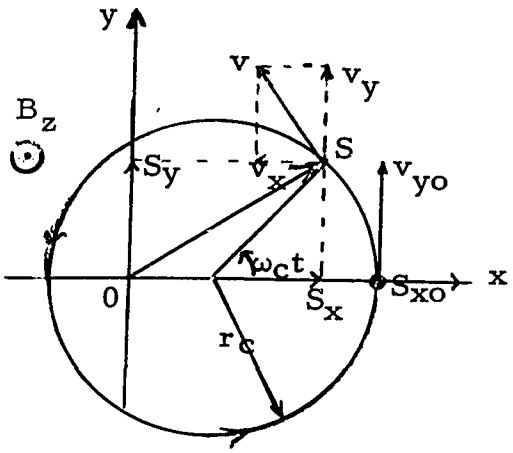

FIG. 5. The circular path of an electron with an initial position $S = S_{xo}$, and velocity $v = v_{yo}$, at $t = 0$, moving in a region of a constant and uniform magnetic field B_z.

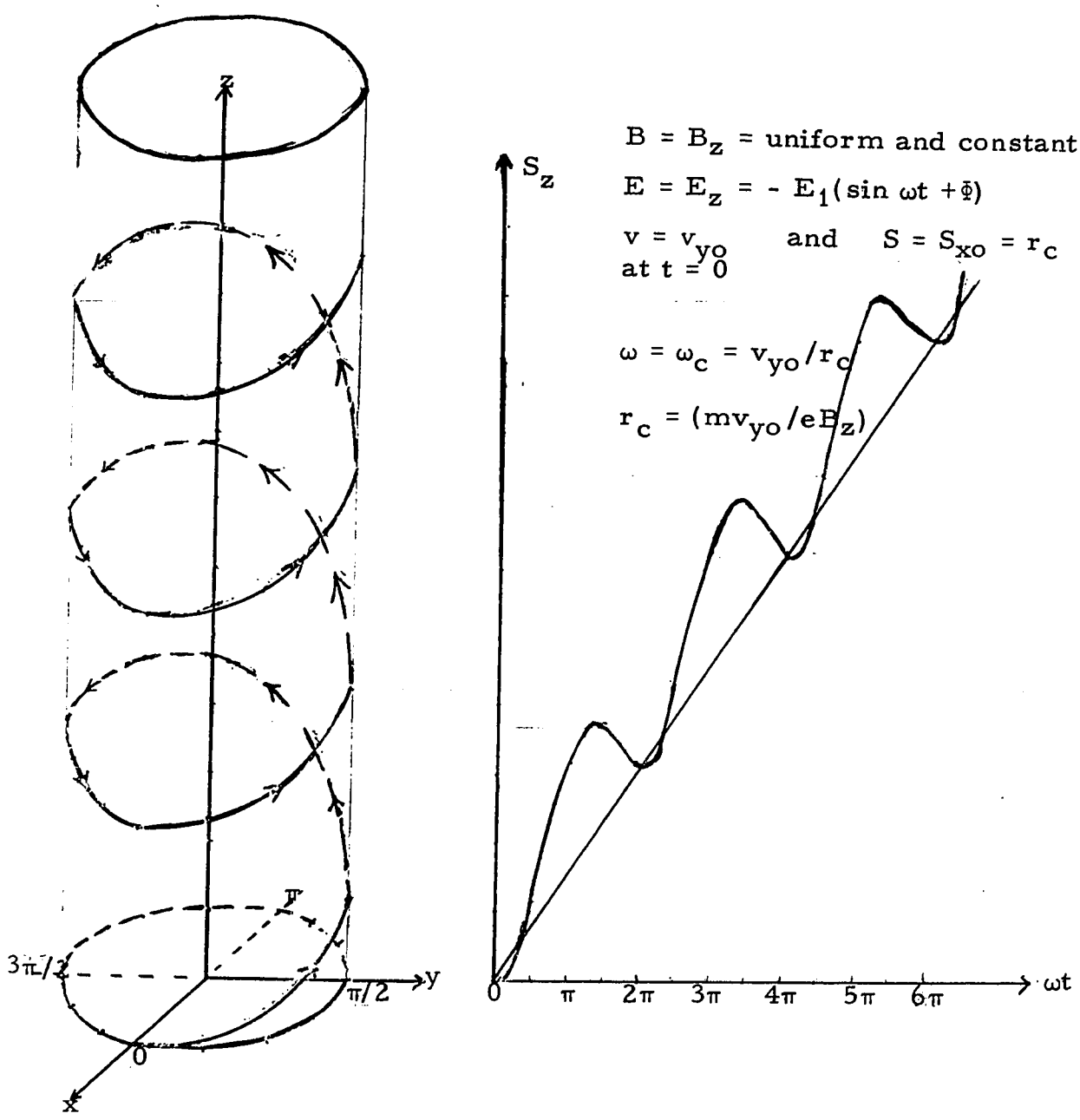

FIG. 6. The path of an electron motion under the conditions specified as described in the figure.

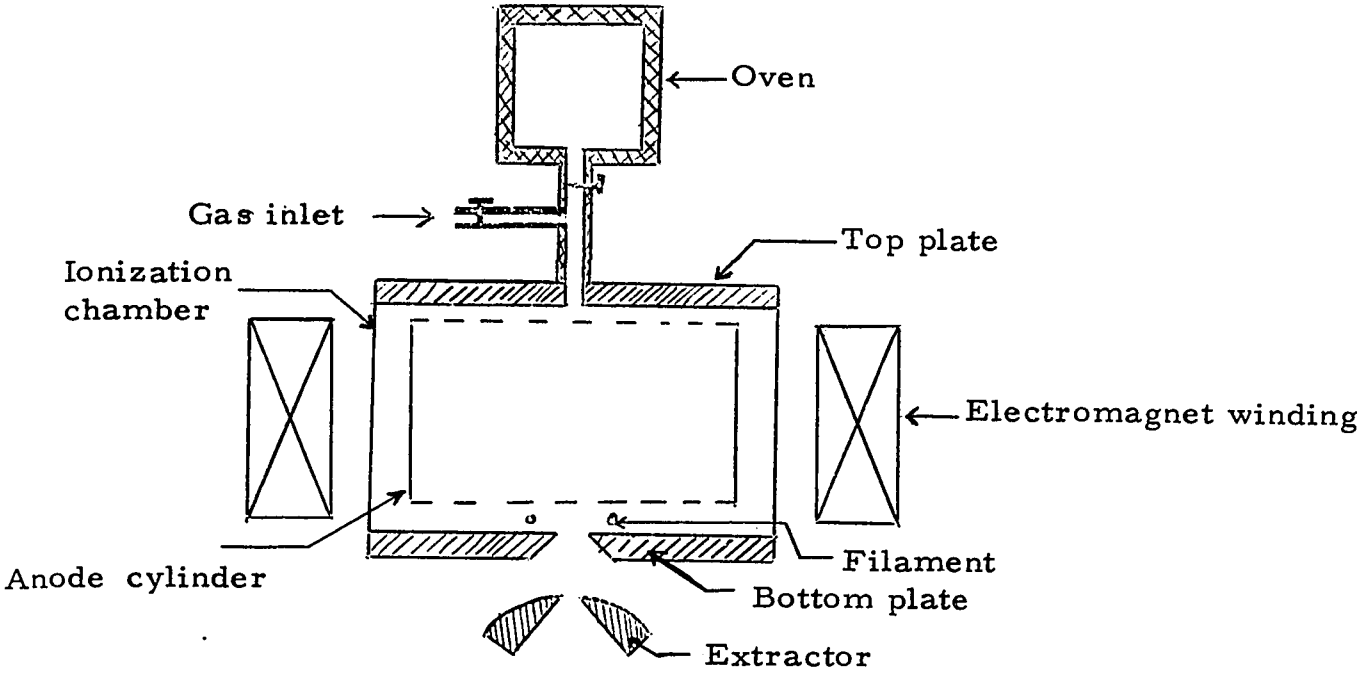

FIG. 7. Magnetic ion source (when used without oven), also called an Oven-ionizer ion source(when used with the oven).

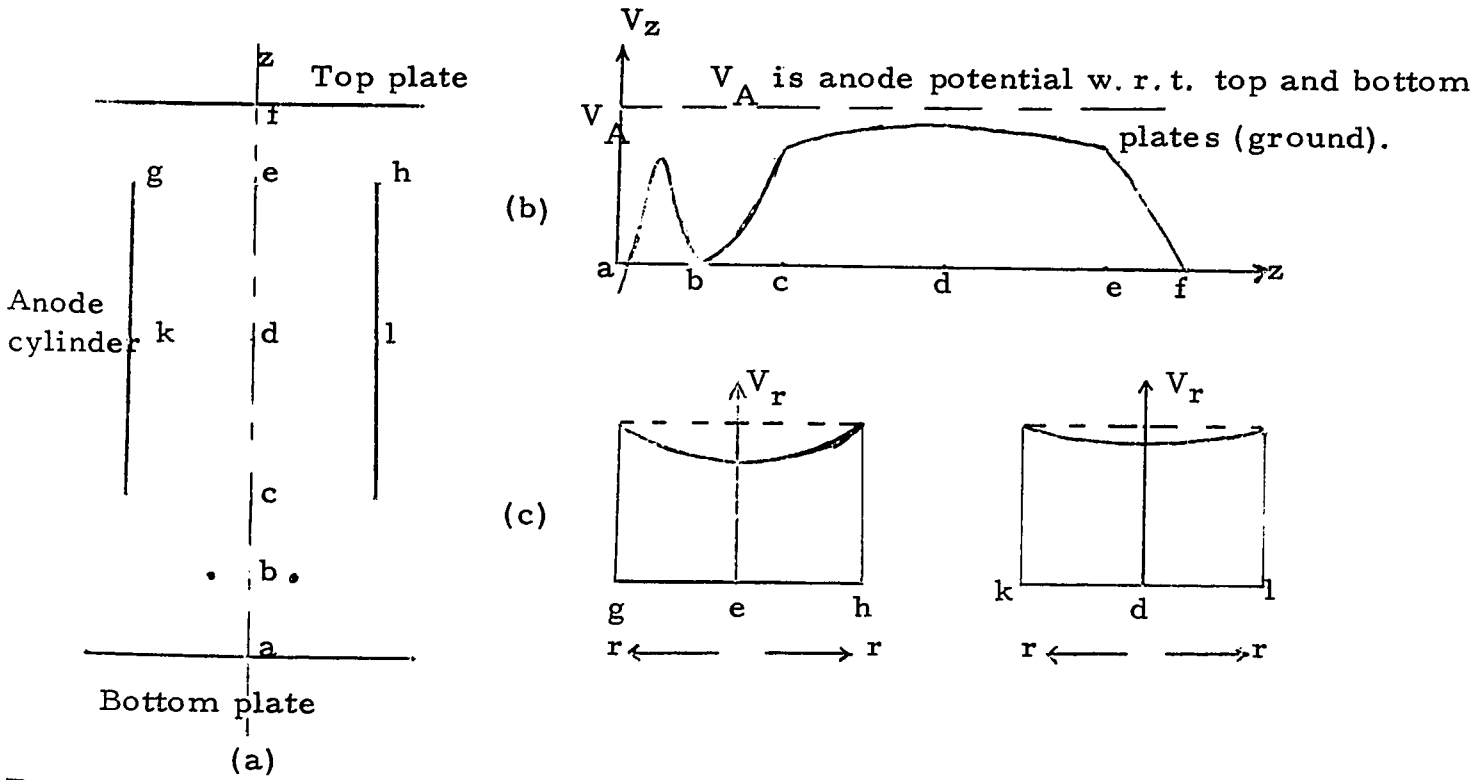

FIG. 8. (a) The ionization chamber of the magnetic ion source.
(b) Axial potential distribution in the chamber.
(c) Radial potential distribution in the chamber.

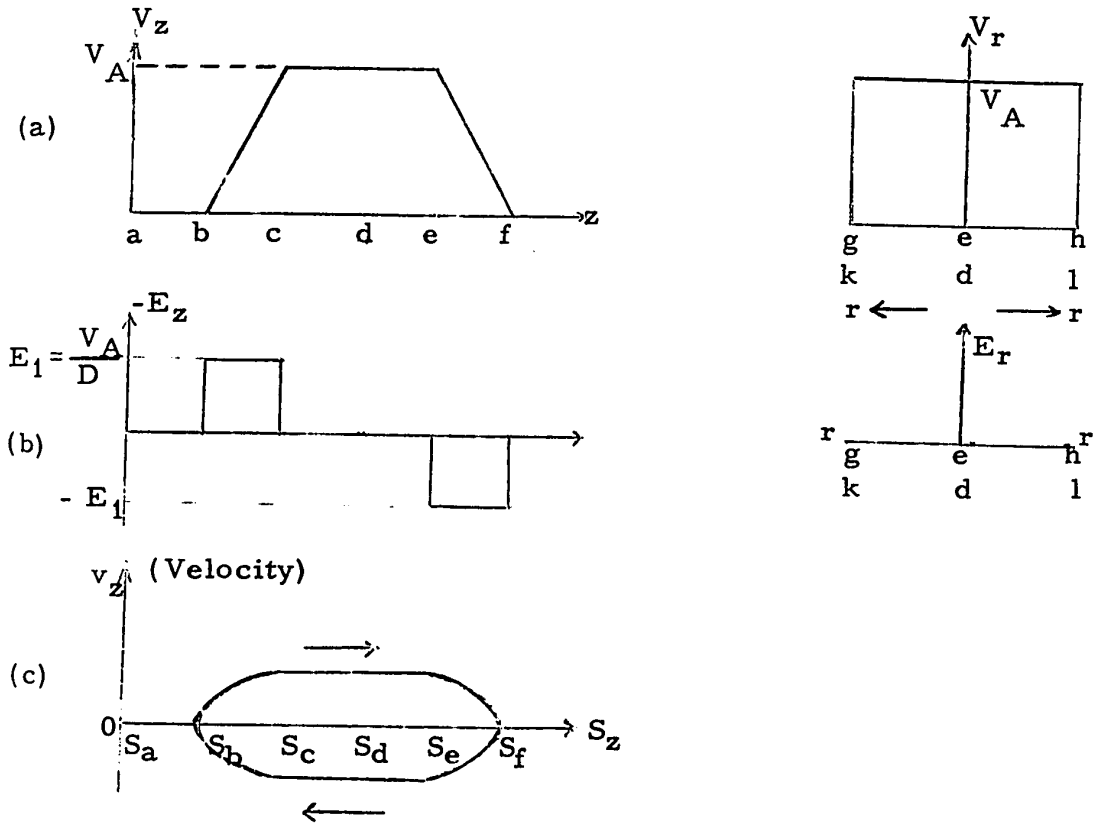

FIG. 9. An idealized potential distribution in a magnetic ion source (without B).
(a) Axial (V_z) and radial (V_r) potential distributions.
(b) Field E_z and E_r corresponding to V_z and V_r.
(c) The velocity of an electron as a function of displacement S_z.

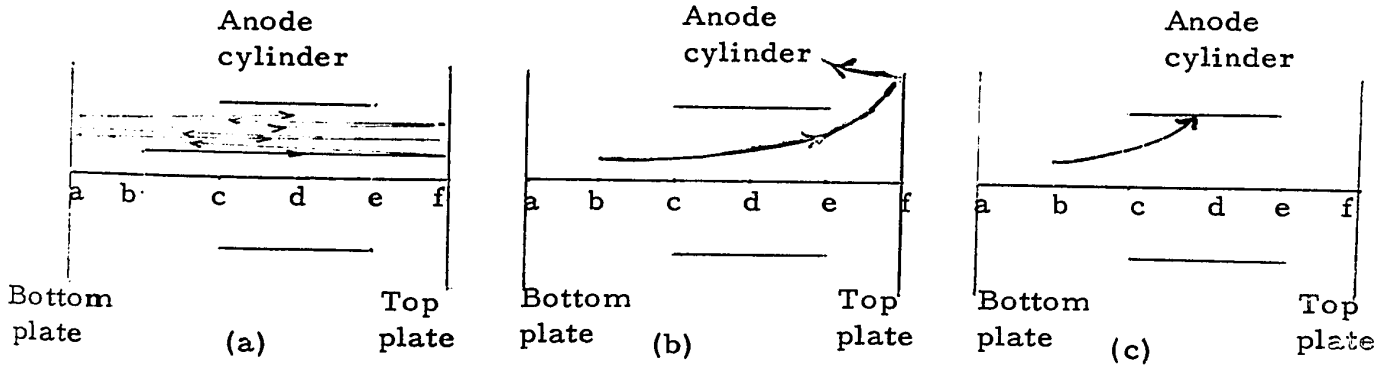

FIG. 11. Paths of electrons moving in the electric field of Fig. 10 (b).
(a) $E_1 >> E_{r3}$, electrons oscillate several times before reaching anode.
(b) $E_1 \leq E_{r3}$, electrons cannot turn back to the inside of the anode cylinder.
(c) $E_1 \leq E_{r3}$, electrons catured by the anode before reaching the top plate.

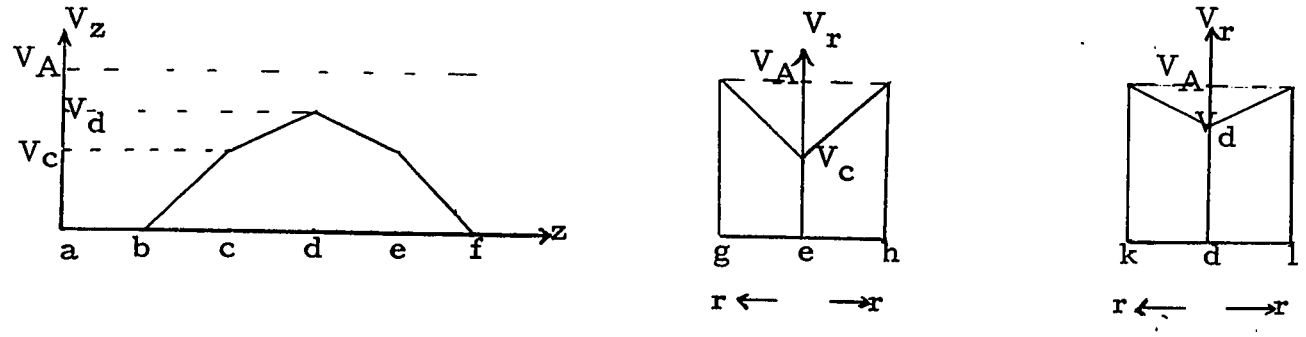

(a) Potential distribution.

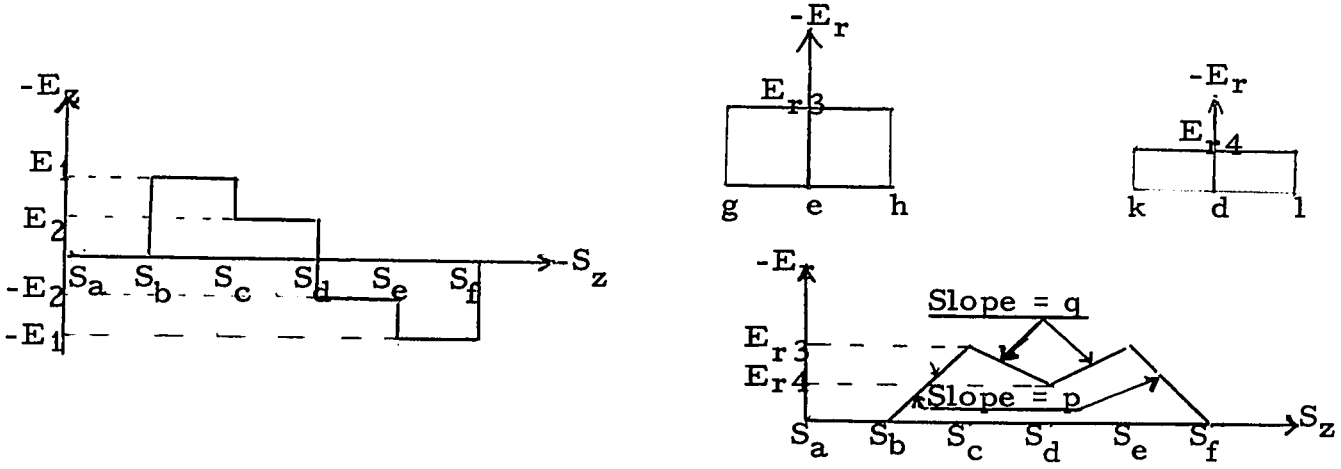

(b) Electric field distribution.

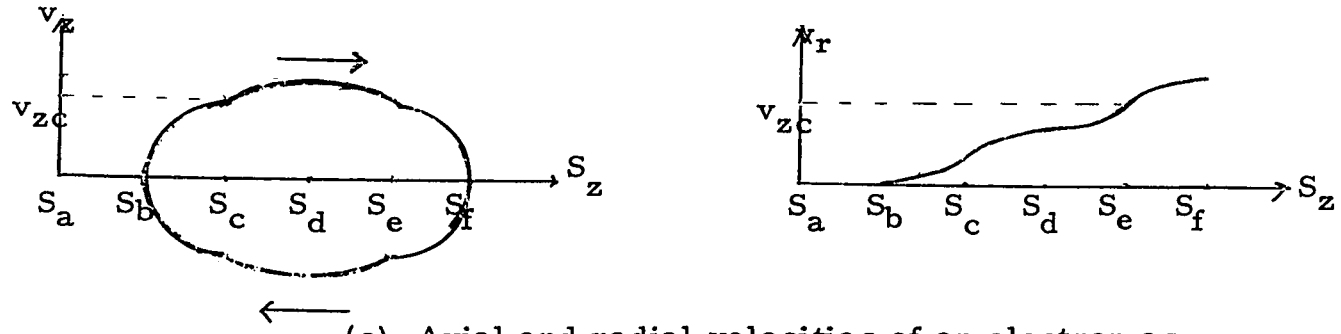

(c) Axial and radial velocities of an electron as a function of its position along the axis

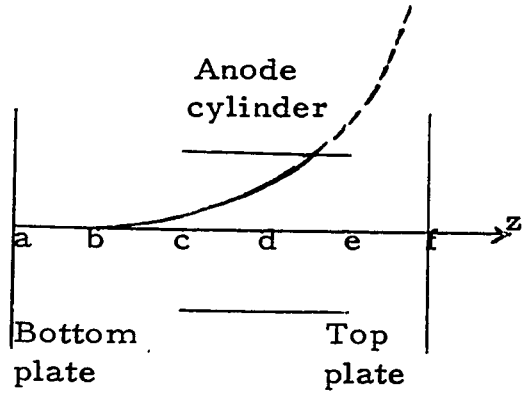

(d) Path of an electron drift away from the axis.

FIG. 10. A simplification of a real distribution of potential in a magnetic ion source (without magnetic field).

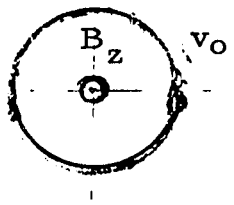

(a) Gyration in an upward uniform B_z without electric field.

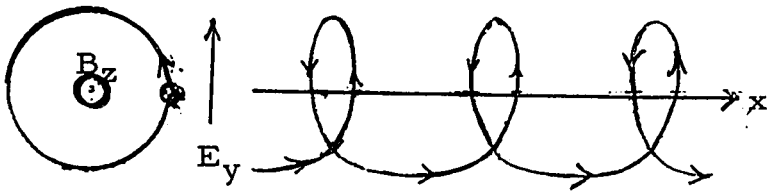

(b) Drift along 'x' axis produced by an electric field E_y.

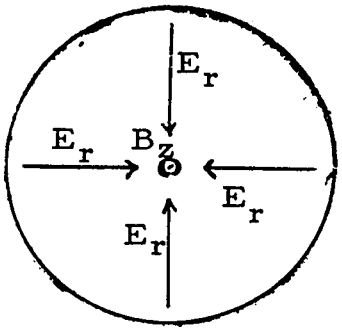

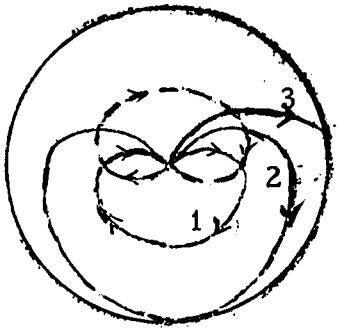

(c) Paths of electron motion in a region with an radial electric field E_r and an uniform upward magnetic field B_z.

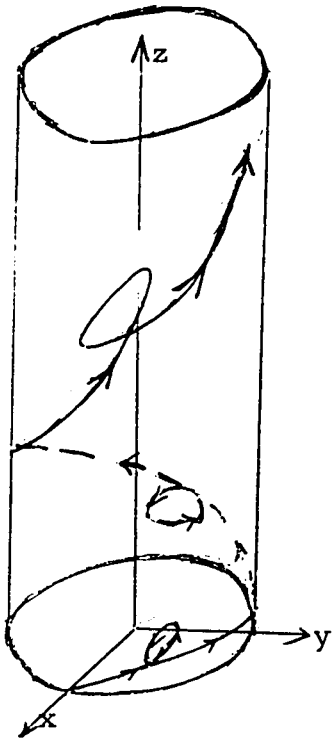

(d) Path of an electron moving in constant B_z, E_z, and E_r fields.

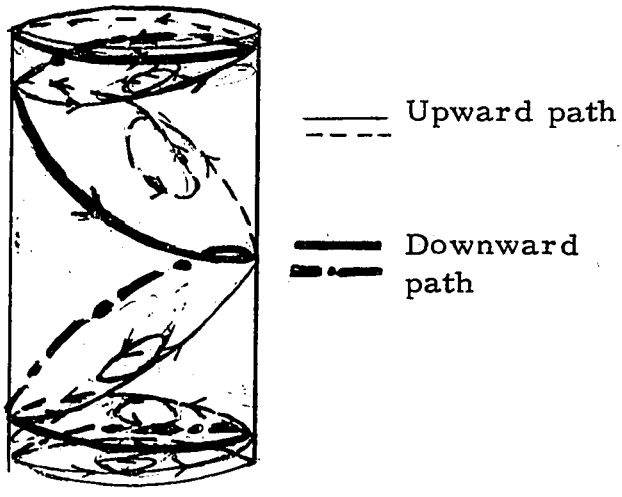

(e) The oscillatory motion of an electron in uniform B_z and E corresponding to V in Fig. 8.

FIG. 12. Paths of electron motion in specified electric and magnetic field.

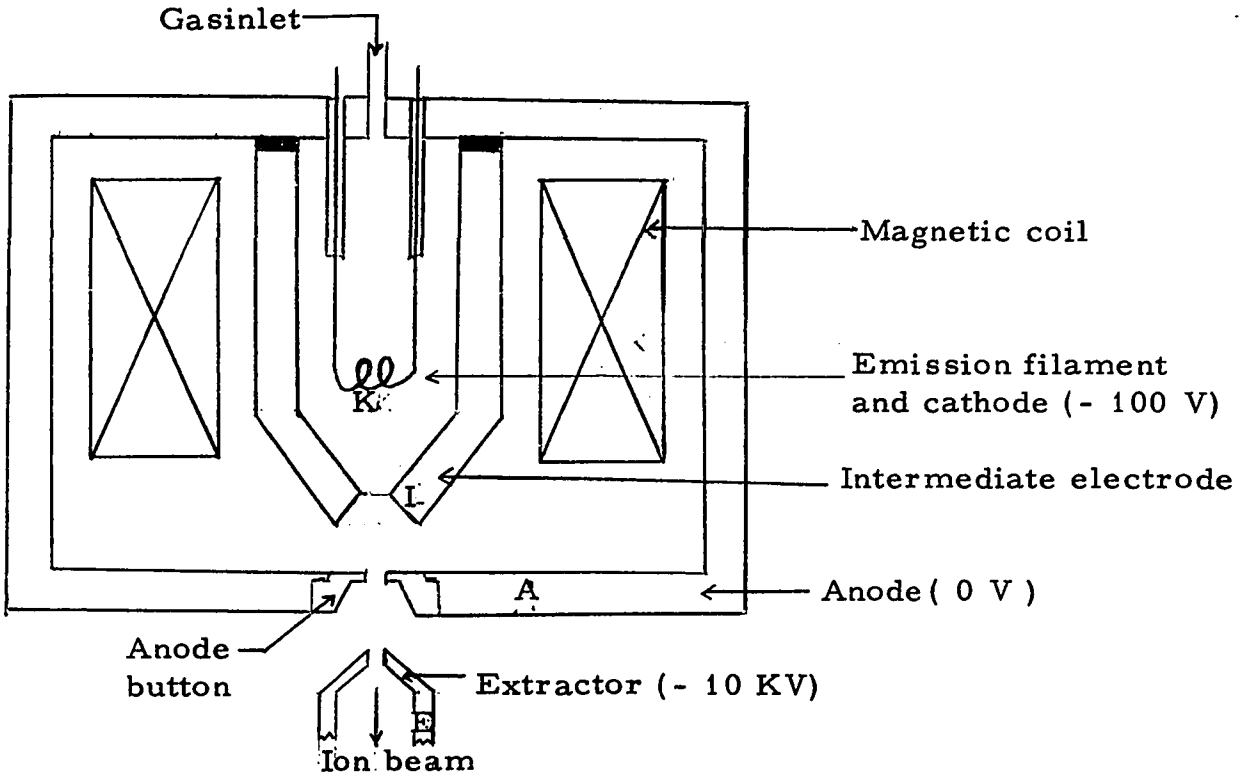

FIG. 13. The basic configuration of a duoplasmatron ion source.

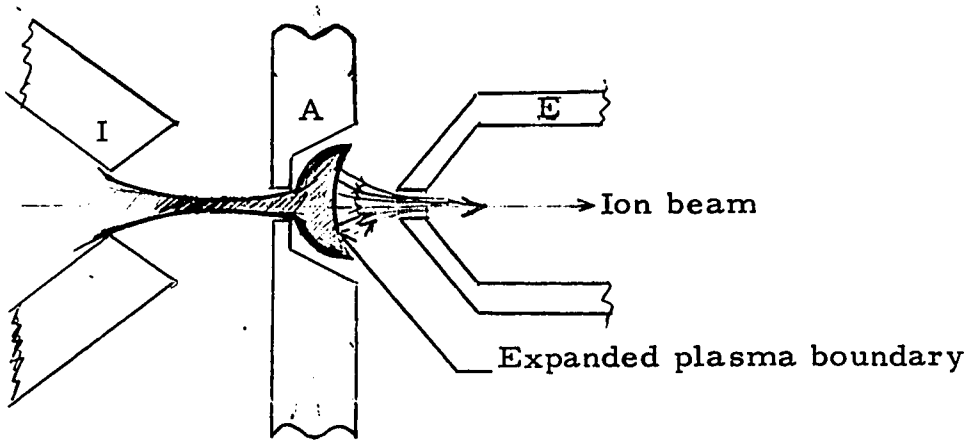

FIG. 14. Ion-beam extraction from the expanded plasma boundary.

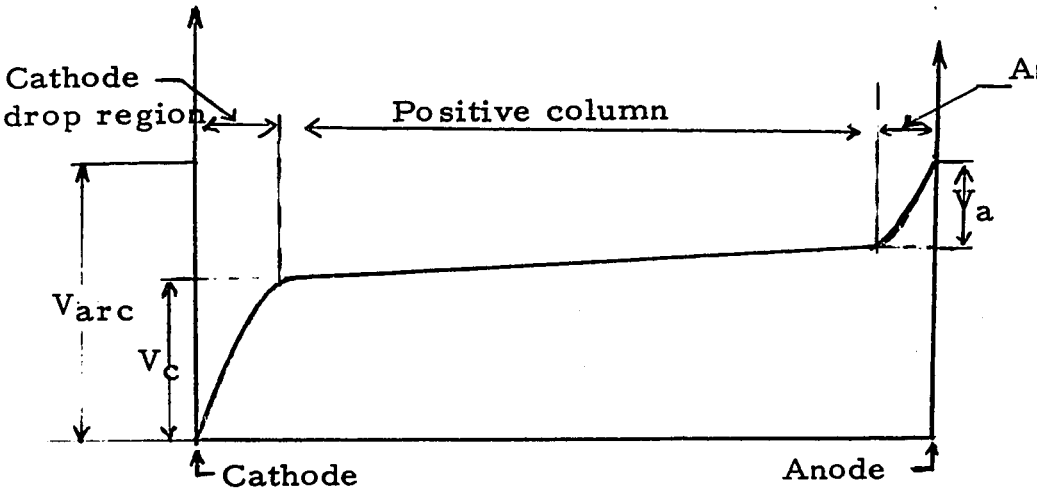

FIG. 15. Potential distribution in an arc.

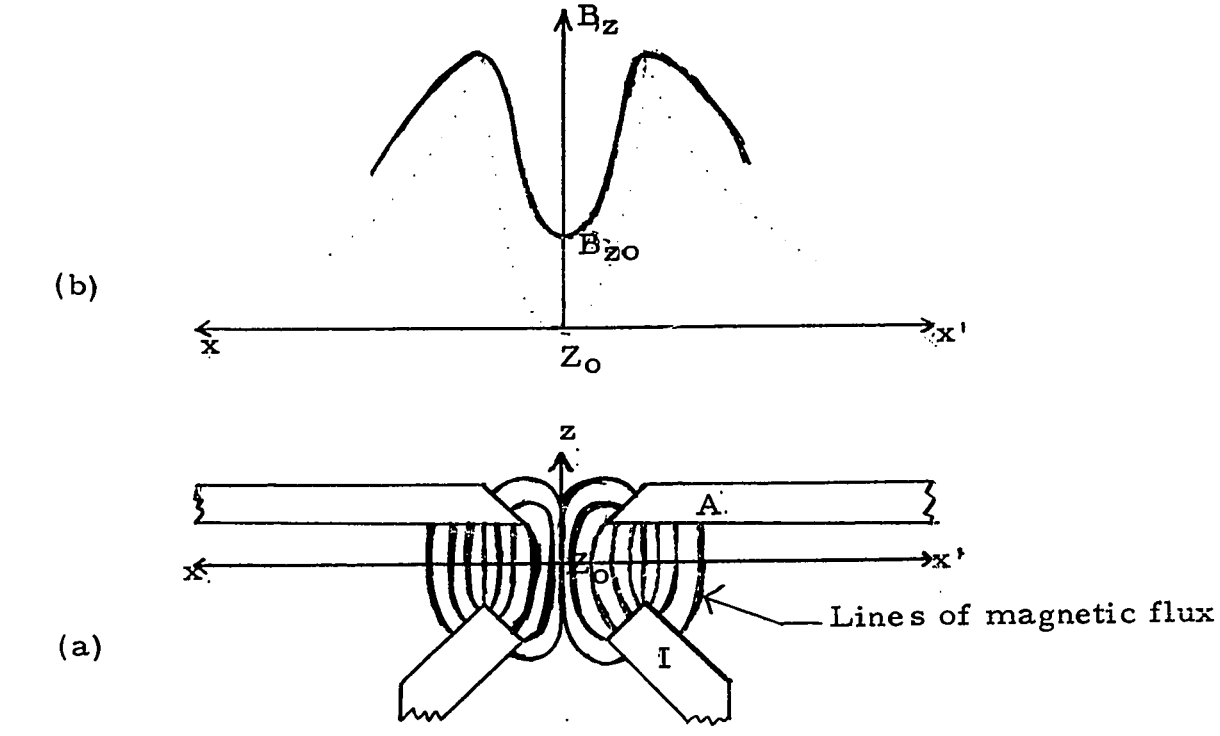

FIG. 16. Distribution of magnetic flux and the relative magnetic field strength.
(a) Lines of magnetic flux.
(b) Relative magnetic field strength at a level Z_o and cros-section xx'.

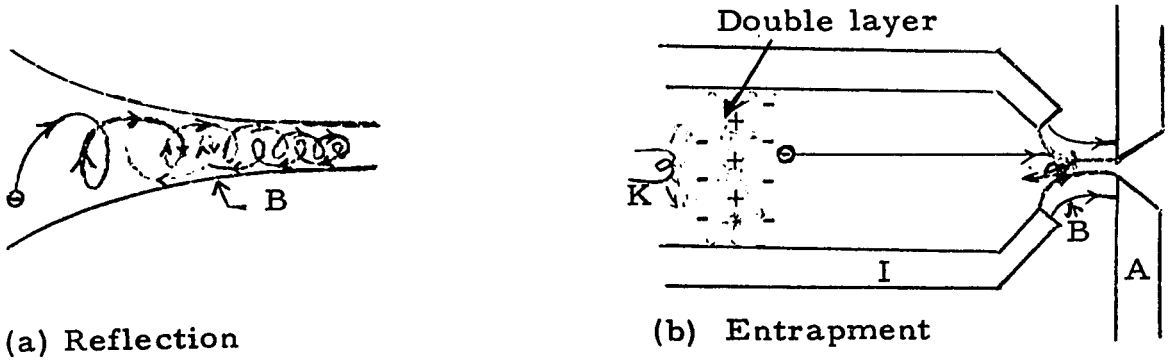

(a) Reflection

(b) Entrapment

FIG. 17. Electron reflection and entrapment in the duoplasmatron ion source.
(a) Electron reflection due to magnetic bottle effect.
(b) Electron entrapment due to double layer near the cathode and magnetic bottle effect near the anode.

INVESTIGATION OF THE EXISTING ION SOURCE AND MODIFICATION PROPOSALS

The existing ion-beam source (Fig. 18) designed and built by W. J. Jirafe (Jirafe, 1966) was expected to have an efficiency of better than 90 % and an ion current in the order of milliamperes. It actually produced an ion current of less than one microampere during its initial tests. Because of the smallness of the current, its efficiency could not be measured. To find the reasons for this and to propose ways in which to increase this current, it was decided to make thorough investigation of the operation of the original ion-source and to repeat the measurements made by the previous author.

As mentioned on p. 25 in the review of the principles of operation of ion sources, the ionization process in the existing ion source can be roughly divided into two stages:

1. In the first stage, the charge material is vaporized and its vapor is ionized in the evaporation chamber in a way similar to that of a low pressure Penning discharge.
2. In the second stage, by constraining the semi-ionized plasma by mechanical and magnetic means in the narrow channel of the chamber, further ionization is enhanced through collisions with gyrating electrons.

In this process we need a heating system to evaporate the solid charge material, a magnetic field system to produce a sufficient magnetic field to constrain the path of electrons, and a cooling system to maintain safe low temperatures in the magnetic core. In what follows, each of these systems is investigated in some detail.

Heating System:

The majority of elements used in the ion-beam techniques of making microcircuits are solids at room temperatures. To ionize their atoms, the solid charge material contained in a crucible has to be vaporized in an evaporation chamber, i.e. heated up to a temperature corresponding to the required pressure (Honig, 1962). This temperature should then be maintained constant during the period of operation.

The evaporation chamber, made of molybdenum (melting point 2617 °C), is heated primarily by a 15 turn 0.2 in. i.d. filament made of 40 mil (AWG 18) tungsten wire (See Appendix B), capable of dissipating 500 watts of power, and designed to raise the chamber temperature to 1500°C (Jirafe, 1966). In addition to this, a considerable amount of heat is produced in the system by the emission filament which has 15 turns of a 20 mil (AWG 24) tungsten wire and dissipates 150 watts. The power for these two filaments is supplied from two low voltage transformers, one capable of supplying 80 A at 15 V, the other 15 A at 11 V. During the operation, a vacuum estimated at about 10^{-3} torr is maintained inside the chamber.

The electric power is supplied to the heating and the emission filaments by an 8 pin high vacuum feedthrough (Ultek, Model 80-323). Since the current rating of the feedthrough is 5 A per pin, therefore, to reduce overloading, two pins of the feedthrough were used in parallel for each current path of the heating filament, which would, normally, allow the use of a current of 10 A. Unfortunately, a higher current (up to 30 A) had to be used, which resulted in overheating of the pins of the feedthrough and consequently in its damage.

To eliminate this danger the heating filament should be redesigned for higher voltage and lower current.

A high temperature thermocouple (Thermo Electric Canada Ltd., Type P13 R), located in the hollow of the bolt that holds the chamber in position (Fig. 19), is used to measure the chamber temperature. To be able to control this temperature, the amount of power supplied to the heating filament is regulated by a simple control system (See Appendix A), which is capable of maintaining the temperature in the chamber within about 3 %.

Magnetic Field System:

In the second stage of the ionization process, the primary and secondary electrons in the semi-ionized plasma are accelerated to the chamber walls and eventually to the anode by the electric field which exists between the chamber walls, the anode, and the plasma. To prevent the electrons in the plasma from striking the channel walls and thus becoming lost from the ionization process, an adequate axial magnetic field is required to limit the radial excursion of the electrons in their helical paths along the axis to the anode. The magnetic circuit which was used for this purpose by the previous author is shown in Fig. 20 (Jirafe, 1966). In his report, W.J. Jirafe indicated that this circuit was capable of producing about 2 kilogauss of magnetic flux density at the channel exit while the calculated value required for proper operation of ion source was 6.74 kilogauss. While he was aware of this discrepancy, nothing could be done about it at that time. Since the inadequate magnetic field seems to be the primary reason which limits the value of the ion current (too large radius

of gyration and the consequent loss of electrons to the channel walls), therefore, to increase the ion current, the magnetic field would have to be increased. To determine the characteristics and capabilities of the existing magnetic circuit and to decide on the extent of the required modifications, a careful analysis and a series of measurements have been carried out on it.

The measurement of the magnetic flux density in the air gap surrounding the poles has been done with a light-beam type fluxmeter (General Electric Co., Cat. No. 9892910G153) and a small search coil, having 100 turns of enamelled wire (AWG 44). From the coil dimensions (inside radius r = 0.15 mm, outside radius R = 0.6 mm) and the diameter of the wire (a = 0.054 mm), the effective area A_{eff} of the coil was calculated:

$$A_{eff} = \pi \times (2(R^2 + Rr + r^2) + (R - r))/6$$
$$= 0.5073 \text{ mm}^2 = 0.005073 \text{ cm}^2$$

This figure applies to a regularly wound coil, whears the actual coil was mass wound. It was, thus, necessary to confirm the above figure, and this was done by calibrating the fluxmeter together with the search coil, with a precisely known field having rated accuracy of 5 parts in 100,000 (Magnetic Field Regulator set; Magnion Inc., Model FFC-4). The field B used in this measurement was 10 kilogauss, the fluxmeter deflection D = 16 mm, the number of turns N in the search coil was 100. Since the sensitivity constant of the fluxmeter K was 388 linkages per mm, the measured effective area A_m of the coil was

$$A_m = KD/NB = 388x16/100x10000$$
$$= 0.006208 \text{ cm}^2$$

The calculated value was about 18 % less than the measured one. Since the accuracy of the measured field was significantly better than 1 %, therefore, the accuracy of A_m was mainly determined

by the errors due to the reading of the fluxmeter, its sensitivity constant, and the position of the search coil during the measurement. The indication of the fluxmeter in this measurement was accurate to within 1 part in 16, and its sensitivity constant was assumed to be of about 5 % accuracy. Thus, the actual value can be regarded as being within about 12 % of the measured value, i.e. $A = 0.006208\ (\pm 12\ \%)\ cm^2$. This measurement confirms the intuitive feeling that, because of the irregular winding, The actual value of the effective area of the coil was probably greater than the calculated one. To compromise between the calculated and the measured values, the effective area of the search coil was assumed to be $0.006\ cm^2$ for the subsequent measurements.

Since the structure of the magnetic circuit is cylindrical, the magnetic field in the region of the anode button may be considered as being symmetrical with respect to the channel axis. Thus, the magnetic flux density was measured along arbitrary diameters in 12 equidistant planes normal to the channel axis. The resulting curves are shown in Fig. 21. Curve No. 0 shows the flux density distribution at the surface level of the top plate, and curves No. 1, 2, ------ , 12 show the flux density distribution at 1, 2, ------, 12 mm below the surface, respectively. These curves are symmetrical with respect to the axis of the core, as expected. One may note here that the maxima of the flux density occurs not on the axis of the channel but in the cylindrical region above the tip 'T' of the core (curves 3, 4, and 5). The significance of this is discussed below in connection with the saturation of the core.

Since the plasma is confined to a relatively narrow region in the vicinity of the channel axis AA', the data from Fig. 21 were used to plot the flux density distribution along that axis, as shown in Fig. 22. As expected, the maximum 'X' of the field occurs at the channel exit. It is about 25 times greater than that at the entrance of the channel. Since we wish to produce a higher density plasma at the exit of the channel than at its entrance, this field distribution is acceptable, in general. Thus, the shape of the poles of the existing magnetic circuit seems to be all right. However, from the point view of reducing the electron loss to the channel walls, as described later, the flux density at the entrance of the channel seems to be too low. Because of this, the shape of the poles should be modified to increase the magnetic flux density at the channel entrance.

Figure 23 shows the flux density at the channel exit as a function of the magnetomotive force (mmf). While the magnetic circuit is capable of producing mmf in excess of 10,000 ampere-turns, the above figure shows that the magnetic core begins to saturate at a relatively low excitation of about 1,500 ampere-turns. Since most of the flux lines are concentrated at the tip 'T' of the core, as shown in Fig. 21, therefore, the change in the slope of the magnetization curve (SS' in Fig. 23) may be caused by the local saturation of the iron near that tip.

Let us now calculate the reluctance of the existing magnetic circuit (Fig. 20) and, from it, the magnetic flux density B, and then compare it with the measured values.

The total reluctance of this magnetic circuit is the sum of the individial reluctances R_a, R_b, R_c, R_d, R_e, and R_f (See

Appendix C) corresponding respectively to the sections a, b, c, d, e, and f in the flux path as shown in Fig. 20. The total reluctance R is therefore:

$$R = R_a + R_b + R_c + R_d + R_e + R_f$$
$$= 0.0216 + 0.00138 + 0.0121 + 0.00029 + 0.00048 + 0.00014$$
$$= 0.036 \text{ ampere-turn/maxwell}$$

where R_a, R_c, and R_e are the reluctances of the air gaps, and R_b, R_d, and R_f are the reluctances of the magnetic material of the magnetic circuit.

The magnetomotive force F is equal to the magnetic flux φ multiplied by the total reluctance R, i.e.

$$F = \varphi R$$

Substituting $\varphi = BA$, we have

$$B = F/RA$$

where B is the magnetic flux density in the area A. For example, the magnetic flux density for F = 500 ampere-turns at the channel exit in Fig. C-2 in Appendix C is,

$$B = \frac{500 \times (0.0216/0.036) \times 0.427 \times 2\pi \times 0.03}{\pi \times (0.03)^2 \quad (2.54)^2}$$
$$= 1.325 \text{ kilogauss}$$

The corresponding measured value was 0.97 kilogauss as shown in Fig. 23. The percentage difference between the measured and the calculated values was thus about 30 %.

The accuracy of the measurement was affected by the following errors:

1. Reading error:

The deflection of the fluxmeter was only about 1.5 mm

for F = 500 ampere-turns, and the width of the hairline in the light spot of the meter was nearly 1 mm. The readings were made with the greatest care by observing the position of one of the edges of the hairline, but the error could not have been expected to be less than about 10 %. To be on the safe side it was assumed to be 20 % for the calculations below.

2. Search coil effective area error:

   The value of the effective area was assumed to be between the calculated and the measured values. Since the difference between these was about 18 %, therefore, by taking a value which was roughly half-way between these values, we obtained a figure for the effective area of the coil, which should not differ from the true value by more than some 10 %.

Thus, the limits of the errors of the measurements of the flux density could be as great as 30 %.

The accuracy of the calculated value of the flux density in Fig. 20 has been estimated as follows:

1. Field mapping methods are capable of up to 1 % accuracy. While the field plots have been made with care, no great effort was made to obtain high accuracy, for there seemed to be no need for this at this stage of work. Because of this the error in the calculations of the reluctance of the section 'a' in Fig. 20, by this method, was assumed to be as much as 10 %.
2. The error made in the measurements of the widths of the stray air gaps 'c' and 'e' was estimated to be 30 % and 50 % respectively (See p. 90).

3. The rated permeability μ_r of the magnetic core material was 2000. If we assume that, because of the temperature dependence of μ_r, this value is accurate within only 50 % then, from Eq. 20 in p. 55, the error in the calculation of B due to the inaccuracy in μ_r is less than 10 %.

Thus, the limits of the errors in the calculations of the flux density could be as high as 20 % (See Appendix C).

Since the accuracies of the measured and the calculated values of the flux density were about $\pm$ 30 % and $\pm$ 20 % respectively, and since the measured value of the magnetic flux density at the channel exit (for F = 500 ampere-turns) differed by about 30 % from the calculated value, therefore, the calculations of the magnetic flux density seemed to be within the limits of errors and, therefore, reasonable and, hopefully, dependable. The accuracy of those calculations and their dependability could be further improved by the elimination of the stray air gaps, by determining the temperature dependence of μ_r, and by improving the accuracies in the field plotting.

The cyclotron radius of an electron moving in a uniform magnetic field can be determined from Eq. 9 in the previous chapter as follows,

$$r_c = mv/eB$$

where r_c is the cyclotron radius of the moving electron, m is the mass of the electron, e is the electron charge, and v is the radial velocity of the electron. The velocity v of an electron moving in a constant electric field can be determined from

$$v = (2eV/m)^{1/2}$$

where V is the difference of potential between the extreme points of the electron's path. Thus,

$$r_c = (2mV/e)^{1/2}/B$$

The radius of the channel of the evaporation chamber is 172 μ, and the potential difference between the evaporation chamber and the filament can be set to any value between 50 and 250 V (Jirafe, 1966). Let us consider the worst condition and find the least value of B which would prevent an electron from colliding with the channel walls.

For r_c = 172 μ, i.e. the cyclotron radius equal to the radius of the channel, and V = 250 V, the required value of the magnetic field B_2 at the entrance of the channel is

$$B_2 = 3.37 \times (250)^{1/2}/172 = 3.09 \text{ kilogauss}$$

For the existing magnetic circuit, the corresponding field B_1 at the channel exit would have to be

$$B_1 = 3.09 \times 25 = 77.4 \text{ kilogauss}$$

Since for ordinary magnetic materials the practical limit of flux density is about 15 kilogauss, therefore, the ratio B_1/B_2 should not be greater than 5 to keep B_1 below this maximum value. The magnetic poles in the existing magnetic circuit should therefore be modified in such a way as to increase B_2 and, at the same time, to keep the ratio B_1/B_2 as high as possible.

There is a number of possible modifications to achieve this. Let us consider them in detail:

1. An alteration of the configuration of the magnetic poles: Figure C-2 shows that the majority of the flux lines leak from the surface near the top of the magnetic core to the top plate (Area A). This leakage can be decreased by increasing the distance between the top plate and this surface, and at the same time, by decreasing the air gap between the poles. A sketch of the suggested modification

in the shape of the magnetic poles is shown in Fig. 24. The corresponding field is mapped in Fig. 25, according to which the number of the flux lines passing through the tip is 6 out of the total of 18 lines. Thus about 30 % of the flux lines pass through the space within the tip of the magnetic core while, in the present magnetic circuit, the corresponding figure is only about 9 %. From the field map in Fig. 25 and Fig. C-2, we can calculate the relative flux density in different cross-sections of the magnetic core, and plot it as shown in Fig. 26-C. Curve 2 gives a lower and more uniform flux density than curve 1. This means that not only the flux density in the air gap between the poles can be increased but also that the nonuniform flux distribution inside the core may be equalized to prevent the undesirable local saturations which reduce the maximum flux obtainable in the magnetic circuit.

2. A modification of the tip of the magnetic core:

To increase the flux density at the entrance of the channel of the evaporation chamber, we have to guide the flux lines which leave the pole through the lower portion of the core. Figure 27 shows some of the equipotentials and flux lines for two different pole shapes of the magnetic core. The flux line 1 in (b) is lower than the corresponding one in (a). This means that the flux density at the entrance of the channel in (b) will be higher than that in (a). Such considerations may serve as a guide in making the modifications of the pole tips to produce an optimum pole design.

3. Elimination of the unnecessary air gaps:

The reluctance R_c of the air gap between the magnetic core and the bottom plate ('c' in Fig. 20), which is due to the presence of the coolant-seal, is 0.0121 ampere-turn per maxwell while the total reluctance R of the present circuit is 0.036. This means that about one third of the total mmf is lost in this air gap. To increase the efficiency of the magnetic circuit, this loss should be either eliminated or decreased to a minimum. Since the permeability and the cross-sectional area in this region is fixed, therefore, the reluctance R_c is directly proportional to the length of the air gap. Similar considerations apply to the seal air gap 'e' in Fig. 20, although, because of the greater total cross-section and closer distance, this gap does not seem to be as detrimental as the one above. The future design, however, should take these gaps into consideration. Attention should also be paid to welded seams. The welding material should be ferromagnetic, the gap between the welded parts should be reduced to a minimum and the area of contact between these parts be made as large as possible.

4. The use of high permeability material for the core:

The value of the flux density in a closed magnetic core is, within certain limits, proportional to the permeability of the material used for the core. Thus, in general, the use of a material of high permeability for the magnetic core is preferable if higher flux density are required. However, because of the air gap mentioned above, the magnetic flux density at the channel exit is

no longer directly proportional to the permeability of the magnetic core. In Fig. 20, for example,

Total Reluctance R = Reluctance of Air Gaps R_A + Reluctance of Iron R_I

where $R_A = R_a + R_c + R_e = 0.03418$ ampere-turn/maxwell

$R_I = R_b + R_d + R_f = 0.00182$ ampere-turn/maxwell

Since $R_A >> R_I$, therefore, the change in the total reluctance R due to a change in the reluctance of the magnetic material is very small. Now let us consider the change in the flux density B_1 at the channel exit as a function of the change in the relative permeability μ_r. This flux density is given by

$$B_1 = F \times (R_a/R) \times P_1 \times 2\pi r/\pi r^2 \qquad (17)$$

where F is the applied mmf, R_a is the reluctnace of the section 'a' in Fig. 20, R is the total reluctance of the magnetic circuit, P_1 is the permeance of the air gap per unit length (inch) at the channel exit, and r is the radius of a ring-like unit volume at the channel exit. Rewriting B_1 as

$$B_1 = (2P_1 F R_a)/(rR) = k/R \qquad (18)$$

and substituting $R = R_A + R_I$, we get

$$B_1 = k/(R_A + R_I) = k/\left(\frac{\ell_A}{\mu_o S_A} + \frac{\ell_I}{\mu_r \mu_o S_I}\right)$$

Differentiating B_1 with respect to μ_r, we get,

$$\frac{dB_1}{B_1} = \frac{R_I}{R}\,\frac{d\mu_r}{\mu_r} \qquad (19)$$

i.e. the smaller is the reluctance of the iron path (the better magnetic material we use) in comparison to that of the air gap, the lesser is the change in B due to an increase in the permeability. For example, in our case $\mu_r = 2000$, $R = 0.036$, and $R_I = 0.00182$, then

$$dB_1/B_1 = (d\mu_r/\mu_r)/20 \qquad (20)$$

which shows that if we wish to increase the flux density in the air gap by using a magnetic material having higher permeability, we can expect a change of only about five percent for a small change of μ_r. For a large increase of μ_r from 2000 to 4000, the percentage gain in the magnetic flux density would be about 3 %. This indicates that the choice of the magnetic material for the magnetic path is of secondary importance, and that in designing this path all attention should be given to the air gaps and to the shape of the poles.

A proposed modification of the magnetic circuit designed according to the above considerations is shown in Fig. 28. The shape of the poles is by no means final and a careful analysis and, perhaps, an optimization of the design should be carried out. To make it possible to experimentally check different pole shapes, the pole-containing section may be made removable.

To see how much improvement in the magnetic flux density we could get in this modified type, let us take Fig. 24 as an example. In this figure every section of the magnetic circuit is the same as that in Fig. 20, i.e. as in the existing circuit, with the exception of the shape of the magnetic poles and of the distance between the top plate and the magnetic core. From the distribution of the flux lines, as shown in Fig. 25, we can find the permeance of the air gap (section 'a' in Fig. 24)

$$P_a = 0.32 \times 2\pi \times (1 + 0.92 + 0.84 + 0.76 + 0.69 + 0.62 + 0.55 + 0.50 + 0.45 + 0.40 + 0.35 + 0.31 + 0.27 + 0.23 + 0.18 + 0.13 + 0.09 + 0.05)$$

$$= 0.32 \times 2\pi \times 8.34 = 16.7 \text{ maxwells/ampere-turn}$$

The corresponding reluctance is

$$R_a = 1/P_a = 0.0595 \text{ ampere-turn/maxwell}$$

Since the reluctance of the other section of the modified magnetic circuit was assumed to be the same as that of the present one, i.e.

$$R_b + R_c + R_d + R_e + R_f = 0.0144 \text{ ampere-turn/maxwell}$$

therefore, the total reluctance R is

$$R = R_a + R_b + R_c + R_d + R_e + R_f$$
$$= 0.0739 \text{ ampere-turn/maxwell}$$

For F = 500 ampere-turns, the magnetic field B_1 at the channel exit is

$$B_1 = \frac{500 \times (0.595/0.739) \times 0.32 \times 2\pi \times 0.05}{\pi \times (0.05)^2 \times (2.54)^2}$$

$$= 0.83 \text{ kilogauss}$$

The corresponding field B_2 at the entrance of the channel is

$$B_2 = 0.83/(3)^2 = 0.092 \text{ kilogauss}$$

The magnetic field sufficient to confine an electron with a 250 V energy within a cyclotron radius $r_c = 172\ \mu$ is

$$B = 3.09 \text{ kilogauss}$$

To produce a magnetic field of 3.09 kilogauss at the entrance of the channel, the magnetic flux density in the modified magnetic core, ignoring saturation, would be 32.4 kilogauss, while in the present magnetic core it would be 114 kilogauss. Since the saturation of ordinary magnetic materials occurs in the range of 10 to 15 kilogauss, therefore, the modified magnetic circuit is better than the existing one. However the value of 32 kilogauss is still too high for the used materials, and the shape of the magnetic poles should be modified e.g. as shown in Fig. 28 to reduce the flux density further. Should these modifications be still insufficient, the diameter of the channel of the evaporation chamber would have to be enlarged to allow for a larger cyclotron radius of moving electrons.

Cooling System:

To evaporate the charge material, the evaporation chamber has to be maintained at a high temperature. Its surrounding magnetic core, however, should be kept below the temperatures which might cause either a serious reduction of the permeability of the magnetic core material, or any other damage. Because of the large temperature difference between the chamber and the core (about 800 °C), a certain amount of heat is transfered from the chamber to the core by means of radiation and conduction. Thus, since the heating system supplies the heat to the evaporation chamber continually (at the rate of about 250 watts), we have to use a cooling system to remove the heat from the core, and also the heat produced by the copper losses (less than 100 watts) in the electromagnet coil.

The cooling system consists of the cylindrical tank (CT) housing the magnetic core (C) surrounding the evaporation chamber (EC) and the electromagnet coil (MC), the centrifugal pump (P), the radiator (R), and the coolant, as shown in Fig. 30. The connecting tubes between the parts are made of flexible plastic (Poly-Flo) tubing. The coolant originally used in this system was FC 75 (Jirafe, 1966), then water, and, because of the low demands on the cooling system and the corroding properties of water, it may ultimately be possible to replace it by oil.

The cylinder tank (o.d. = 8.75 in., height = 8.875 in., and the wall thickness = 0.375 in.) and the magnetic core (0.d. = 2 in., height = 7.5 in., and the wall thickness = 0.2 in.) are made of mild steel. The electromagnet coil of 500 turns of AWG No. 9 enamelled wire wound on a brass cylinder ($5\frac{3}{8}$ in. long) can carry currents

of up to 20 amperes. The evaporation chamber, which is located inside the magnetic core, is made of molybdenum (melting point 2617 °C). The coolant inlet and outlet tubes, four of each, are made of steel tubing, 0.25 in. i.d., and are located radially near the top and the bottom of the tank respectively. To avoid the collection of air, an air-vent was placed near the top of the tank.

The centrifugal pump is driven by a sealed electric motor (110 V, 3.5 A). The rated pump-flow is 760 cc/sec (12.5 gal/men.). However, the measured value, under the operating conditions, was below 200 cc/sec.

A commercial automobile-heater is used as a radiator. As the coolant flows down, it is cooled by the air forced through the radiator by a domestic-type electric fan with a 110 V, 0.5 A, motor. The rate of heat-removal from the radiator can be determined by measuring the flow velocity and the temperature difference of the coolant entering and leaving the radiator. A preliminary check indicated that the heat removing capacity of the radiator should be ample in this application.

The flow velocity of the coolant was determined by measuring the time needed to pump a fixed amount of water at different voltages applied to the centrifugal pump. The resulting curve was plotted in Fig. 30.

There are several heat sources which contribute to the total amount of heat which has to be removed by the coolant. These are:

1. heating filament: about 250 watts
2. emission filament: about 100 watts
3. electromagnet coil: less than 100 watts

The total amount of heat which has to be removed by the coolant is, therefore, about 500 watts*. This amount of heat is small and no problems connected with the removal of heat have been encountered during the experimental work. On the contrary, it was necessary to reduce the coolant flow to be able to raise the temperature in the evaporation chamber to 900 °C required for the evaporation of Silver.

The hottest part of the evaporation chamber is near its top where the second stage of ionization process takes place. Because of this, the coolant is injected at the top of the magnetic core, and removed from the bottom of the cylindrical tank. Since the permeability of the magnetic material is temperature sensitive (e. g. See Soohoo, 1960), and since the hottest part of this system is near the top of the core, a special cooling system for the poles may be needed. This would have to be investigated in the future.

---

* The coolant, while passing through the centrifugal pump, may be absorbing some 5 % of the heat dissipated by the pump's motor (less than 200 watts). This amount (about 10 watts) seems to be too small to merit special consideration.

Summary of Modifications and Suggestions:

1. Magnetic Field System:

   a. To increase the flux density in the desired region between the magnetic poles, and to decrease the leakage outside of it, a modified magnetic circuit was proposed. This modification should, for a given mmf, increase the flux density at the entrance of the channel by a factor of nearly two. In addition to this, the flux lines should be guided to leave the pole through the lower portion of the core to increase the flux density at the channel entrance even further.

   b. Because of the presence of the coolant seals, the stray air gaps exist between the bottom plate and the magnetic core or the cylindrical walls of the tank. This decreases the efficiency of ~~the~~ producing flux density in the main air gap between poles greatly. Those stray gaps should be either eliminated or minimized (e.g. by using 'O' rings rather than gaskets). Furthermore, a ferro-magnetic material should be used for welding the seams between the top plate and the cylindrical wall of the tank.

   c. In selecting a suitable magnetic material for the magnetic circuit, the considerations of the permeability should be linked with its temperature dependence. To get the relevant data for these considerations, the working temperatures of the inner and the outer surfaces of the magnetic core should be measured.

2. Evaporation Chamber:

a. If the flux density in the channel is found to be insufficient after a maximum effort has been put into the modifications of the magnetic circuit, as described above, then the diameter of the channel of the evaporation chamber would have to be enlarged. The flux density required to confine electrons within the channel can then be decreased proportionally. Thus, the size of the diameter of the channel and the magnetic ~~field strength~~ flux density are, to some extent, mutually compensating.

b. To avoid losing electrons to the walls in the straight portion of the evaporation chamber, and to reduce heat losses, the evaporation chamber may be made of an insulating material, e.g. of a ceramic.* To apply an electric field between the evaporation chamber and the emission filament, a metalic film (e.g. Molybdenum) deposited on the inner sloping wall of the chamber could be used.*

3. Temperature Control System:

To prevent overheating of the chamber in case of misadjustment of R_s (Fig. A-1), a protective switch operated by a circuit consisting of a Schmitt trigger, a power amplifier, and a relay should be incorporated in the temperature control system.

---

* I would like to thank Mr. Mohammed Husain Master for this suggestion.

References:

1. General Electric Co.,
'Light-beam Type Fluxmeter',
Cat. No. 9892910G153

2. Honig, R.E.,
'Vapor Pressure Data for the Solid and Liquid Elements',
RCA Review, Vol. XXIII, No. 4, Dec. 1962

3. Jirafe, W.J.
'A Duoplasmatron Ion Source For Ion Beam Deposition',
Tech. Rep. No. 66-15, Univ. of Ottawa, Dec. 1966

4. Magnion Inc.,
'Magnetic Field Regulator Set', Model FFC-4
Burlington, Massachusetts, USA

5. Soohoo, Ronald F.
'Theory and Application of Ferrites',
Prentice-Hall Inc., New Jersey, p. 143, 1960

6. Thermo Electric CanadaLtd.,
'Operation and Maintenance Instruments for Metal
Sheated Thermocouples',
Brampton, Ontario

7. Ultek Corporation,
'High Vacuum Feedthroughs', Bulletin No. B-1288,
Palo Alto, Calif., USA

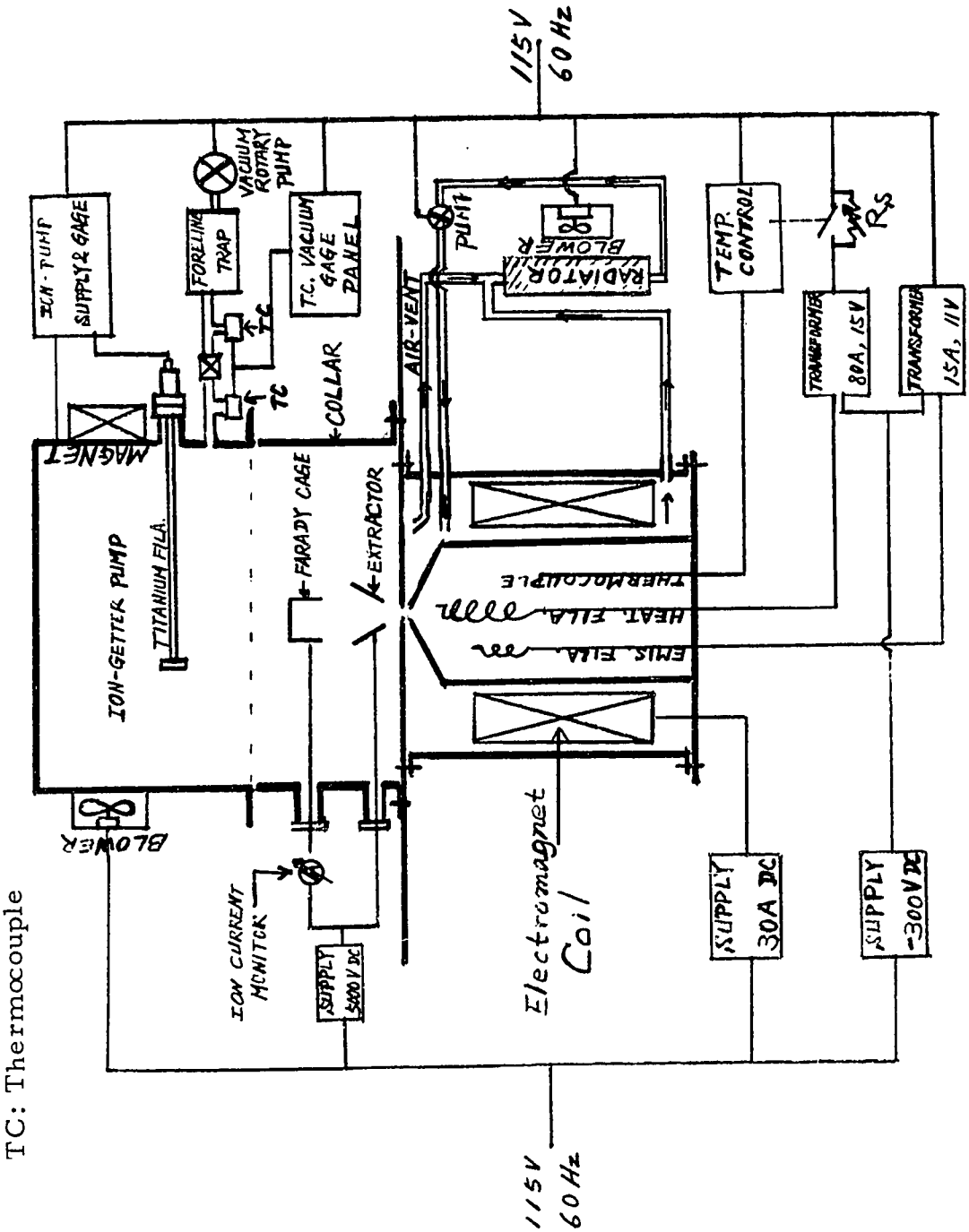

TC: Thermocouple

Fig. 18 Block Diagram of the Ion Source

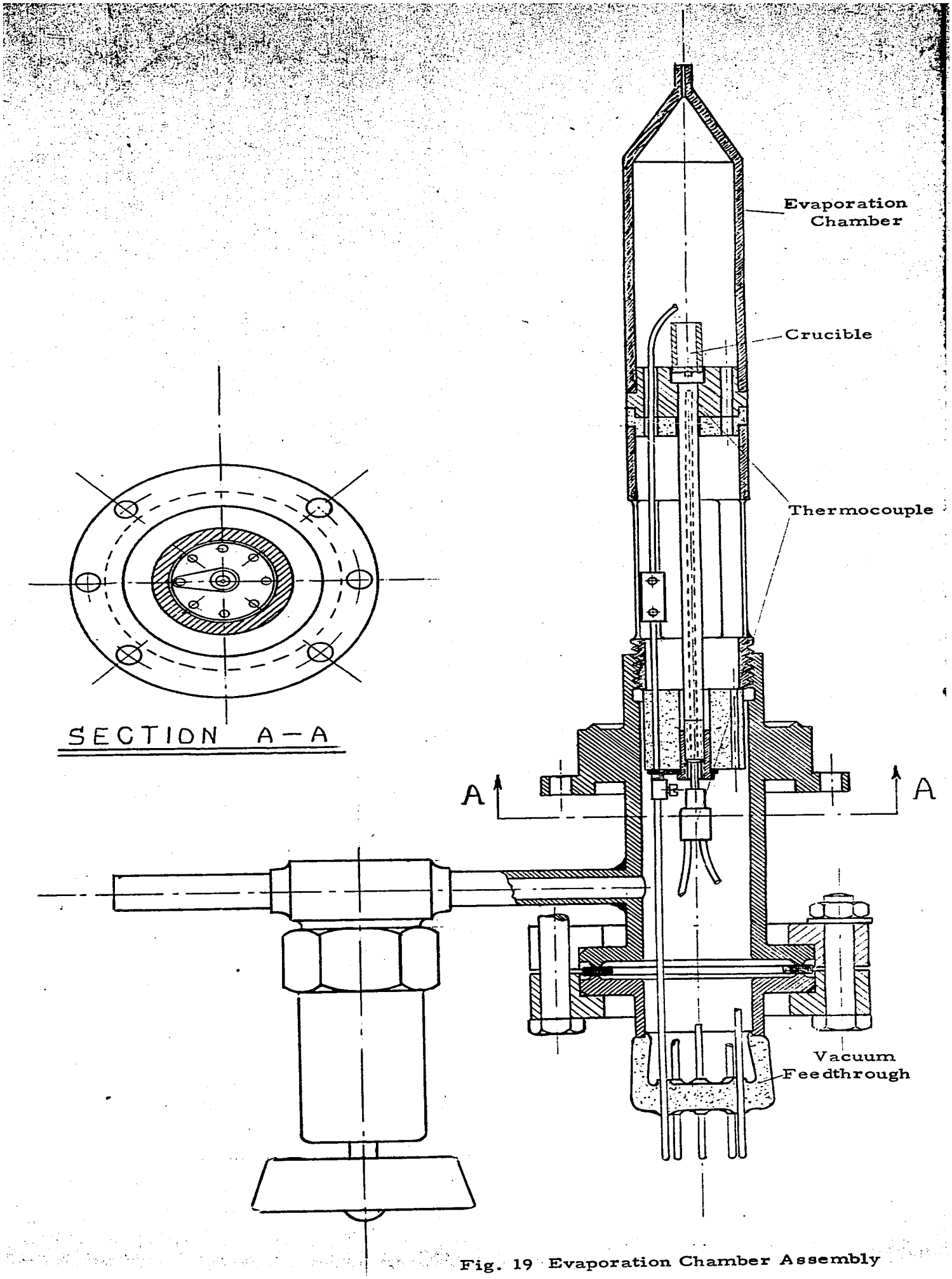

Fig. 19 Evaporation Chamber Assembly

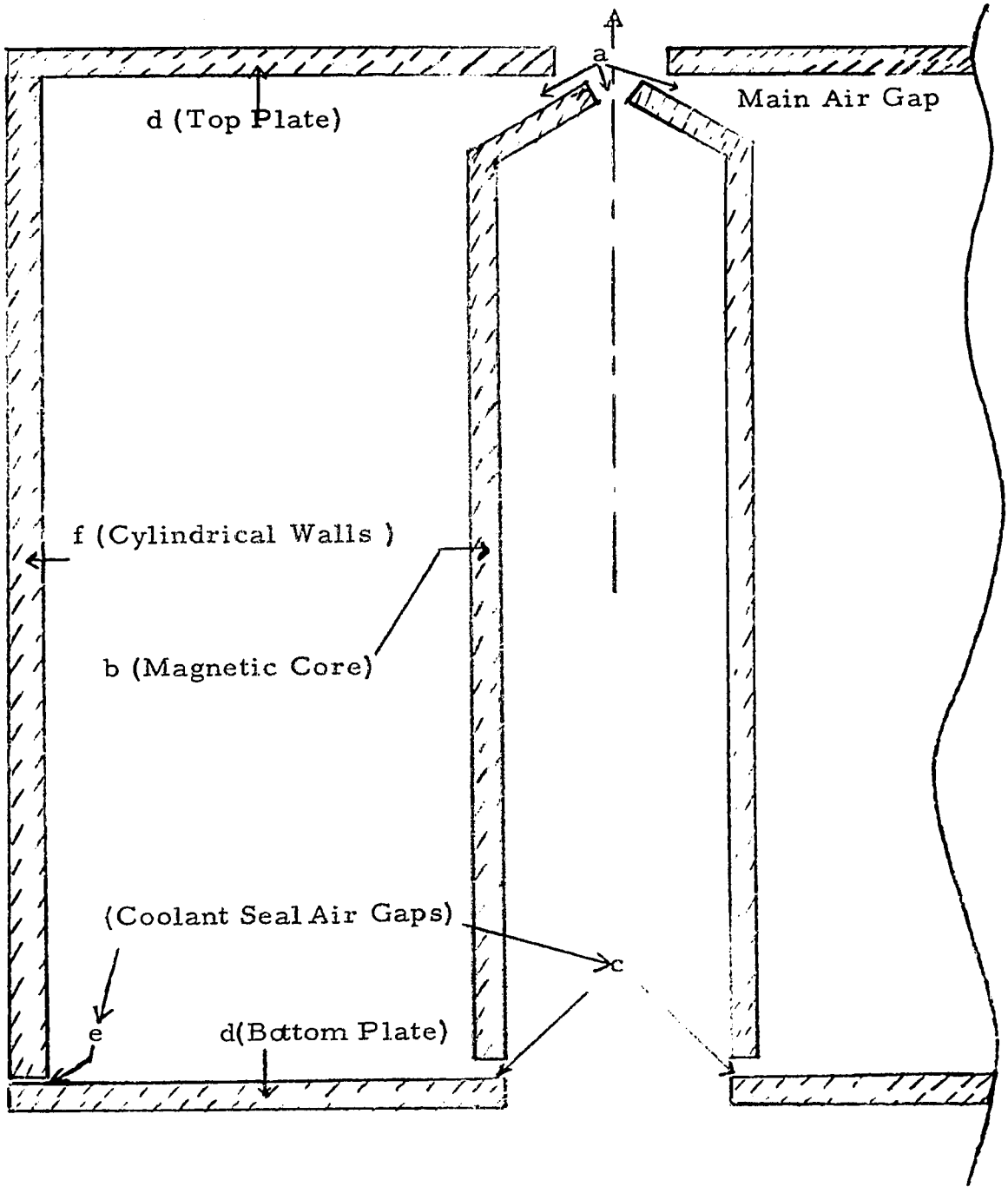

Fig. 20 Magnetic Circuit of the Ion Source.

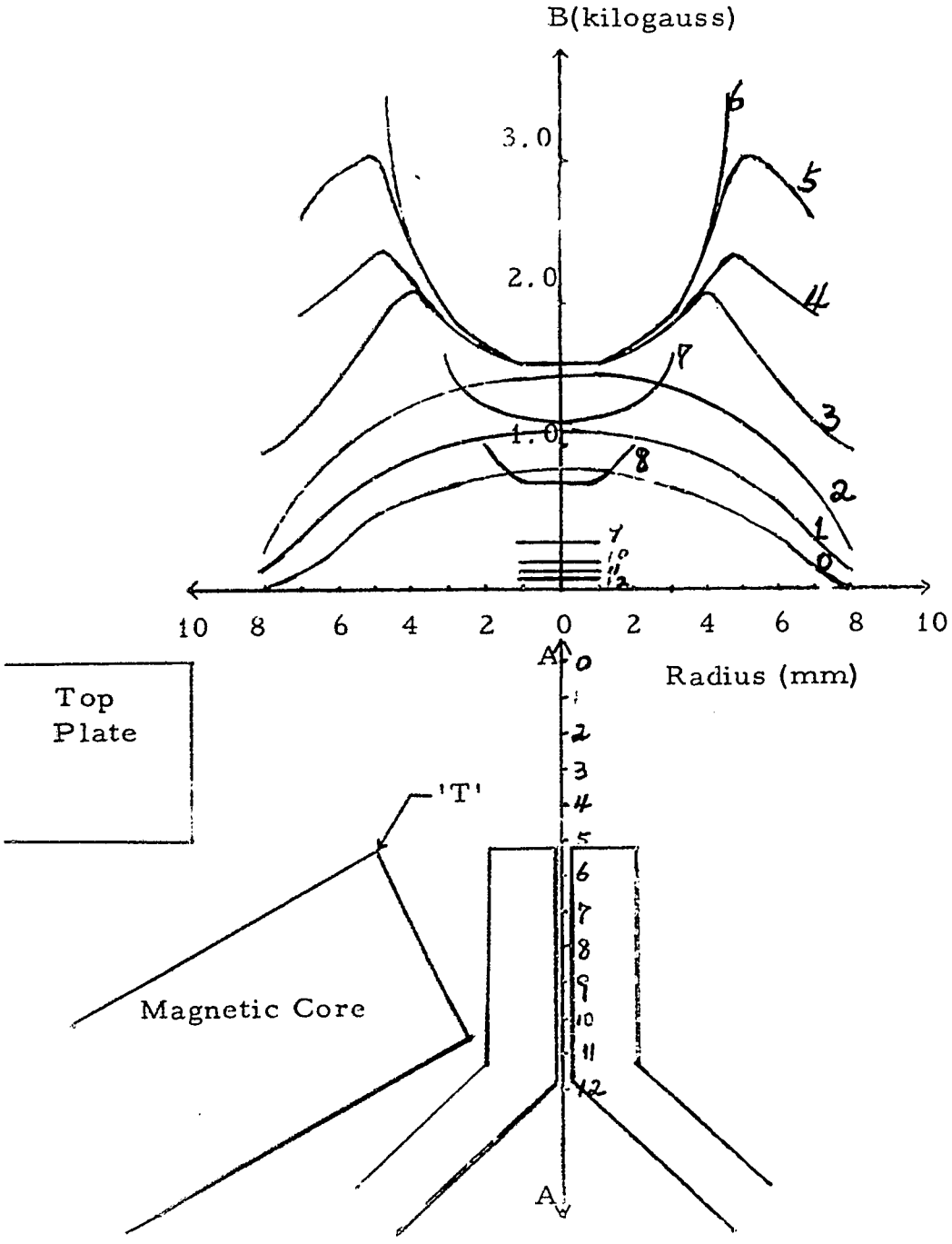

Fig. 21 Magnetic field density in the air gap between the magnetic poles. Curves 0 to 12 show the field distribution measured at different levels from the top plate (level '0') down to the channel entrance (level 12). The magnetomotive force was 1000 ampere-turns.

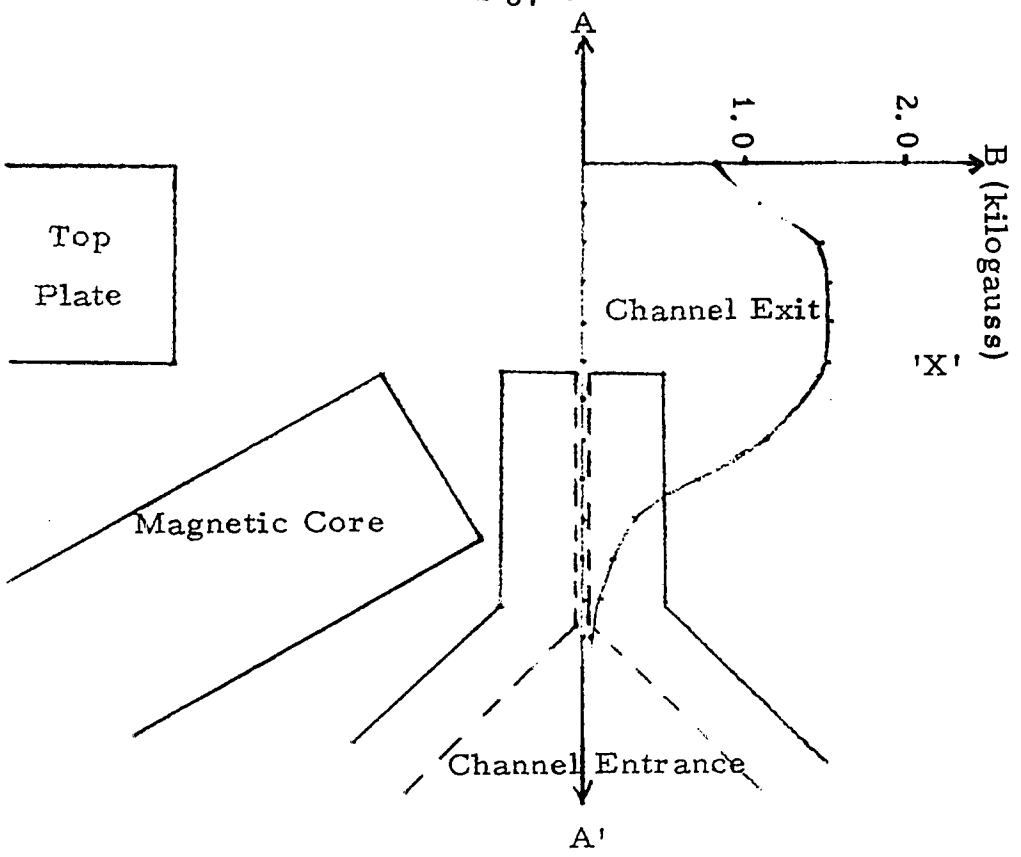

Fig. 22 The Flux Density Distribution Along the Axis AA' for F = 1000 ampere-turns.

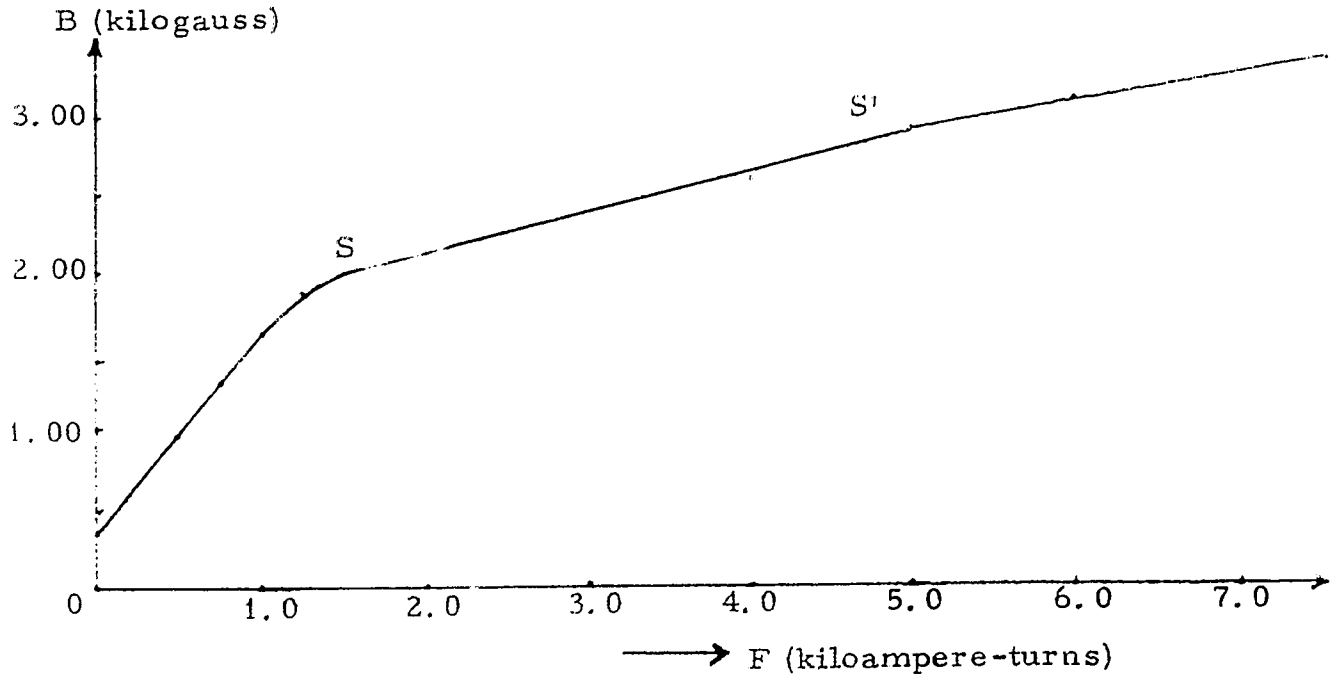

Fig. 23 Flux Density B Measured at the Channel Exit as a Function of the Magnetomotive Force F.

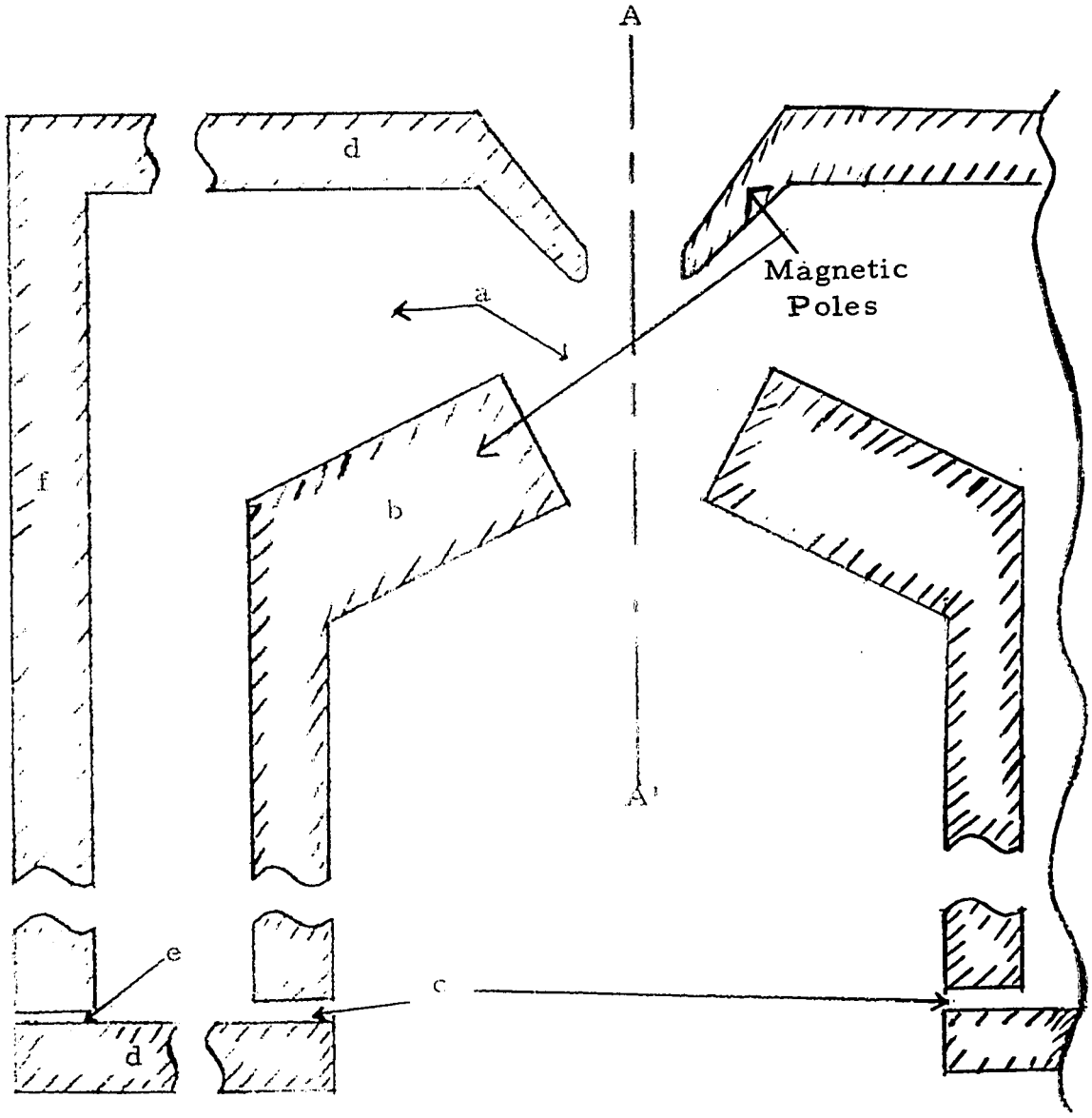

Fig. 24 Suggested Modification in the Shape of Magnetic Poles.

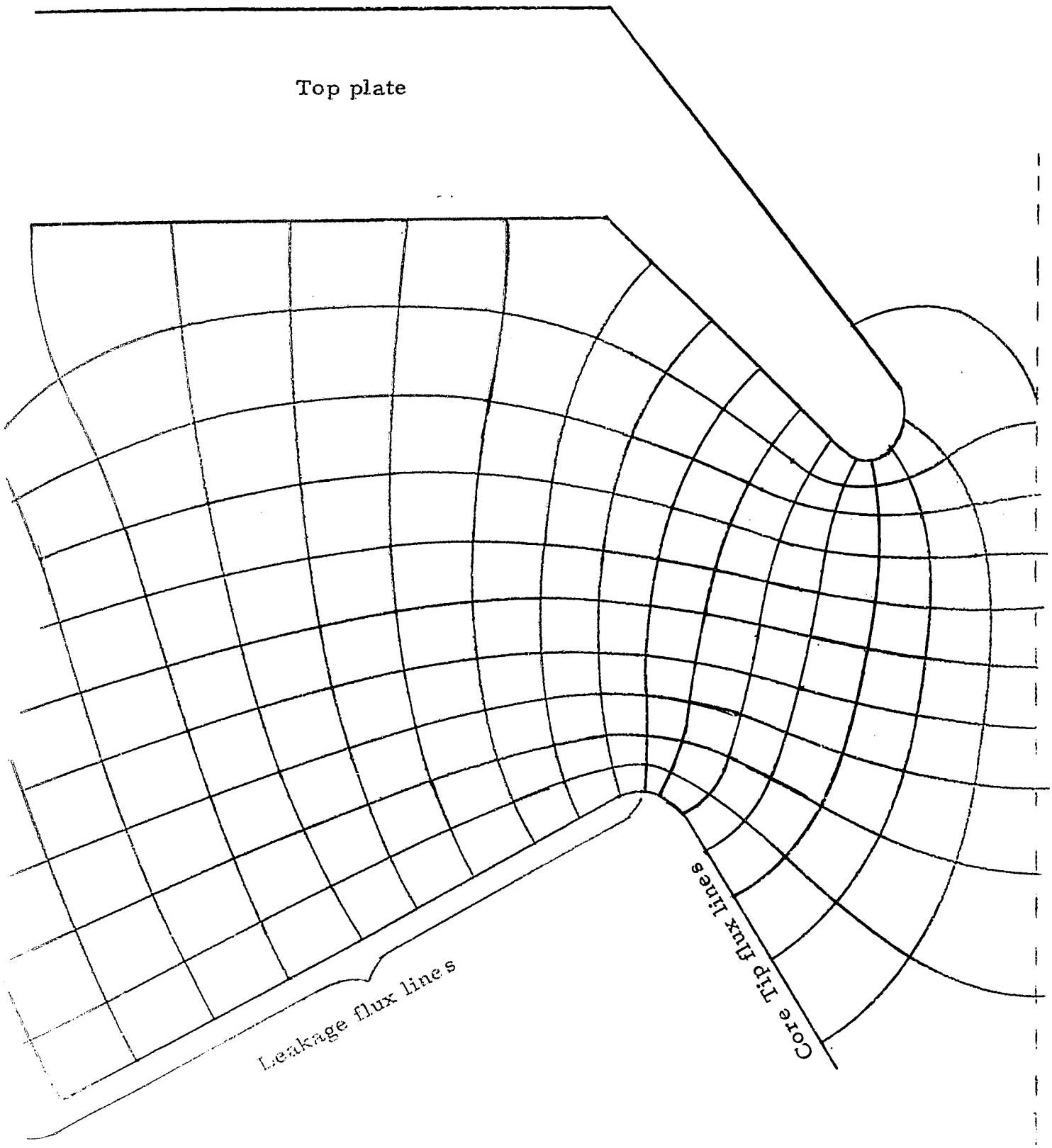

Fig. 25 Field mapping in the space between the Magnetic Poles of Fig. 24

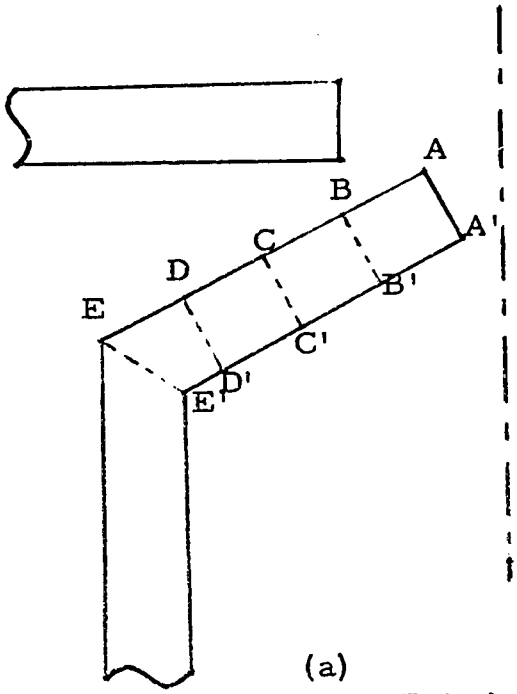

(a)

The Pole Shape of the Existing Magnetic Circuit

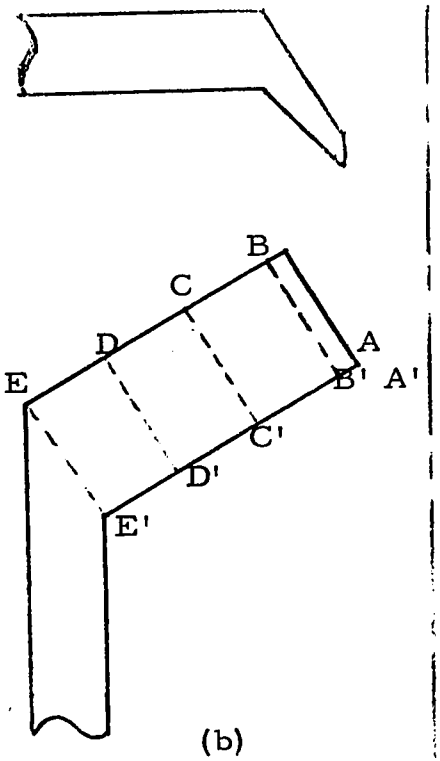

(b)

The Pole Shape of the Suggested Magnetic Circuit

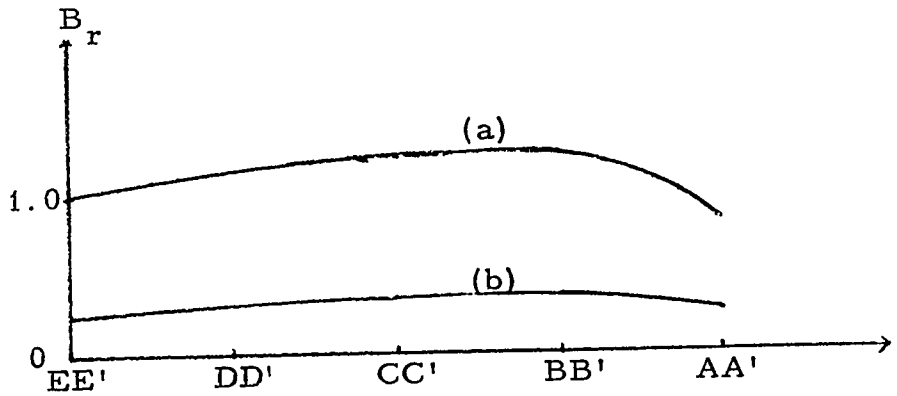

(c)

The Relative Flux Density Distribution Inside the Magnetic Core. The Letter Pairs Indicate the Corresponding Sections in (a) and (b).

Fig. 26 Comparison of the Magnetic Flux Density Distribution in the Iron of the Magnetic Poles of the Existing and the Suggested.

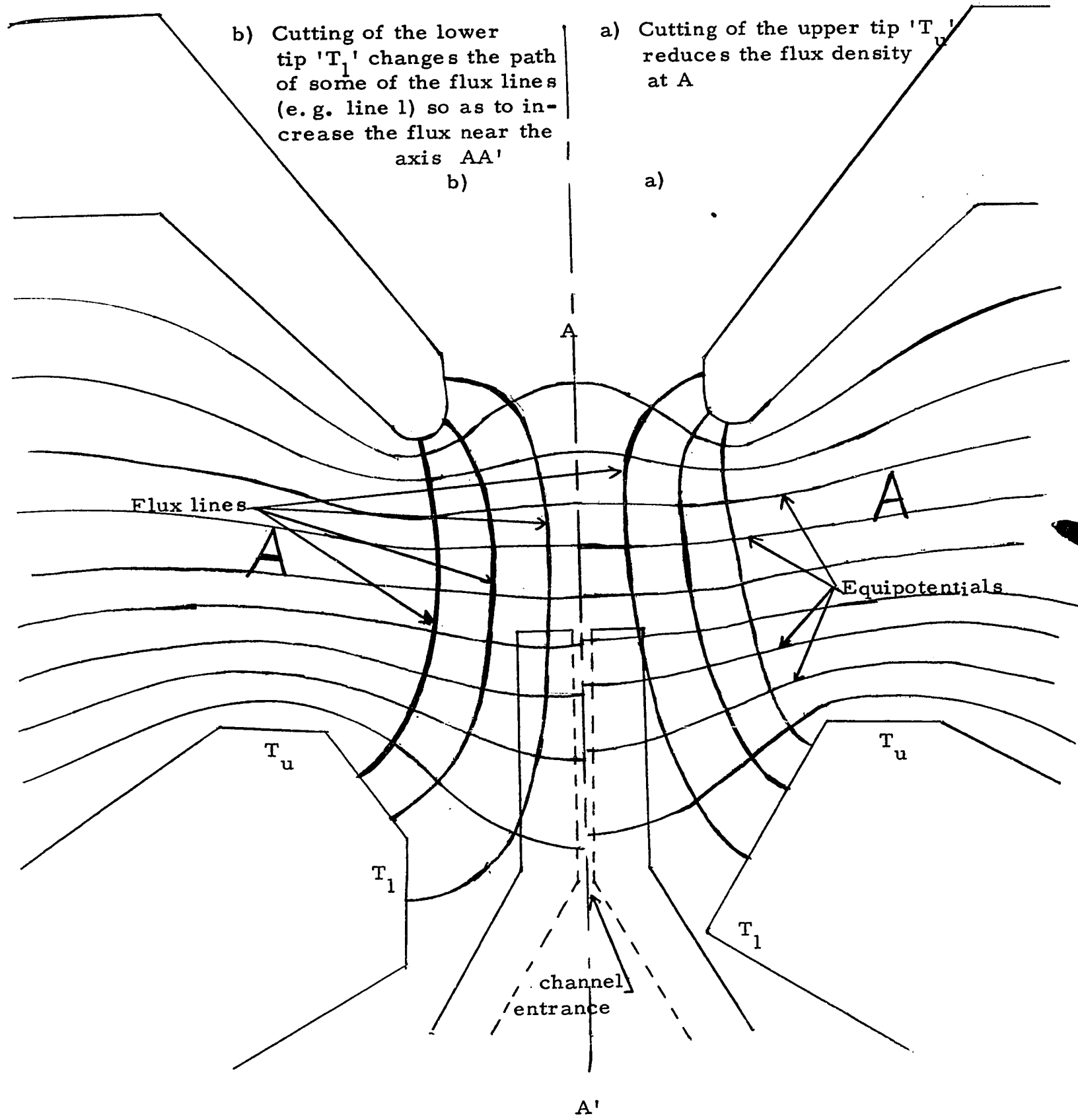

Fig. 27 The influence of additional modifications of the shape of magnetic poles on the flux distribution in the air gap.

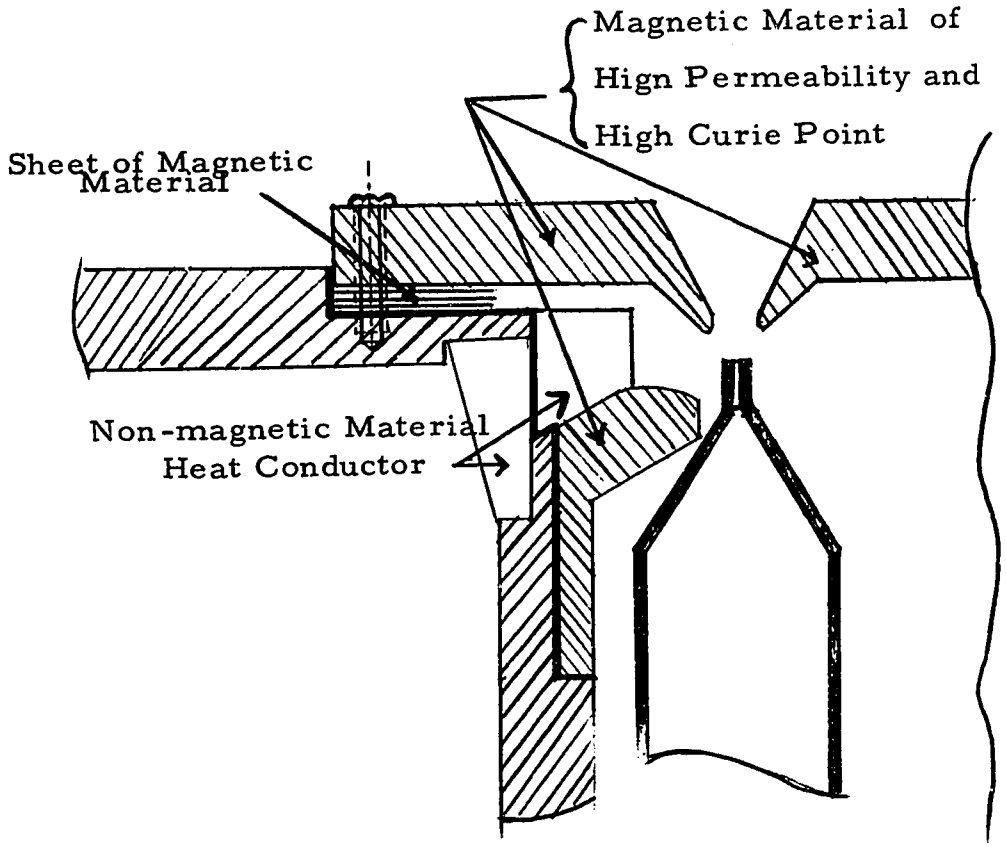

Fig. 28 Details of the Proposed Modifications of the Poles of the Magnetic Circuit. (Bold line indicates the removable section). The Remainder of the circuit is assumed to be the same as that in Fig. 24.

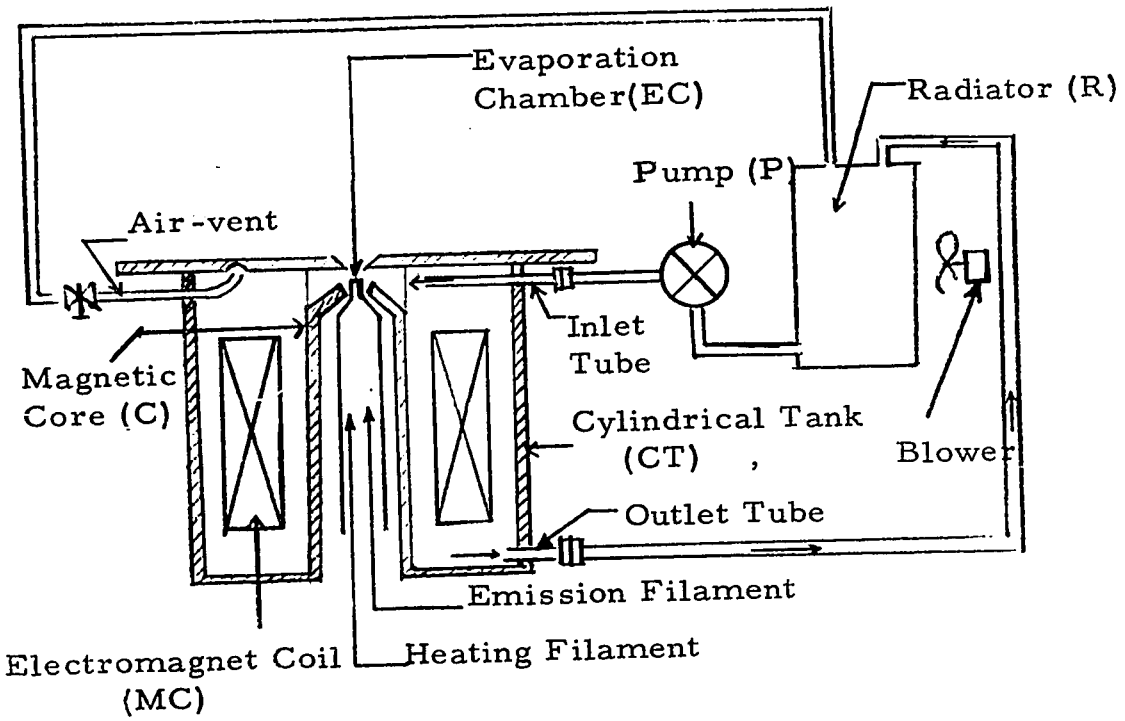

Fig. 29 Block Diagram of the Cooling System

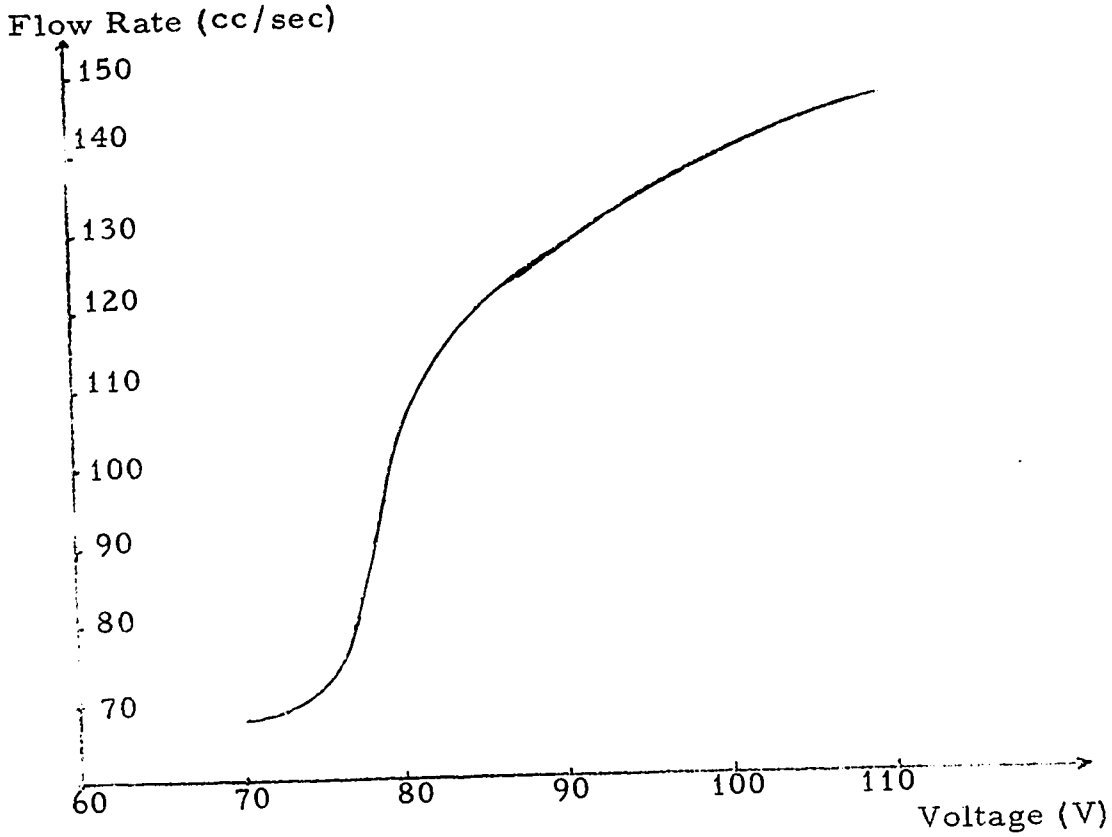

Fig. 30 The Flow Rate of Coolant as a Function of the Voltage Applied to the Pump.

CONCLUSION

The Duoplasmatron ion source was originally designed to produce ions of the elements which are gases at room temperatures. The ion source described in this thesis seems to have been the first attempt to use a Duoplasmatron to produce ions of materials which are solids at these temperatures. Because of this, and the consequent lack of the published data which could be used in aiding the design of this source, the usual research, and development procedure had to followed.

The originator of this ion-source W. J. Jirafe had designed and constructed, in a remarkably short time of one year, an apparatus which made an excellent starting point for further development. The author of this thesis could not obtain any measurable ion current from this source, in its original form. However, W. J. Jirafe made some measurements which indicated that the source did function, though not as well as anticipated. At the start of this work, the reason for this inadequate functioning was unknown. At its conclusion, however, it was possible to make a set of definite suggestions which, if incorporated in the source, should improve its performance. It seems that the principal reason for the malfunctioning was an inadequate magnetic field, and that it should be increased as much as possible. Following such an increase, further modifications might have to be made in the dimensions and profile of the channel of the evaporation chamber. The amount of time which was needed to analyse the ion-source, and to design and construct the temperature control system, excluded the possibility of actual testing of the intended modifications. They have been left as suggestions which may serve as a starting point for the worker who is continuing the development of the ion-source.

Appendix A Temperature Control System

To maintain constant temperature in the evaporation chamber, the heating filament which is used to produce a vapor of the element which is ionized is switched ON and OFF by a simple control system, shown in Fig. A-1. This system consists of a thermocouple, a dc reference voltage (adjustable by the potentiometer P), a differential amplifier, a Schmitt trigger circuit, a power amplifier, and a dc relay. The dc reference voltage (E_2) can be set to control the temperature level of the evaporation chamber. The emf of the thermocouple (E_1) is a measure of the chamber temperature at any time. The difference ($E_2 - E_1$) is amplified by the differential amplifier. The Schmitt trigger circuit converts the slow variations of the output of the differential amplifier into an ON-OFF type of signal needed for an unhesitant operation of the relay Ry which is driven by the power amplifier. The relay controls the power supply of the heating filament by short-circuiting the variable resistor R_s on the supply side of the filament transformer. R_s is adjusted so as to reduce the current surge and frequency of relay operation, in the circuit to a minimum.

I. Tolerance Considerations:

The purpose of the temperature control circuit is to maintain the temperature of the evaporation chamber within certain limits of the desired level. The range of temperatures for evaporating the elements mentioned in the introduction is from 44 °C (Phosphorus) to 1420 °C (Silicon). At the time of writing,

there is no guide for establishing the allowable tolerance limits of temperature fluctuations in the evaporation chamber. However, it seems reasonable to try to maintain the deviation from the normal working temperatures within about 1 %.

The value of the threshold input voltage of the Schmitt trigger circuit is about $\pm$ 2 mV, whereas the minimum input to the differential amplifier, corresponding to 1 % deviation from the 1000 °C level is about 0.132 mV, for the thermocouple used. Thus, the minimum gain of the differential amplifier has to be higher than 16.

This circuit will responds to the input voltages on the order of 0.132 mV at the input terminals of the differential amplifier. Since the ac hum present at these terminals is of the same order of magnitude as that of the input signals, therefore, the bandwidth of the differential amplifier was reduced by means of a capacitive feedback to about 1 Hz to eliminate relay chatter due to 60 Hz hum. An additional low-pass RC filter is used to further reduce the bandwidth and, effectively, the excess of gain.

II. Elements of the Control System:

II-1 Thermocouple:

To measure the chamber temperature, a thermocouple (Type P13 R (Thermo Electric Co., Inc.)), selected for the required temperature range, is used. It is made of Pt, Pt-13 % Rh junction, and can measure temperatures up to 1500 °C. For accurate measurement of the evaporation chamber temperature

the thermocouple would have to be located somewhere inside the chamber. In such case, however, apart from constructional difficulties, the vapor of the charge material would be condensing on the thermocouple, and thus creating additional problems. Because of this, the thermocouple is protected from the metal vapour by placing it in the hollow of the bolt that holds the chamber in position, as shown in Fig. 19. The temperature sensing tip of the thermocouple is close to the bottom of the crucible containing the charge material. The error in the temperature reading introduced by this arrangement should not be great, and can be eliminated by a suitable calibrations of the thermocouple. The relation between the emf of the thermocouple P13 R and its temperature with the reference junction at 25 °C are given by the manufacture. The data from this source are plotted in Fig. A-2. During the preliminary experiments the reference junction was kept at the room temperature which was maintained around 25 °C by an air conditioner.

II-2 Differential Amplifier:

An integrated circuit, type ZEL 1 (Zeltex Inc.) was used as a differential amplifier (Fig. A-3). With a resistive feedback, the general input-output relation of this amplifier was approximately:

$$E_3 \simeq -\frac{R_2}{R_1}(E_2 - E_1)$$

where E_1 and E_2 are two input signals, and E_3 is the output, R_1 is the input resistance and R_2 is the feedback resistance.

Thus, the closed-loop gain of this amplifier is roughly proportional to the ratio R_2/R_1. Since the rated open-loop gain of this amplifier is 100,000, therefore, we can get the desired system sensitivity by adjusting the value of R_2/R_1.

The curve 1 of Fig. A-3-c shows the open-loop characteristic of this amplifier as a function of frequency giving a bandwidth of about 15 Hz. To eliminate the 60 Hz hum, and to reduce the relay chatter, this bandwidth was reduced to about 1 Hz by means of a capacitive feedback. The closed-loop frequency characteristic is shown as curve 2 in Fig. A-3-c.

II-3 Schmitt Trigger Circuit:

Figure A-4 is a temperature compensated Schmitt trigger circuit (Robinson, 1964). The change of the output level E_4 of this circuit is controlled by its input signal E_3. In this circuit, transistors Q_1 and Q_3 are coupled through transisror Q_2 which is used as a diode. This diode apart from its temperature compensating junction offsets the base-to-emitter voltage drop in Q_1 and thus brings the quiescent level of the input voltage to ground potential. Its minimum control signal E_3 is about $\pm$ 2 mV as shown in Fig. A-4-b. Figure A-4-c shows the wave forms of the input and the output signals.

II-4 Power Amplifier:

A power amplifier (Fig. A-5) was needed to drive the dc relay Ry. Since the relay required 0.6 A to energize its coil whereas the maximum current which could be drawn from Schmitt trigger circuit was about 9.4 μA, therefore, a considerable current gain was needed. This amplifier consisted of three cascaded transistors. One of these, Q_6, was a PNP power transistor, type 2N554 with 3 A maximum emitter-collector current and a minimum current gain of 30. The other two, Q_4 and Q_5, PNP switching type transistors 2N4402 had a minimum current gain of 50 each. Thus the overall current gain was at least 75,000, and about 8 μA at the input terminal of Q_4 was sufficient to drive the dc relay.

A Zener diode Q_7 (20 Volts) was connected across the coil to protect the power transistor Q_6 from overvoltages (up to 60 V) induced in the relay coil, due to current switching.

III. Measurements of Performance:

The temperature control system seemed satisfactory during the preliminary tests and measurements. These, however, could not be carried out in full because of a breakdown in a vacuum feedthrough, which made the ion-source temporarily inoperative.

References:

1. Robinson, Donald D.
'Diode-coupled Schmitt Trigger',
Electronics, Vol. 37, Dec. 14, 1964.

2. Thermo Electric Canada Ltd.,
'Operation and Maintenance Instruments for
Metal Sheated Thermocouples',
Brampton, Ontario

3. Zeltex, Inc.,
'Differential Amplifier, Type ZEL 1',
Concord, California, USA

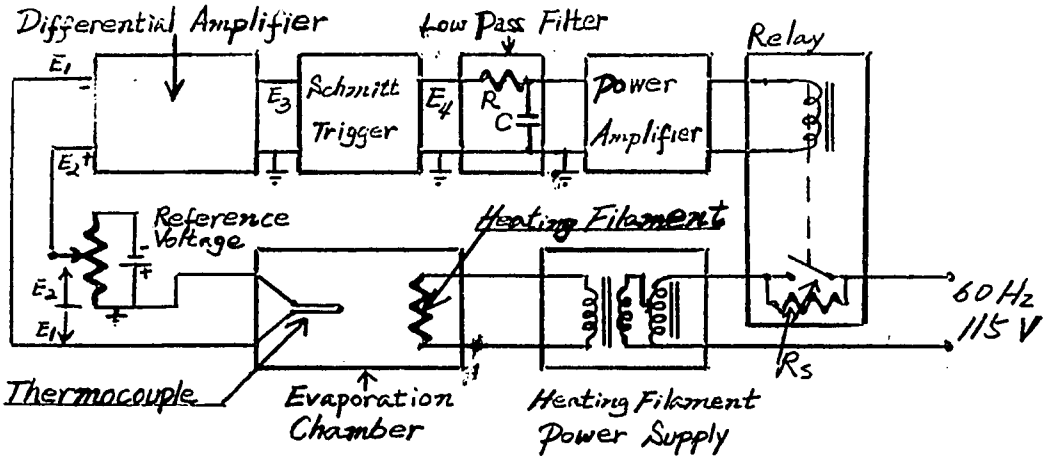

Fig. A-1 Block Diagram of the Temperature Control System. Rs is a by Pass Resistance to Minimize Filament Current Surge.

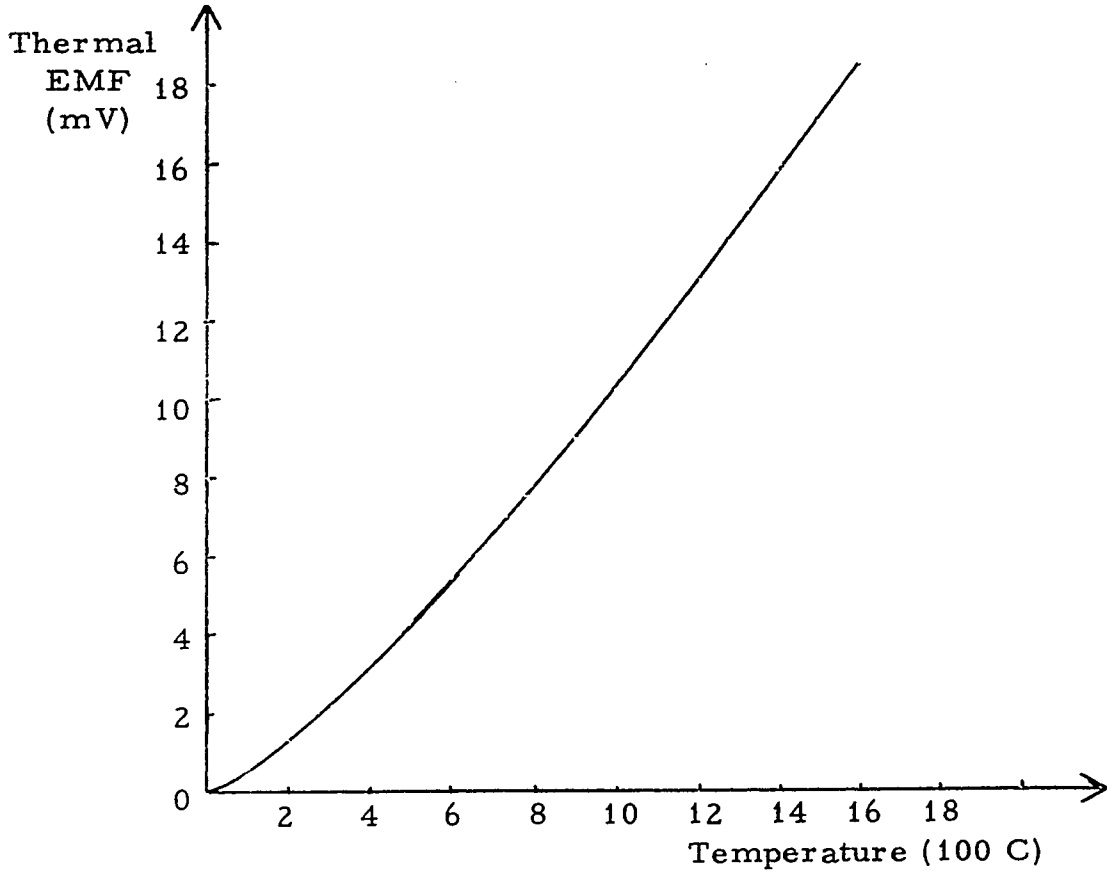

Fig. A-2 Temperature vs Thermal EMF of the Thermocouple (P13 R).

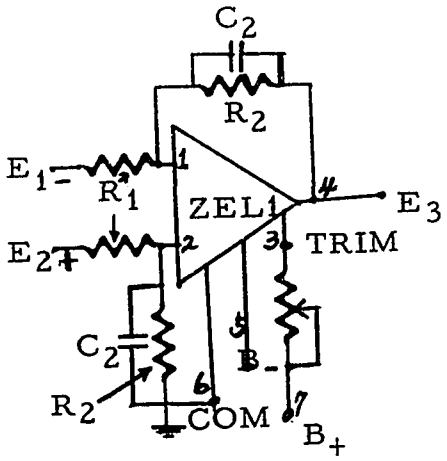

(a) External Circuit Connections.

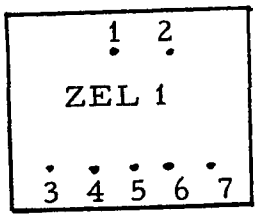

(b)

Pin Connections of the Amplifier (looking at the bottom of the package).

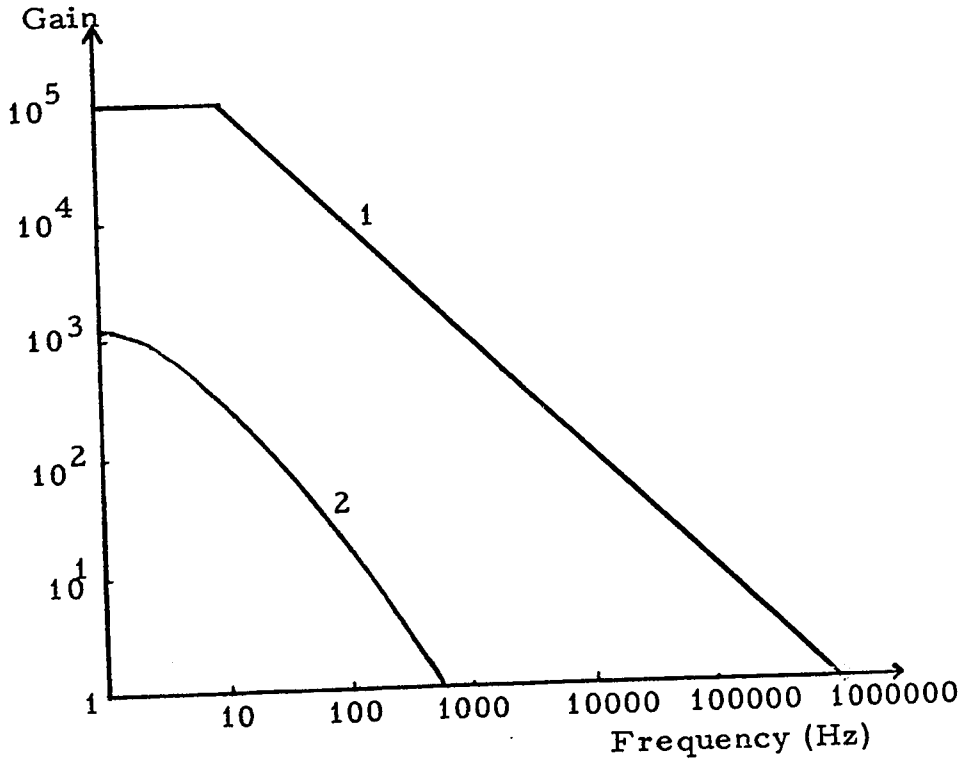

(c) Frequency Characteristics:
Curve 1: Open Loop Characteristic.
Curve 2: Closed Loop Characteristic with RC Feedback (R_2C_2 = 0.3 sec).

Fig. A-3 Differential Amplifier (Integrated Circuit ZEL 1).

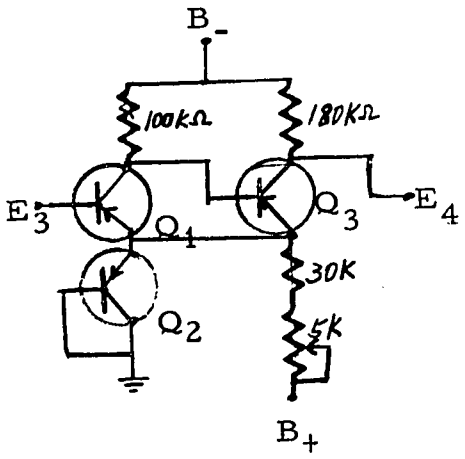

(a) Circuit Diagram

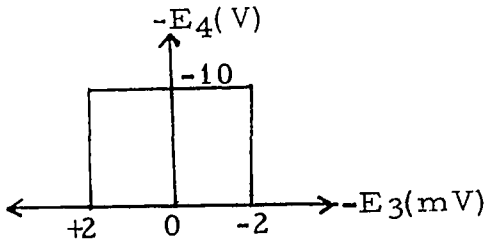

(b)
Threshold Voltage
Characteristic

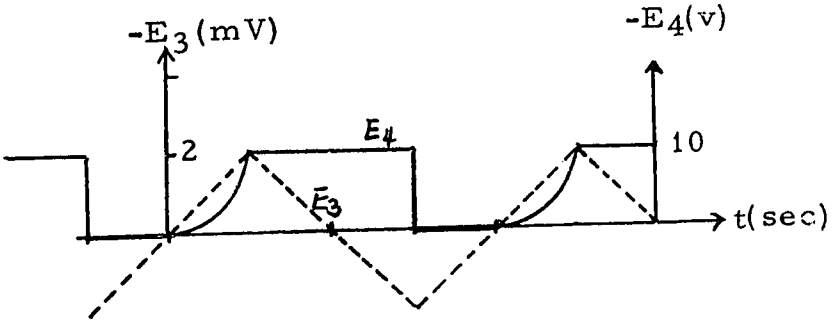

(c) Waveforms of E_3 and E_4.

Fig. A-4 Schmitt Trigger Circuit.

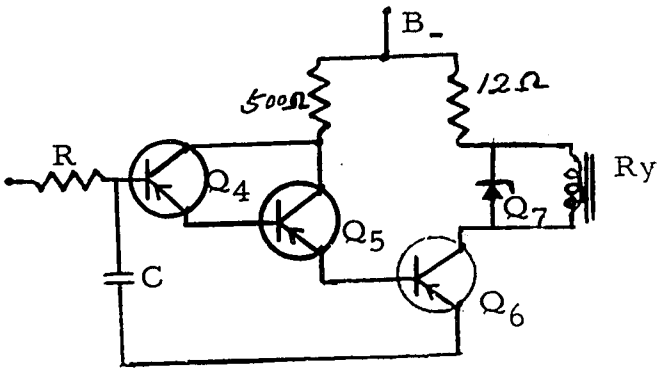

Fig. A-5 Circuit Diagram of Power Amplifier.

Appendix B

The filaments used to heat the evaporation chamber were not available commercially and, therefore, had to be specially wound. Because of its fragility, the 40 mil tungsten wire had to be heated during the winding by passing a current of about 20 A through it. Since hand winding of these filaments was awkward, and since the life of a filament was short, therefore, a simple winder (Fig. B) was designed for making these.

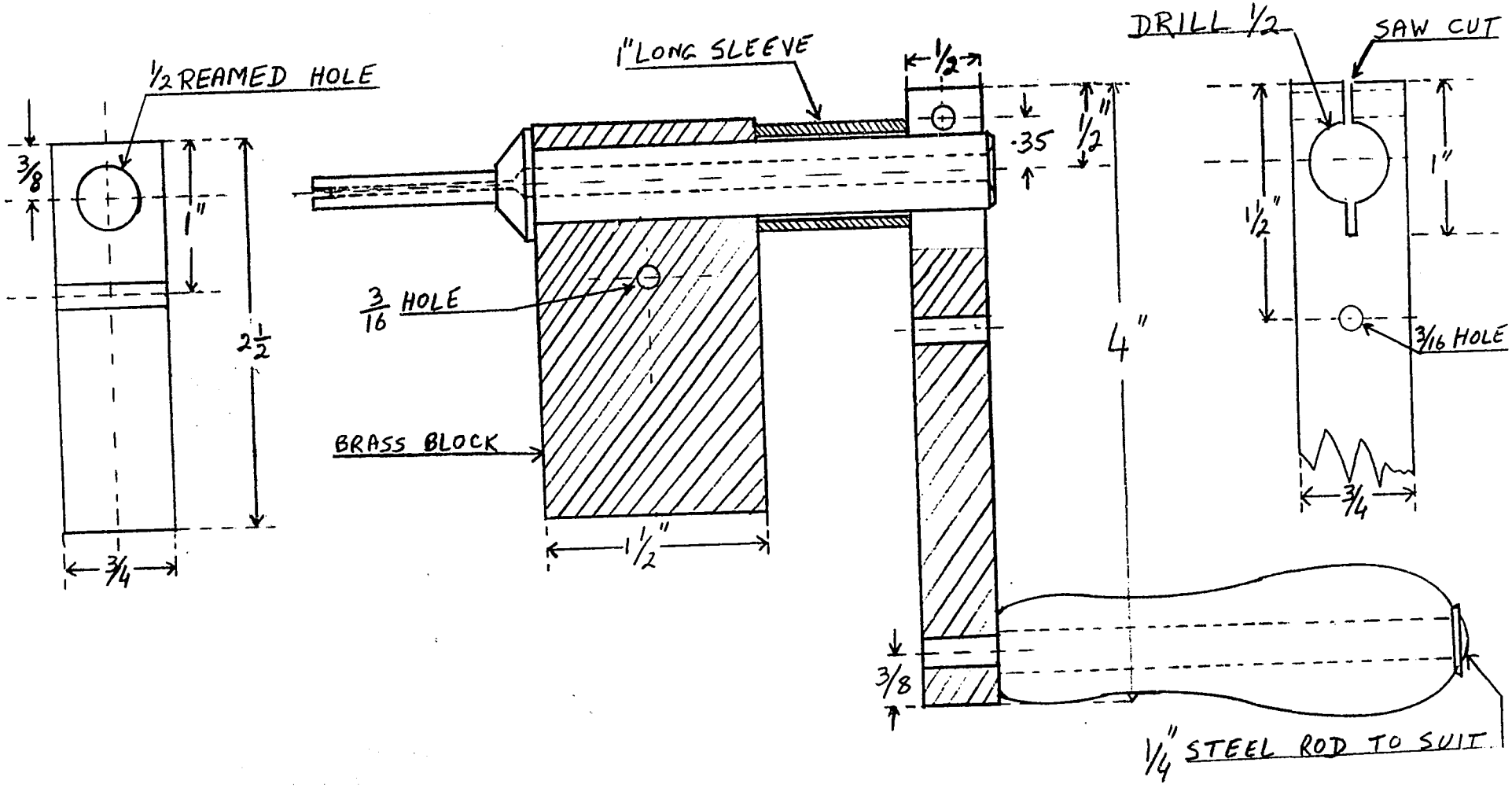

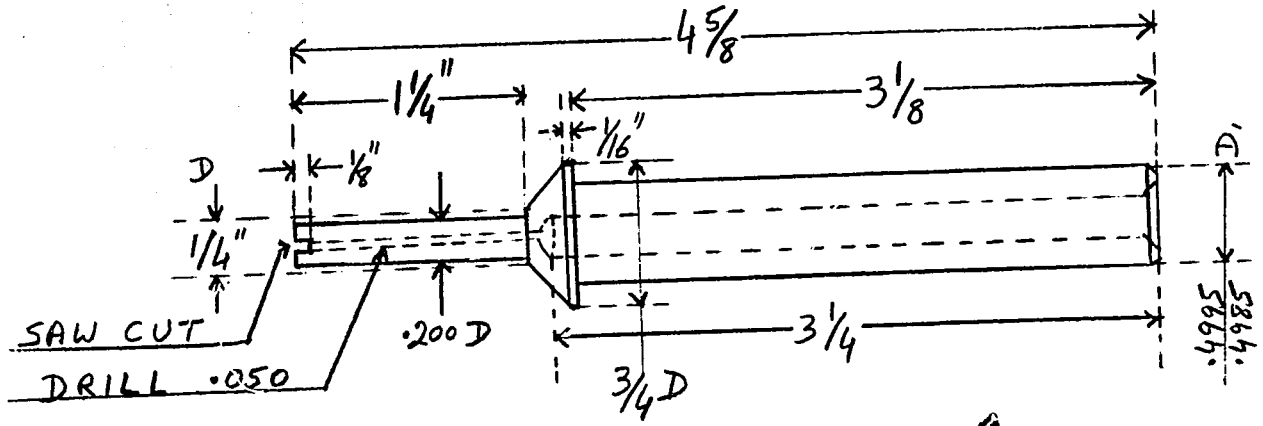

FILAMENT WINDER FIGURE - B

Appendix C Calculation of the total Reluctance of the Existing Magnetic circuit

The total reluctance of the magnetic circuit in Fig. 20 is the sum of the individial reluctances of the sections a, b, c, d, e, and f in the flux path. In the following calculations permeance (the inverse of reluctance) was used:

Section 'a':

The permeance of the air gap between the top plate and the magnetic core has been calculated by the field mapping method. This has been done by using an analog field plotter (Sunshine Scientific Instrument) and the resulting equipotential lines are shown in Fig. C-1. The distribution of the magnetic flux lines has been drawn in this plot by trial and error to form curvilinear squares as shown in Fig. C-2. The permeance of a volume element in the air gap was determined from the dimensions of these squares and from other known dimensions of the cylindrically symmetrical air gap (Fig. C-3). The following formula was used (Roters, 1941):

$$P_u = \mu_r \mu_o S/\ell \qquad (C-1)$$

where μ_r is the relative permeability of the medium (for air gap $\mu_r = 1$), μ_o is the permeability of the free space, S is the area of an elemental square in the equipotential surface in in.^{2}, and ℓ is the distance between the adjacent equipotential surfaces in inches.

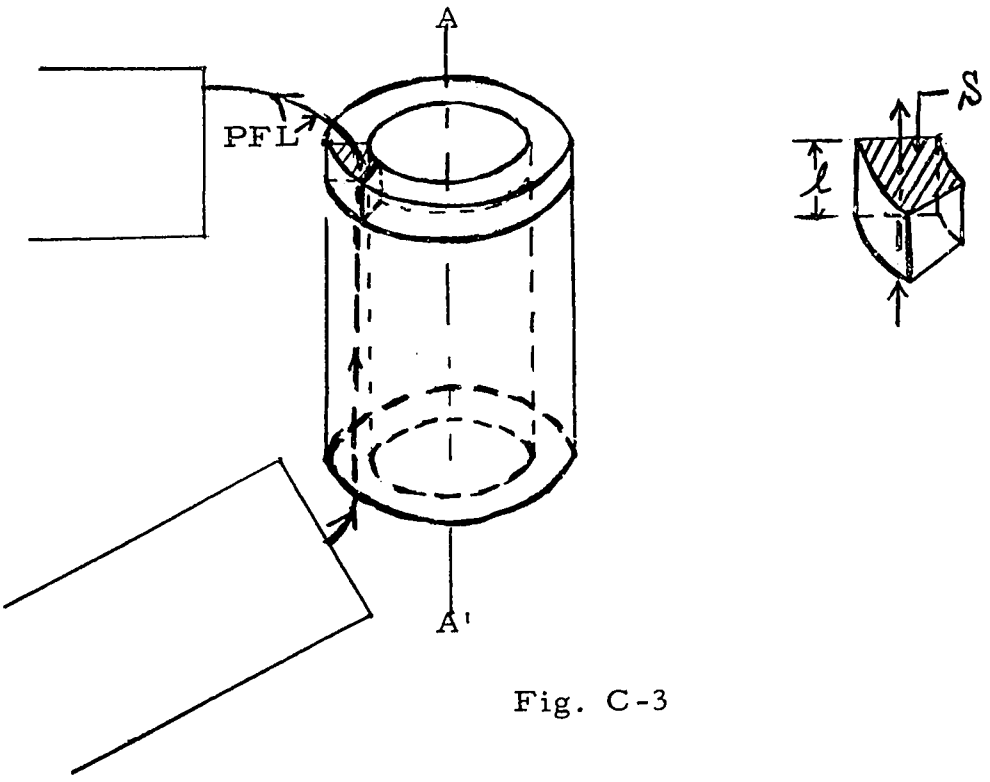

Fig. C-3

The permeance of a cylindrical element in the air gap was found by suitably adding the permeances of the volume elements in series and in parallel to get

$$P_c = P_u n_p / n_s \qquad (C-2)$$

where P_c is the permeance of the desired cylindrical region, n_p is the total number of the elemental squares in the annulus A in the equipotential surface, and n_s is the number of the elemental squares in the path PFL of the flux lines. For example, in Fig. C-2, where S = 1/7.5 sq. in./in., ℓ = 1/10 in., the elemental permeance per unit length is

$$P_u = 3.2\,(1/7.5)/(1/10)$$
$$= 4.27 \text{ maxwells/ampere-turn in.}$$

The permeance per unit length of annulus A in the equi-potential surface of each flux path was found by substituting $n_p = 1$ and $n_s = 10$ into Eq. (C-2)

$$P_1 = 4.27 \cdot (1/10) = 0.427 \text{ maxwell/ampere-turn in.}$$

Since the cross-section of each annulus was varying from one equipotential surface to another, and from one flux line to another, therefore the overall permeance of the air gap was calculated from

$$P_a = P_1 2\pi R \qquad \text{(C-3)}$$

where R is the sum of the averaged radii of individual annuli of flux lines. Therefore,

$$\begin{aligned} P_a = 0.427 \times 2\pi \,(&1 + 0.95 + 0.90 + 0.85 + 0.80 + 0.75 \\ &+ 0.71 + 0.68 + 0.65 + 0.62 + 0.59 + 0.56 + \\ &0.54 + 0.52 + 0.50 + 0.48 + 0.46 + 0.445 + \\ &0.43 + 0.42 + 0.41 + 0.405 + 0.40 + 0.39 + \\ &0.38 + 0.37 + 0.35 + 0.33 + 0.31 + 0.29 + 0.26 \\ &+ 0.23 + 0.20 + 0.17 + 0.14 + 0.11 + 0.07 + \\ &0.03) \\ = 0.427 &\times 2\pi \times 17.7 \\ = 46.4 &\text{ maxwells/ampere-turn} \end{aligned}$$

Because of simple geometries the calculations of the permeances of the other sections were simple. Equation C-1 was used in all these calculations.

Section 'b':

The cylindrical magnetic core, Here relative permeability $\mu_r = 2000$, ~~has been calculated from Eq. (C-1). Here~~ $\mu_o = 3.2$, cross-section area $S = \pi(1 - 0.8^2) = 1.1$ sq. in., the length $\ell = 7.5$ in.

Thus,

$$P_b = 2000 \times 3.2 \times 1.1/7.5$$
$$= 965 \text{ maxwells/ampere-turn}$$

Srction 'c':

The air gap at the junction between the magnetic core and the bottom plate of the tank. Since $\mu_r = 1$, $\mu_o = 3.2$, $S = \pi(1 - 0.8^2) = 1.1$ sq.in., $\ell = 0.04$ in., therefore,

$$P_c = 3.2 \times 1.1/0.04 = 83 \text{ maxwells/ampere-turn}$$

Section 'd':

The bottom and the top plates of the tank, $\mu_r = 2000$, $\mu_o = 3.2$, S(an average value) $= 2\pi \times 2.5 \times 0.2 = 3.14$ sq.in., and $\ell = 3$ in., thus,

$$P_d = 2000 \times 3.2 \times 3.14/(2 \times 3)$$
$$= 3500 \text{ maxwells/ampere-turn}$$

Section 'e':

The air gap at the junction between the bottom plate and the cylindrical walls of the tank, $S = \pi(4.375^2 - 4^2) = 10.24$ sq.in. and $\ell = 0.015$ in., therefore,

$$P_e = 3.2 \times 10.24/0.015$$
$$= 2080 \text{ maxwells/ampere-turn}$$

Section 'f':

The cylindrical walls of the tank. For $\mu_r = 2000$, $\mu_o = 3.2$, $S = \pi(4.375^2 - 4^2) = 10.24$ sq.in., and $\ell = 8.875$ in., thus,

$$P_f = 2000 \times 3.2 \times 10.24/8.875$$
$$= 7030 \text{ maxwells/ampere-turn}$$

The reluctance of the different sections of the magnetic circuit were

$$R_a = 1/P_a = 0.0216 \text{ ampere-turn/maxwell}$$

$$R_b = 1/P_b = 0.00138 \text{ ampere-turn/maxwell}$$

$$R_c = 1/P_c = 0.0121 \text{ ampere-turn/maxwell}$$

$$R_d = 1/P_d = 0.00029 \text{ ampere-turn/maxwell}$$

$$R_e = 1/P_e = 0.00048 \text{ ampere-turn/maxwell}$$

$$R_f = 1/P_f = 0.00014 \text{ ampere-turn/maxwell}$$

The total reluctance of the magnetic circuit was

$$R = R_a + R_b + R_c + R_d + R_e + R_f$$
$$= 0.036 \text{ ampere-turn/maxwell}$$

The accuracy of the above value of the reluctance was affected by the following errors:

1. The error in the calculation from the field plot was assumed to be not greater than 10 % (See p. 49), thus,
$$\Delta R_a = 0.0216 \ (\pm 10\ \%)$$
2. The lengths of the air gaps 'c' and 'e' were measured by inserting wires of different diameters in the gaps. This was not very satisfactory as a measurement and, therefore, the error in R_c and R_e was estimated to be as much as 30 % and 50 % respectively, thus
$$\Delta R_c = 0.0121 \ (\pm 30\ \%)$$
$$\Delta R_e = 0.00048 \ (\pm 50\ \%)$$

3. The error in the calculation of the reluctance of the magnetic material $R_I = R_b + R_d + R_f$, due to a 50 % inaccuracy in the knowledge of μ_r, is less than 10 %, thus,

$$\Delta R_I = 0.00182 \ (\pm 10\ \%)$$

Therefore

$$\Delta R = \Delta R_a + \Delta R_c + \Delta R_e + \Delta R_I$$
$$= \pm 0.006212 \text{ ampere-turn/maxwell}$$

Thus the error in the calculation of the total reluctance of the magnetic circuit was about 17 %. From the above figures, the accuracy of the calculations of the flux density in the air gap at the channel exit was found

$$B_1 = \frac{F \times (R_a/R) \times P_1 \times 2\pi r}{\pi r^2}$$

$$= \frac{500\left(\frac{0.0216 \pm 10\ \%}{0.036 \pm 17\ \%}\right) \times 2(0.427 \pm 10\ \%)}{0.03}$$

Since P_1 is inversely proportional to R_a, their errors cancel out and we get

$$B_1 = 1.325 \ (\pm 17\ \%) \text{ kilogauss}$$

This gave a 17 % error in the calculated value of B_1.

References:

1. Roters, Herbert C.
'Electronmagnetic Devices',
John Willey and Sons Inc., New York, 1941

2. Sunshine Scientific Instrument Co.,
'Use and Theory of the Analog Field Plotter',
Phila. 15, PA.

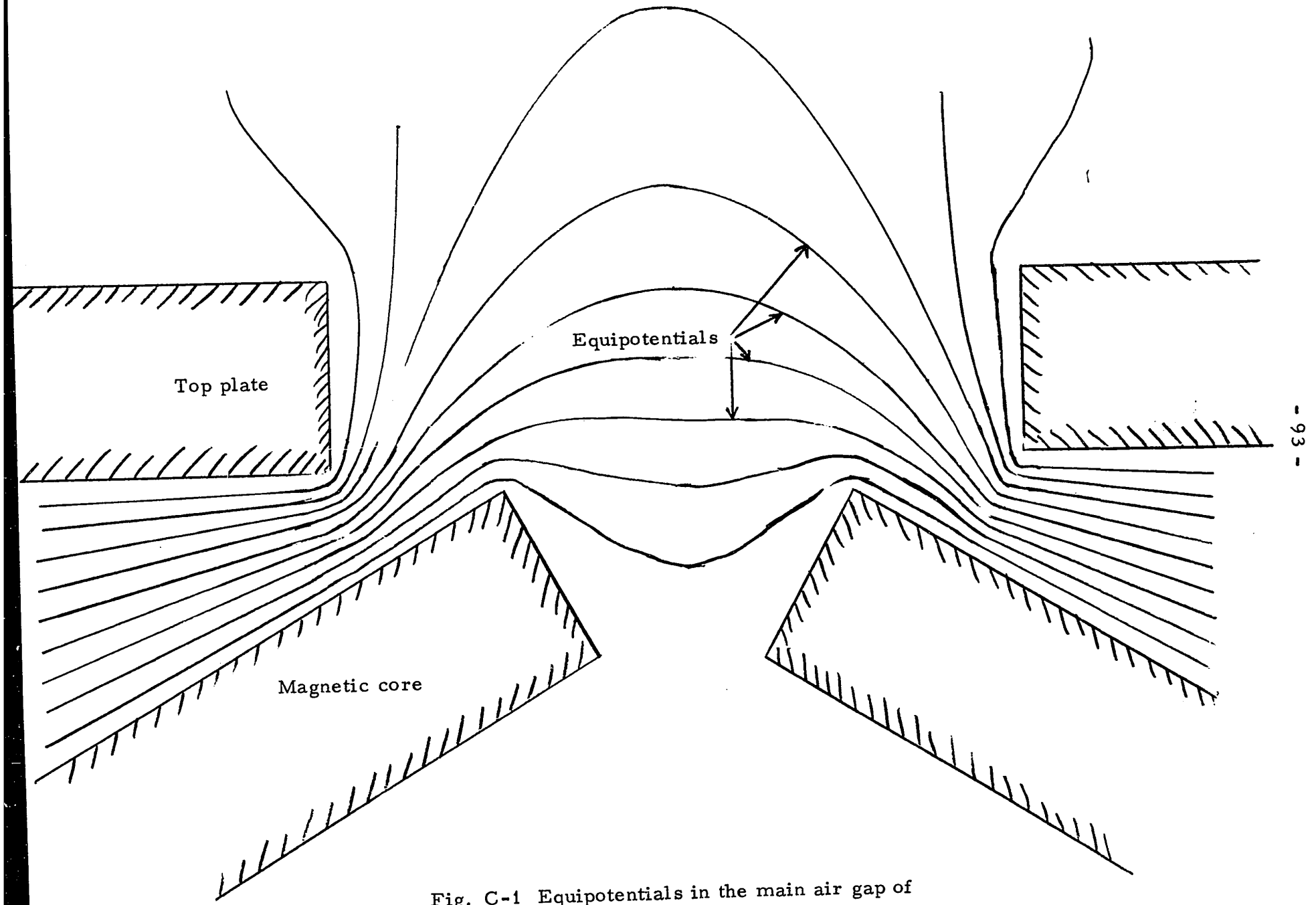

Fig. C-1 Equipotentials in the main air gap of the existing magnetic circuit.

Fig. C-2 Mapping of the Field in the Main Air Gap Between the Existing Magnetic Poles.

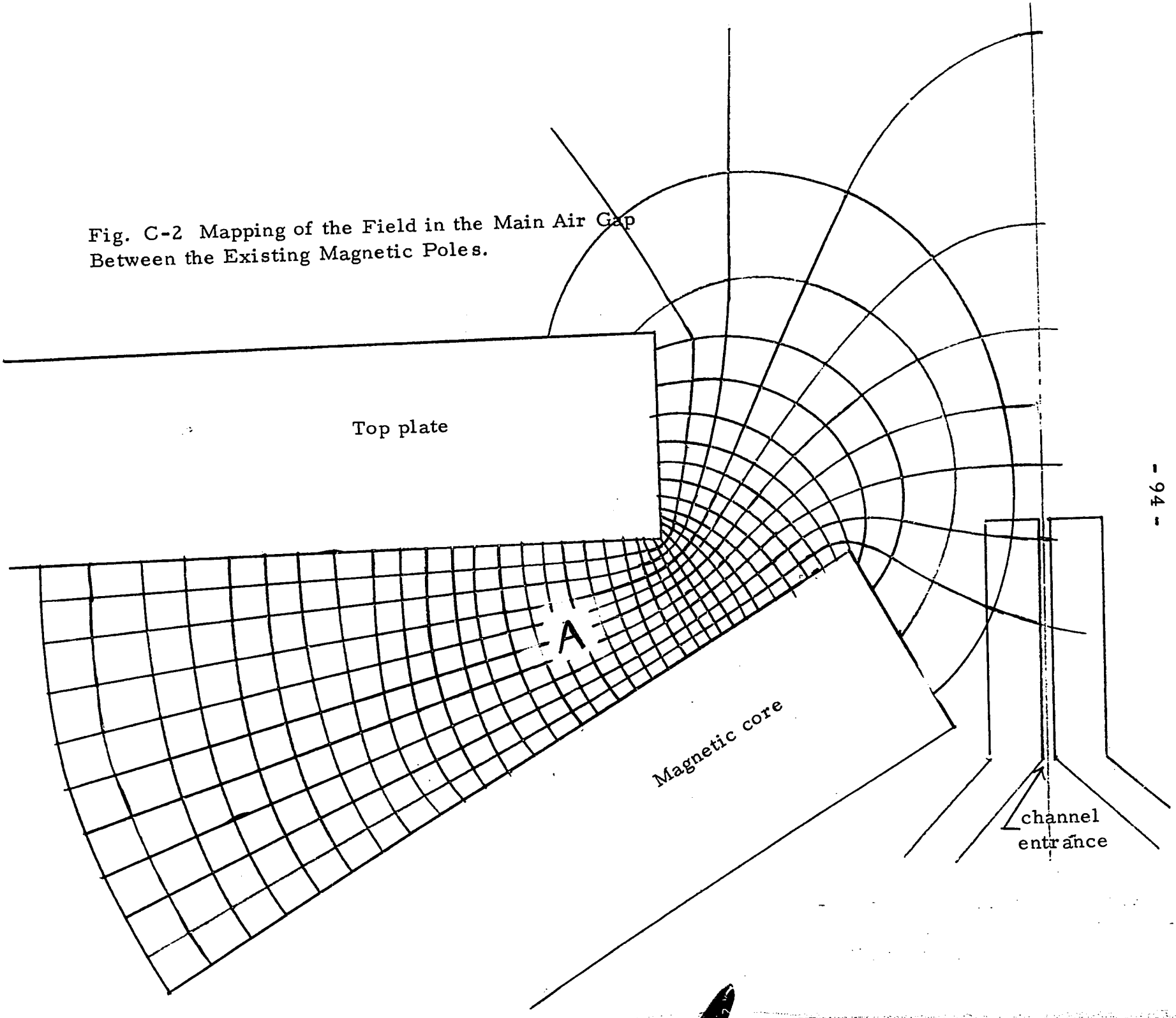

VITA

Name: Chin-Chi Tsai

Born: 11 June, 1940 Changhua, Taiwan

Educated:

Primary: Provencial Changhua High School, Taiwan

Secondary: Provencial Changhua High School, Taiwan

University: Cheng Kung University, Taiwan

1963 Bachelor of Science in Electrical Engineering (B.S.E.E.)